ISSN : 0019-5693

INDIAN JOURNAL
OF
THEORETICAL PHYSICS

VOLUME 64 NOS. 3, 4

JUNE, 2016 — DECEMBER, 2016

Published by the
CALCUTTA INSTITUTE OF THEORETICAL PHYSICS
(Formerly, INSTITUTE OF THEORETICAL PHYSICS)
"BIGNAN KUTIR"
4/1, MOHAN BAGAN LANE, KOLKATA-700 004

(UGC approved and refereed Journal)

ISSN : 0019-5693

INDIAN JOURNAL
OF
THEORETICAL PHYSICS

VOLUME 64 **NOS. 3, 4**

2016

Published by the

CALCUTTA INSTITUTE OF THEORETICAL PHYSICS
(Formerly, INSTITUTE OF THEORETICAL PHYSICS)
"BIGNAN KUTIR"
4/1, MOHAN BAGAN LANE, KOLKATA-700 004

(UGC approved and refereed Journal)

ISSN : 0019-5693

INDIAN JOURNAL
OF
THEORETICAL PHYSICS

[Founder President : Late Prof. K. C. Kar, D.Sc.]

VOLUME 64 **NOS. 3, 4**

2016

Director **: D. K. Basu**
Secretary **: S. K. Sarkar**

Co-Published by the

WILCOX BOOKS & PERIODICALS CO.
8/2/A, Neogipara Road, Kolkata – 700 036

INDIAN JOURNAL
OF
THEORETICAL PHYSICS
"BIGNAN KUTIR"
4/1, MOHAN BAGAN LANE, KOLKATA-700 004, INDIA

SUBSCRIPTION RATE

INDIA : (For Library & Institute)
₹ 1500.00 for Vol. 64, 2016 and onwards
FOREIGN : $ 350 for Vol. 64, 2016 and onwards
Drafts, Orders, Enquiries & Claim for Non-Receipt of Journal should be sent to :

WILCOX BOOKS & PERIODICALS CO.
8/2/A, NEOGIPARA ROAD
KOLKATA – 700 036 (INDIA)
Website : www.wilcoxjournals.com
E-mail : wilcoxbooks@yahoo.com
: wilcoxbooks@gmail.com
Phone : 91-3325771147
Mobile : 91-9231675520

BLANK

C O N T E N T S

BLANK

INDIAN JOURNAL OF THEORETICAL PHYSICS, VOL. 64, NOS. 3 & 4, 2016

Theoretical investigation on electronic structure and optical properties of zinc-blende and rocksalt structures of HgSe: A DFT study

P. K. Saini[1,2*], D. S. Ahlawat[1]

[1]Department of Physics, Chaudhary Devi Lal University,
Sirsa (HRY) 125055, India
[2]Department of Physics, Govt. PG College,
Hansi (HRY) 125033, India

and

D. Singh

Department of Physics, MM University,
Ambala (HRY) India

(Received for publication in July, 2016)

[**Abstract :** Electronic band structure and optical properties of *HgSe* with zinc blende (*ZB*) and rocksalt (*RS*) type structures are studied using a*b initio* density functional method with generalized gradient approximation (*GGA*).The band structure and density of states are calculated to discuss the electronic properties and orbital hybridized properties of the compound. The optical properties, including the complex dielectric function, absorption coefficient, refractive index and electron energy loss function, are discussed for radiation up to 14 *eV* by analysis of the energy band structures and density of states calculated. The common trends and the differences between the two structures of *HgSe* are presented in details. The calculated optical properties indicate that *HgSe* can serve as shielding devices for ultraviolet radiation.]

Keywords : Electronic structure, density of states, optical properties, DFT and GGA

1. Introduction

The mercury chalcogenides, *HgX* [*X= S, Se, Te*] have received and still receiving considerable attentions due to their enormous technological importance in optoelectronic applications such as emitter, tunable lasers, photo conductor, *IR* detector, electrostatic imaging, photoelectric conversion devices[1-7]. *HgSe* and *HgTe* crystallize in the zinc-blende structure, but are

*Corresponding Author : pawansaini2005@gmal.com

semimetalic, a deviation from the semiconducting behavior[8]. The phase transition of *HgSe* from cinnabar structure to rocksalt structure under high pressures has been considered in experiments[8-10]. The band gap is a significant parameter which affect on the electrical, magnetic and optical properties of semiconducting compounds. The band gaps of most III–V and II–VI compounds have been correctly measured by various methods[11-12]. However, the band gaps for some of these compounds have been recently a subject of debate. One of the well-known compound is the mercury selenide (*HgSe*) in *ZB* and *RS* structure.

Mercury chalcogenide confirms a large spectrum of properties, making them good candidates for modern spintronic and optoelectronic applications[13-14]. The mercury cadmium telluride is one of the widely used semiconductor material for infrared detectors. Many of their strange properties come from the interaction between the localized semicore d electron with the valence p electron[15]. When compared with other II–VI compounds and their alloys, very few results have been reported for *HgX* compounds[16-19]. Cardona, et. al.[20] have investigated the electronic band structure and the phonon dispersion relations of the mercury chalcogenides in *ZB* structure. Recently, *ZB* and *RS HgSe* have been comprehensively studied theoretically[11,15,21,22-25] and experimentally[8,26-29]. However, detailed descriptions for the two structures of *HgSe* are not available till now to our knowledge. Here, we have taken up this problem purely from theoretical point of view. Earlier, we have carried out similar calculations on both pure *ZnSe* and *ZnTe*[30-31]. This paper presents a systematic study of the structural, electronic and optical properties of *HgSe* in *ZB* and *RS* phases in order to provide a basic understanding of future device concepts and application. In this work, we also have focused on the common trends and the differences in electronic structure and optical properties among the two phases of *HgSe*. The organization of the paper as follows; Section 2 gives method of calculations. Further, results and discussion are presented in section 3 and finally in section 4 the results are summarized and conclusions are drawn.

2. Computational method

The calculations are performed using the full-potential linear augmented plane wave (*FP-LAPW*) method[32-34] using density functional theory (*DFT*)[35] as implemented in the Wien2k code[36]. The exchange-

correlation potential has been calculated using *GGA* within the parameterization of Perdew-Burke-Ernzerhof (*PBE*)[37-38]. Moreover, the Engel-Vosko *GGA* (*EVGGA*) formalism is also applied to optimize the corresponding potential for band structure calculations to improve the energy band gap[39]. The self consistent calculations are considered to be converged only when the total energy of the crystal converged to less than 1 *mRyd*. In the *FP-LAPW* method, the wave function, charge density and potential are expanded by spherical harmonic functions inside non overlapping spheres surrounding the atomic sites [muffin-tin spheres] and plane wave basis set in the interstitial region of the unit cell .The maximum *l* value for the wave functions expension inside the spheres was confined to l_{max} = 10. The plane-wave cut off of $K_{max} = 7.0/R_{MT}$ (where R_{MT} is the smallest muffin-tin radius) is taken for the expension of the wave functions in the interstitial region. Further, the charge density was Fourier expanded up to G_{max} = 14. For the Brillouin-zone sampling, we have applied the Monkhorst-pack *k*-point grids of 12×12×12 for both *ZB* and *RS HgSe*. In *ZB HgSe* the *Hg* and *Se* atoms are at the positions of *Hg*(0,0,0) and *Se*(1/4,1/4,1/4), and *Hg*(0,0,0) and *Se*(1/2,1/2,1/2) for *RS HgSe*.

We first check the structural properties of the *ZB* and *RS HgSe* at zero pressure and the calculated results are listed in Table I, along with the available theoretical and experimental results. It can be seen for *ZB HgSe* that the *GGA* over-estimates the lattice parameter. This finding is consistent with the general trend of this kind of approximation . The lattice constant calculated from *GGA* is 2.9%, larger than the experimental value whereas the results for bulk modulus, well agreed with the experimental findings. It can be noted that the value of our lattice constant calculated from *GGA* is in good agreement with the experimental data[26] and the theoretical value of Ref.[22]. In case of *RS HgSe*, since we have neither theoretical nor experimental values available in literature to compare with, we leave these obtained results as a reference for future investigation about the said compound.

Table I

Lattice constants, bulk modulus B_0 [in *GPa*] and pressure derivative of the bulk modulus B_0' of *ZB* and *RS HgSe*.

Material	Phases	Calculations	Lattice constant a a_0 [*Å*]	Bulk modulus B_0 [in *GPa*]	Pressure derivative of the bulk modulus B_0'
HgSe	*ZB*	Present work	6.25	53.15	3.23
		Theory [Ref.22]	6.19	41.8	–
		Exp. [Ref.26]	6.07	57.6	–
	RS	Present work	5.79	57.07	4.16
		Others	–	–	–

3. Results and discussion

3.1. Electronic structure results :

Based on the optimized structural results, electronic structures including the band structure, total density of states (*TDOS*) and atomic site projected density of states (*PDOS*) are computed for the structures of *ZB* and *RS HgSe*. The energy gap, at Γ point, calculated using the two approximations *GGA* and the Engel-Vosko (*EV*) correction[39] are listed in Table II. The approximation (*EV*) yields a better band splitting in the spectrum. The energy band structures of the *ZB* and *RS HgSe* at zero pressure are compared in Fig. 1. The Fermi level (*EF*) is selected to locate at 0 *eV* as reference level and coincides with the top of the valence band . From Fig. 1, the valence band maximum (*VBM*) is found to be 0.2 *eV* at Γ point for the *ZB*, 0.3 *eV* at *L* point for the *RS HgSe*, respectively. The conduction band minimum (*CBM*) is obtained to be ⁻2 *eV* at Γ point for the *ZB*, ⁻2.3 *eV* at *X* point for the *RS*, *HgSe*, respectively. Consequently, we found that the *ZB* structures of *HgSe* have a negative direct band gap of ⁻2.3 *eV*. The band gap values computed by using *EV-GGA* scheme are found to be improved and lying closer to their experimental results available in literature[26].

Further, we find from Fig.1 that the electronic structures near the valence band maximum of *HgSe* are very similar for *ZB* and *RS* structures except the band gap at Γ point in the spectrum. However, a small difference

in the band position on energy scale may be seen. In the case of *ZB* phase the lowest lying band in the valence band region is found at ⁻12.5 *eV*. It mainly arises due to the 4*s* states of *Se* while the bands just below E_F are composed of *Hg-d* and *Se-p* states. The *d* states of *Hg* are more important in the valence bands than the *s* states.

The bottom of the conduction bands is mixer of the hybridization states of *Hg-s* and *Se-p*, and also some states from *Hg-d*. Similarly, the band gap is also calculated for high pressure *RS* phase of *HgSe*, which is found to be reduced as a function of pressure as one can see from the comparative study of band structures and partial *DOS* of both the *ZB* and *RS* phases. This may be due to the fact as mentioned above in high pressure rock salt phase of *HgSe* that the hybridization interaction of the *d* electrons with

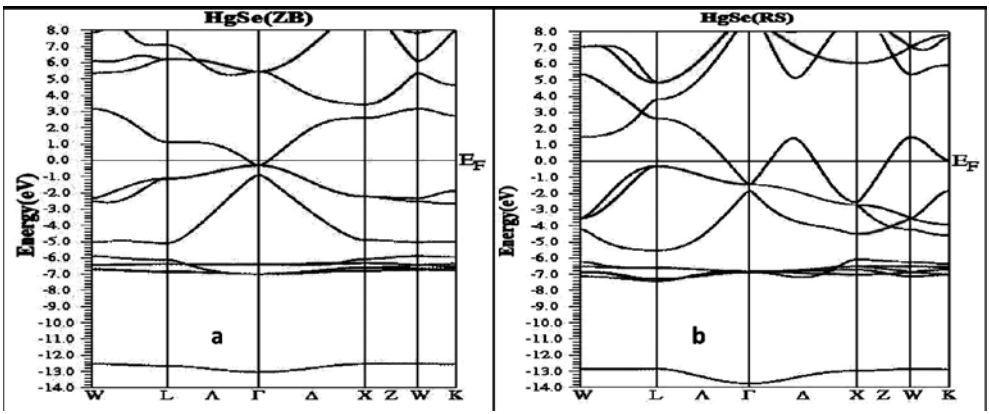

Fig. 1

Band structure of *ZB* and *RS HgSe* using *EV-GGA*.

anion *p* electrons responsible for the repulsion of the involved states and an increased width of the upper valence bands region and hence a decrease in the band gap obtained.

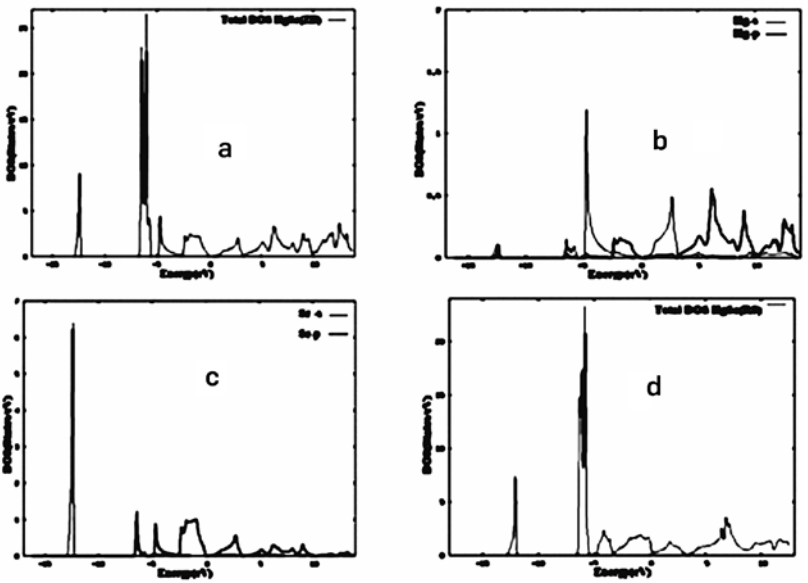

Fig. 2

Calculated total and partial density of *ZB* and *RS HgSe* at zero pressure.

This decrease in the band gap is due to *Se*-4*p* states which are pushed up in energy towards the *Hg-s* derived conduction bands by *p-d* interaction. It can be noticed that the conduction band and the valence band overlap at several places in the spectrum. On the basis of this, it can be explained that the rocksalt phase of *HgSe* under high pressure has metallic properties.

Table II

Calculated direct-band gap for zinc-blende phase of *HgSe* along with the other theoretical and experimental work.

Compound	Calculations	Static dielectric constant, $\varepsilon_1[0]$
HgSe	Present work [using *EV-GGA*]	-0.23
	Present work [using *GGA*]	-0.1
	Theory [Ref.15]	-0.4
	Theory [Ref.23]	-1.2
	Experimental [Ref. 26]	-0.2

Calculated total density of state (*TDOS*) and atomic site projected densities of states (*PDOS*) are displayed in Fig. 2 for the *ZB* and *RS* structures of *HgSe*, respectively. From Fig. 2, we can see that the lower part of the valence band is mainly dominated by *Se* 4*s* states with some contributions from *Hg* 4*s* states, while the upper part by *Se* 4*p* and *Hg* 5*p* states for the *ZB* and *RS* structures of *HgSe*. Further, the upper valence bands of *HgSe* are shown to localize in different energy regions for different structures from the *TDOS* as shown in Fig. 2(*a*) and 2(*d*), *i.e*. from the Fermi level to ⁻2.2 *eV* for the *ZB* and ⁻3.5 *eV* for the *RS* structure, which is due to the hybridization of *Se p* states with the *Hg p* and *Hg s* states. The lower conduction bands positioned above the Fermi level with the energy ranging at 3.2 *eV* and 1.6 *eV* for *ZB* and *RS* structures of *HgSe*, respectively, are mainly from the contribution of *Hg p* states.

3.2. Optical properties :

In this part, the optical properties of *HgSe* at zero pressure are analyzed for the *ZB* and *RS* phases, based on our *DFT* calculations. The optical properties are obtained from the complex dielectric function $\varepsilon(\omega)$, which correspond to the linear response of the system in an external electromagnetic field with a small wave vector. It can be expressed as[40-43]

$$\varepsilon_{\alpha\beta}(\omega) = Re\,\varepsilon_{\alpha\beta}(\omega) + i\,Im\,\varepsilon_{\alpha\beta}(\omega) = \varepsilon_1(\omega) + i\varepsilon_2(\omega) \quad \ldots \quad (1)$$

In calculations we include the local field effect but ignore the excitonic effects. The interband contribution to the imaginary part of the dielectric function is computed by taking all possible transitions from occupied to unoccupied states. The imaginary part of the dielectric function is given by[44-46]

$$Im\,\varepsilon_{\alpha\beta}(\omega) = \frac{4\pi e^2}{m^2\omega^2}\sum_{c,v}\int_0^\infty dk \left\langle c_k \left| P^\alpha \right| v_k \right\rangle \left\langle v_k \left| P^\beta \right| c_k \right\rangle \left(\varepsilon_{ck-}\varepsilon_{vk-}\omega\right) \quad \ldots \quad (2)$$

where c_k and v_k are the wave functions corresponding to the conduction and the valance bands with the wave vector *k*, respectively .

The real part of the dielectric function can be extracted from the imaginary part using the Kramers-Kroning relation given[47]:

$$Re\ \varepsilon_{\alpha\beta}(\omega) = 1 + \frac{2}{\pi} P \int_0^{\infty} \frac{\omega' Im\, \varepsilon_{\alpha\beta}(\omega')}{\omega'^2 - \omega^2} d\omega' \qquad \ldots \quad (3)$$

where P is the principal value of integral in the equation.

Other optical constants such as the refractive index $n(\omega)$, extinction coefficient $k(\omega)$, optical reflectivity $R(\omega)$, absorption coefficient $I(\omega)$ and energy-loss spectrum $L(\omega)$, can be computed using the complex dielectric function (ω), through the relations as given in Ref.[48-49]. The calculated optical properties at the equilibrium lattice constant are given in Figs. (3-5) for the energy range up to 14 *eV*. Figs. 3(*a-b*) gives the real and imaginary parts of calculated dielectric function for the *ZB* and *RS* structures of *HgSe*. The spectrum of $\varepsilon_2(\omega)$ in Fig. 3 indicate that the threshold energy of the dielectric function starts at 0.012 *eV* for both *ZB* and *RS* structures of *HgSe*.

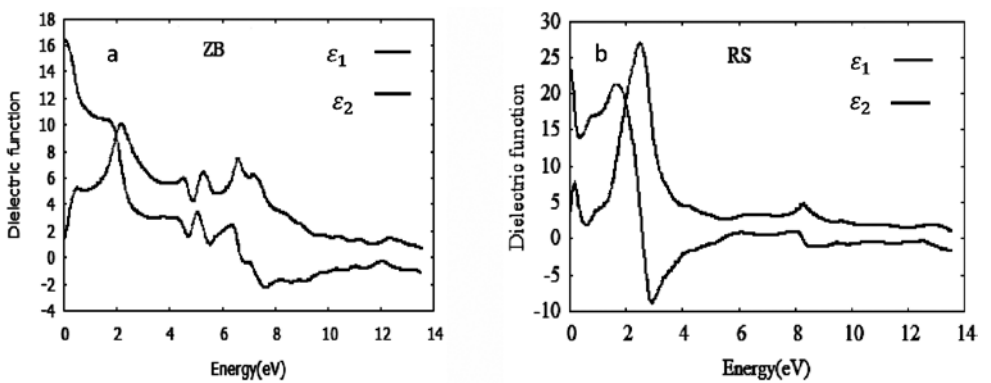

Fig. 3

Calculated real and imaginary part dielectric function for *ZB* and *RS HgSe*, respectively.

The $\Gamma_V - \Gamma_C$ splitting for both the *ZB* and *RS HgSe* are shown in Fig.1, and give the threshold for direct optical transitions between the highest valence and the lowest conduction bands, which is known as the fundamental absorption edge of spectrum. Away from these points, the

peak increases rapidly, which is due to the fact that the number of points contributing towards $2(\omega)$ increases abruptly. With the increase of energy, the absorptive part of the dielectric function $2(\omega)$ exhibits two structures positioned at 0.8 and 2.3 *eV* for the *ZB* as well as 0.3 and 2.8 *eV* for the *RS* structure *HgSe*, respectively. The first structures obtained primarily from the transitions of *Se* 4*p* electrons into *Hg* 5*p* conduction bands, while the second structures due to the transitions of *Se* 4*p* electrons into *Hg* 6*p* and 5*s* conduction bands in the spectrum. Unfortunately, there are no experimental data available relating to the origin and the position of these peaks to make a comparison for both structures of the compound.

Table III

Microscopic dielectric constants of *ZB* and *RS* phases of *HgSe*.

Compound	Phase	Calculations	Microscopic dielectric constant, $\varepsilon_1[0]$
HgSe	*ZB*	Present work	16.3
		Theory [Ref.34]	16.4
		Exp. [Ref.35]	15.7
	RS	Present work	23.4
		Others	–

In the real dielectric function, the most important quantity is the zero frequency limit $\varepsilon_1(0)$, since it gives the static dielectric constant in the zero frequency limit. The obtained values of the static macroscopic dielectric constants are given in Table III, in comparison with the data in other literatures. It can be seen that our calculated result of *ZB HgSe* is in good agreement with experimental and other theoretical results. As far as we know, for the *RS HgSe* there are no experimental and theoretical data available related to the static dielectric constants.

Fig. 4(*a*) displays the calculated refractive index $n(\omega)$ results. It can be seen that the refractive index is significant only up to 2.1 of *ZB* and 1.95 *eV* for *RS* phases, beyond this energy value the peak drops sharply.

The calculated static refractive index $n(0)$ is 4.05 and 4.85 for the *ZB* and *RS* structure, respectively. The computed extinction coefficients $k(\omega)$ for *ZB* and *RS HgSe*, are depicted in Fig. 4(*b*). The local maxima of the extinction coefficient $k(\omega)$ corresponds to the zero of $\varepsilon_1(\omega)$ (7.31 *eV*) for *HgSe* in *ZB* phase and 2.81 *eV* for *HgSe* in *RS* phase, respectively. The difference in the spectra of the extinction coefficient for *ZB* and *RS* indicates that there is a shifting of spectra towards lower energy side for high pressure *RS* phase with increase in peak height in the spectrum. This is due to fact that the energy band gap decreases at high pressure rocksalt phase and becomes metallic.

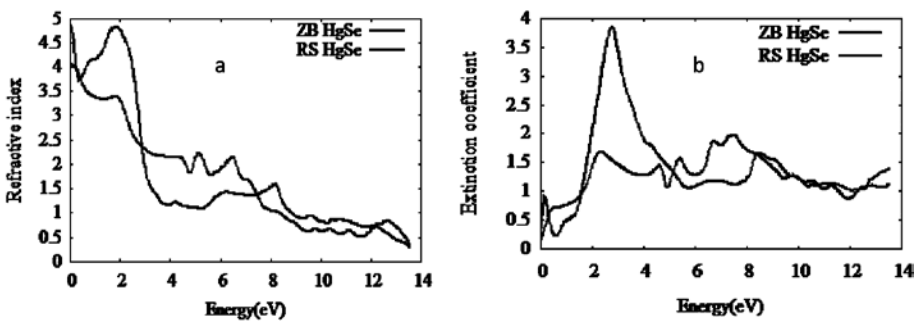

Fig. 4
The calculated refractive index $n(\omega)$ and extinction coefficient for *ZB* and *RS HgSe*, respectively.

Fig. 5 shows the results of the linear absorption spectrum $\alpha(\omega)$, reflectivity function $R(\omega)$ and electron energy loss function $L(\omega)$ for the *ZB* and *RS* structures of *HgSe*, respectively. From Fig. 5(*a*), it can be seen that the absorption edge starts from the energy values of 0.22 and 0.51 *eV*, corresponding to the direct Γ- Γ transition for the *ZB* and *RS HgSe*, respectively.

In Fig. 5(*b*), the maximum reflectivity occurs in the energy regions of (9.21, 13.31 *eV*) and (8.31, 13.42 *eV*) for the *ZB* and *RS HgSe*, respectively, and these are in the ultraviolet region. Therefore, the present calculated results imply that the two structures *HgSe* materials can serve as shields for ultraviolet radiation in optical devices. The electron energy loss function $L(\omega)$, is a important factor related to the energy loss of fast electron traversing in the material. In the Fig. 5(*c*), the most prominent peak in the energy loss spectrum is linked with the Plasmon peak and situated at 11.90 *eV* and 11.99 *eV* for *ZB* and *RS* structure of *HgSe*,

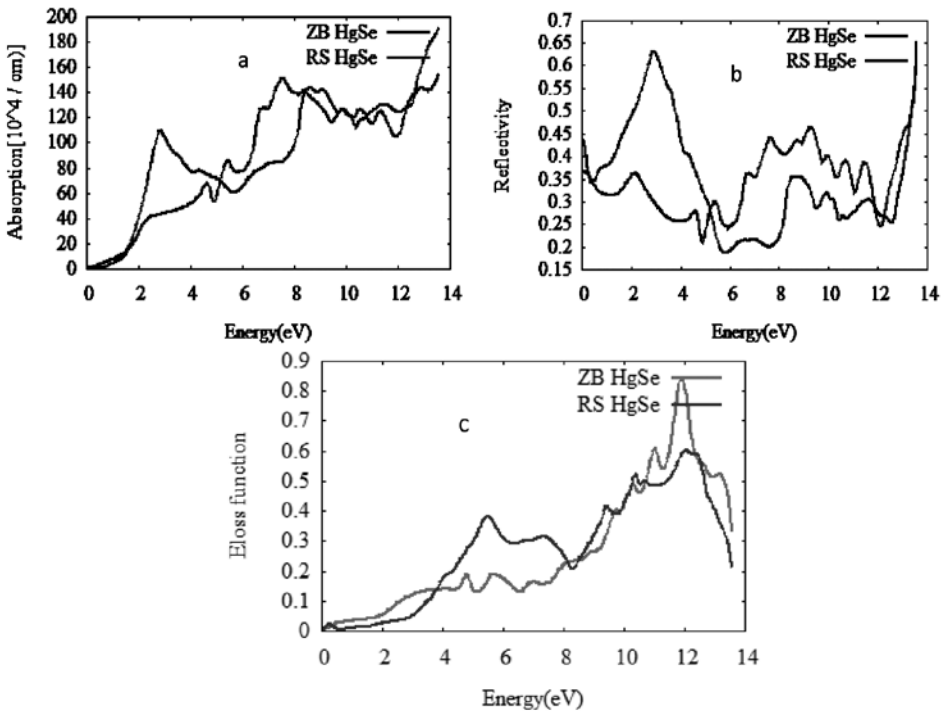

Fig. 5

The calculated absorption coefficient $\alpha(\omega)$, reflectivity $R(\omega)$, and loss function $L(\omega)$ for *ZB* and *RS HgSe*, respectively.

respectively and the corresponding frequency is called plasma frequency ($\hbar\omega_p$) (50). These different peaks correspond to irregular edges in the reflectivity spectrum, and hence an abrupt decline occurs at these peaks values in the reflectivity spectrum and it correlates with the zero crossing of $\varepsilon_1(0)$ shown in Fig. 3(*a-b*).

To the best of our knowledge, we are not aware any results/data related to the optical dispersions of *HgSe* in high pressure rocksalt phase. So a comparison is not possible.

4. Conclusions

This study reports a detailed investigation on the electronic and the optical properties of *ZB* and *RS HgSe* using the first principles calculations *FP-LAPW* method based on the density functional theory. On the basis of the calculated structural results, the electronic structures and optical

properties are compared among the two structures of *HgSe* and the common trends as well the differences are presented in detail. The calculated lattice constants at zero pressure of the *ZB* and *RS HgSe* are in a reasonable agreement with the available experimental and other theoretical results. The calculation provides an excellent description of the electronic band structures of two phases *HgSe*, which could be useful for further experimental investigation and other theoretical calculations. The density of states of *ZB* and *RS* phases is analyzed in more detail, and differences among these two structures have been found. Using the electronic band structure, we have analyzed the interband contribution to the various optical response functions. Moreover, the static macroscopic dielectric constants of high pressure *RS HgSe* are predicted theoretically.

References

1. Tokyo, N. – J. Appl. Phys., **46**, 4857(1975**)**.
2. Whisett, C. R., Broerman , J. G. and Summers, C.J. in: Willardson , R.K. and Beer, A.C. [Eds.] – Semiconductors and Semimetals, Academic Press, New York, Ch. 4, 16 (1981).
3. Hankare, P. P., Bhuse, V.M., Garadkar, K.M. and Jadhav, A.D. – Mater. Chem. Phys., **71**, 9982 (2001).
4. Vankatasamy, V., Jayaraju, N., Cox, S.M., Thambidurai, C., Mathe, M. and Stickney, J. L. – J. Electroanal. Chem., **195,** 589 (2006).
5. Girgis, S.Y., Salem, A. M. and Selim, M. S. – J. Phys: Condens. Matter, **19**, 116213 (2007).
6. Higginson, K.A., Kuno, M., Bonevich, J., Qadri, S.B., Yousuf, M. and Mattoussi, H. – J. Phys. Chem. B., **106**, 39 (2002).
7. Wang, H. and Zhu, J.J. – Ultrason. Sonochem., **11**, 293 (2004).
8. Werner, A., Hochheimer , H. D., Strossner, K. and Jayaraman, A. – Phys. Rev. B., **28**, 3330 (1983).
9. Huang, T. and Ruoff, A. L. – J. Appl. Phys., **54**, 5459 (1983).
10. Huang, T. L. and Ruoff, A.L. – Phys. Rev. B., **31**, 5976 (1985).
11. Moon, C. Y. and Wei, S.H. – Phys. Rev. B.,**74**, 045205 (2006).
12. Madelung, O. [ed] – Semiconductors: Data Handbook 3rd edn [Berlin: Springer] (2003).

13. Chantis, A. N., Schilfgaarde, M.V. and Kutani, T. – Phys. Rev. Lett., **96**, 086405 (2006).
14. Gawlik, K-U, Kipp, L. and Skibowski, M. – Phys. Rev. Lett. , **78**, 16 (1997).
15. Fleszar, A. and Hanke, W. – Phys. Rev. B, **71**, 045207 (2005).
16. Sun, S. R. and Dong, Y.H. – Phys. Rev. B, 72, 174101 (2005); Phys. Rev. B, **73**, 113201 (2006).
17. Boutaiba, F., Zaoui, A. and Ferhat, M. – Superlattice Microstruct., **46**, 823 (2009).
18. Kumar, V., Shrivastava, A. K. and Jha, V. – J. Phys. Chem. Solids, **71**,1513 (2010).
19. Verma, A. S., Singh, R.K. and Rathi, S.K. – Physica B, **404**, 4051 (2009).
20. Cardona , M.R., Kremer, K., Lauck, R., Siegle, G., Muñoz, A. and Romero, A. H. – Phys. Rev. B, **80**, 195204 (2009).
21. Radescu, S., Mujica, A. and Needs, R. J. – Phys. Rev. B, **80**, 144110 (2009).
22. Wei, S.H. and Zunger, A. – Phys. Rev. B, **37**, 8958 (1988).
23. Chen, X., Mintz, A., Hu, J., Hua, X. and Zinck, J. – J. Vac. Sci. Technol. B, **13**, 4 (1995).
24. Deligoz, E., Colakoglu, K. and Ciftci, Y. – Physica B, **373**, 124 (2006).
25. Carrier, P. and Wei, S.H. – Phys. Rev. B, **70**, 035212 (2004).
26. Madelung, O. [Ed.] – Landolt Börnstein: Numerical Data and functional Relationships in Science and Technology, Springer, Berlin, 17b (1982).
27. Strehlow, W. H. and Cook, E.L. – J. Phys. Chem., **2**, 163 (1973).
28. Madelung, O., [Ed.] – Semiconductors: Basic Data, 2nd ed, Springer, Berlin, (1996).
29. Burstein, E., Brodsky, H. and Lucousky, G. – Int. J. Quantum Chem., **1**, 756 (1967).
30 Saini, P. K., Singh, D. and Ahlawat, D. S.– Chalcogenide Letters, **11**, No. 9, 405 (2014).
31. Singh, D., Saini, P. K. and Ahlawat, D. S. – International Journal of Computing Science and Communication Technologies, **6**, No. 1, 904 (2013).
32. Koelling, D. D., Harmon, B. N.– J. Phys. C: Solid State Phys., **10**, 3107 (1977**)**.
33. Schwarz, K., Blaha, P. and Madsen, G.K.H. – Comput. Phys. Commun., **147**, 71 (2002**)**.
34. Madsen, G.K.H., Blaha, P., Schwarz, K., Sjöstedt, E. and Nordström, L.– Phys. Rev. B, **64**,195134 (2001).
35. Hohenberg, P. and Kohn, W. – Phys. Rev., **136,** 864 **(**1964); Kohn , W. and Sham, L.J. – Phys. Rev., **140**, A1133 (1965).
36. Blaha, P., Schwarz, K., Madsen, G.K.H., Kvasnicka, D. and Luitz, J. – WIEN2k, An Augmented Plane Wave + Local Orbitals Program for Calculating Crystal Properties, Vienna University of Technology, Vienna, Austria, (2001).
37. Perdew, J. P., Chevary, J. A., Vosko, S. H., Jackson, K. A., Pederson, M. R., Singh, D. J. and Fiolhais, C. – Phys. Rev. B, **46**, 6671-6687 (1992).

38. Peterson, M., Wanger, F., Hufnagel, L., Scheffler, M., Blaha, P. and Schwarz, K.– Computer Physics Communications, **126**, 294-309 (2000).
39. Engel, E. and Vosko, S.H. – Phys. Rev., **47**, 13164 (1993).
40. Tell, J. S. – Phys. Rev., **104**, 1760 (1956).
41. Kramers, H.A. – Collected Sciences Papers, North Holland, Amsterdam, pp. 333 (1956**)**.
42. Landau, L.D. and Lifshitz, E.M. – Electrodynamics in Continous Media, Pergamon Press, Oxford, (1960).
43. De, R. and Kron, L. – J. Opt. Soc. Am., **12**, 547 (1926).
44. Yu, Y. P. and Cardona, M. – "Fundamentals of Semiconductors: Physics and Materials Properties" 2^{nd} edn. [Berlin: Springer], 241, (1999**)**.
45. Fox, M. – Optical Properties of Solids [New York: Oxford University Press], **6** (2001).
46. Wooten, F. – Optical properties of solids, Academic Press, New York, (1972).
47. Draxl, C. A. and Abt, R. – ICTP lecture notes, unpublished (1998).
48 Fang, R.C. – Solid Spectroscopy. Chinese Science Technology University Press, Hefei, (2003).
49. Zhang, Y. and Shen, W.M. – Basic of Solid Electronics. Zhe Jiang University Press, Hangzhou, (2005).
50. Anderson, O. L.– J. Phys. Chem. Solids, **24**, 909 (1963).

INDIAN JOURNAL OF THEORETICAL PHYSICS, VOL. 64, NOS. 3 & 4, 2016

Natural convection in MHD flow past a uniformly moving vertical plate with variable suction in a slip flow regime in presence of thermal radiation

K. Choudhury and N. Ahmed

Department of Mathematics, Gauhati University,
Guwahati-781014, Assam
E-mail : kangkan22@gmail.com
E-mail : saheel_nazib@yahoo.com

(Received for publication in July, 2016)

[**Abstract :** The present paper deals with the analysis of unsteady *MHD* free convective flow past a moving vertical plate with variable suction in the presence of radiation in a slip flow regime. Slip flow conditions for the velocity, jump in temperature as well as concentration are taken into account in the boundary conditions. The dimensionless governing equations are solved analytically by using perturbation technique. The effects of various parameters on the velocity, temperature, concentration fields as well as the coefficient of skin friction, Nusselt number and the Sherwood number are presented graphically.]

Keywords : Heat and mass transfer; natural convection; slip flow; Nusselt number; Sherwood number; chemical reaction.

Nomenclature

B_0 – strength of the applied magnetic field,
$\vec{B}$ – magnetic induction vector,
C^* – species concentration,
C_∞^* – species concentration in free stream,
C_w^* – species concentration at the plate,
C_p – specific heat at constant pressure,
D_M – mass diffusion coefficient,
$\vec{E}$ – electric field,
Gr – Grashof number for heat transfer,

Gm – Grashof number for mass transfer,
g – acceleration due to gravity,
h_1 – slip parameter due to velocity,
h_2 – slip parameter due to jump in temperature,
h_3 – slip parameter due to jump in concentration,
$\vec{J}$ – current density,
K^* – rate of first order chemical reaction,
K – chemical reaction parameter,
k^* – permeability of porous medium,
k – permeability parameter,
K_T – thermal diffusion ratio,
M – magnetic parameter,
Nu – Nusselt number,
Pr – Prandtl number,
Q – heat sink parameter,
Q^* – heat sink,
R – Radiation parameter,
Sr – Soret number,
Sh – Sherwood number,
T^* – fluid temperature,
T_∞^* – temperature at the free stream,
T_w^* – temperature at the plate,
T_M – mean fluid temperature,
u_w – velocity ratio parameter,
t – dimensionless time,
μ – coefficient of viscosity,
κ – thermal conductivity,
υ – kinematic viscosity,
σ – electrical conductivity,
ρ – fluid density,
θ – dimensionless temperature,
ϕ – dimensionless concentration,
β – coefficient of volume expansion for heat transfer,
β^* – coefficient of volume expansion for mass transfer.

1. Introduction

In the present years, the natural convective flow of heat and mass transfer problems in thepresence of magnetic field through a porous medium have attracted the attention of a numberof research scholars because of their possible application in many branches of science and technology such as fibre and granular insulation, a geothermal system etc. In Engineering Sciences, *MHD* finds its many applications in *MHD* pumps, *MHD* bearing, *MHD* power generators etc. Free convection flow of magneto polar fluid through porous medium in slip flow regime with mass transfer was studied by Rajput, et. al.[4]. Rajesh Johari, et. al.[5] analyzed unsteady *MHD* flow through porous medium and heat transfer past a porous vertical moving plate with heat source. Devi and Raj[6] investigated the effects of thermo-diffusion on unsteady hydromagnetic free convection flow of a viscous, incompressible, electrically conducting fluid with heat and mass transfer past a moving porous vertical plate of infinite length with time dependent suction in the presence of heat source in slip flow regime. Ahmed and Das[10] studied *MHD* mass transfer flow past a vertical porous plate in porous medium in a slip flow regime with radiation and chemical reaction. Balamurugan, et. al.[11] investigated unsteady *MHD* free convective flow past a vertical plate with time dependent suction and chemical reaction in a slip flow regime. Prakash, et. al.[7] have made a systematic investigation of fluid flow with chemical reaction on unsteady *MHD* mixed convective flow over a moving vertical porous plate.

The Soret effect arises when the mass fluxs contains a term that depends on the temperature gradient. Many investigators have carried out model studies on the Soret effect in different heat and mass transfer related problems, some of them are Bhavana, et. al.[9], Ahmed and Bhattacharyya[12].

Radiative heat and mass transfer play an important role in manufacturing industries for the design of fins, steel rolling, nuclear power plants, gas turbines and various propulsion device for aircraft, missiles, satellites and space vehicles are examples of such Engineering applications. The effect of radiation on *MHD* free convective heat and mass transfer flow

becomes more industrially important. Radiation effect on the natural convective flow of a gas past a semi-infinite plate was studied by Soundalgekar and Takhar[1]. Raju, et. al.[8] investigated the combined effect of heat and mass transfer on a free convective flow through a porous medium bounded by a vertical surface with radiation. Radiation effect on free convective flow over a porous vertical plate was studied by Hossain, et. al.[2]. The heat transfer in a porous medium with high porosity in the presence of radiation was analyzed by Raptis[3].

The main objective of the present investigation is to study the problem of an unsteady *MHD* free convective flow past a uniformly vertical porous plate with variable suction in a slip flow regime in presence of thermal radiation. Slip flow conditions for the velocity, jump in temperature as well as concentration are taken into account in the boundary conditions.

2. Basic equations

The equations governing the flow of a viscous incompressible and electrically conducting fluid in the presence of magnetic field are :

Equation of continuity :

$$\vec{\nabla}.\vec{q}=0 \qquad \ldots \quad (1)$$

Momentum equation :

$$\rho\left[\frac{\partial\vec{q}}{\partial t^*}+(\vec{q}.\vec{\nabla})\vec{q}\right]=-\vec{\nabla}p+\vec{J}\times\vec{B}+\rho\vec{g}+\mu\nabla^2\vec{q}-\frac{\mu}{k^*}\vec{q} \qquad \ldots \quad (2)$$

Ohm's law :

$$\vec{J}=\sigma\left[\vec{E}+\left(\vec{q}\times\vec{B}\right)\right] \qquad \ldots \quad (3)$$

Gauss' law of magnetism :

$$\vec{\nabla}.\vec{B}=0 \qquad \ldots \quad (4)$$

Energy equation :

$$\rho C_p\left[\frac{\partial T^*}{\partial t^*}+\left(\vec{q}.\vec{\nabla}\right)T^*\right]=\kappa\nabla^2T^*+Q^*\left(T^*-T_\infty^*\right)+\varphi-\vec{\nabla}.\vec{q_r} \qquad \ldots \quad (5)$$

Species continuity equation :

$$\frac{\partial C^*}{\partial t^*} + \left(\vec{q}.\vec{\nabla}\right)C^* = D_M \nabla^2 C^* + K^*(C^*_\infty - C^*) + \frac{D_M K_T}{T_M}\nabla^2 T^* \qquad \ldots \quad (6)$$

All the physical quantities are defined in the nomenclature.

3. Mathematical analysis

Let us consider a flow of an incompressible viscous electrically conducting fluid past aninfinite vertical porous plate. We introduce a Cartesian coordinate system (x^*, y^*, z^*) with X-axis along the infinite vertical plate, Y-axis normal to the plate and Z-axis along the width of the plate. Initially the plate and the fluid were at same temperature T^*_∞ with concentration level C^*_∞ at all points. At time $t^* > 0$ the plate temperature is suddenly raised to T^*_w and the concentration level at the plate raised to C^*_w. A uniform magnetic field is applied normal to the plate. Due to semi-infinite plane surface assumptions, all the flow variables except pressure are functions of y^* and t^* only.

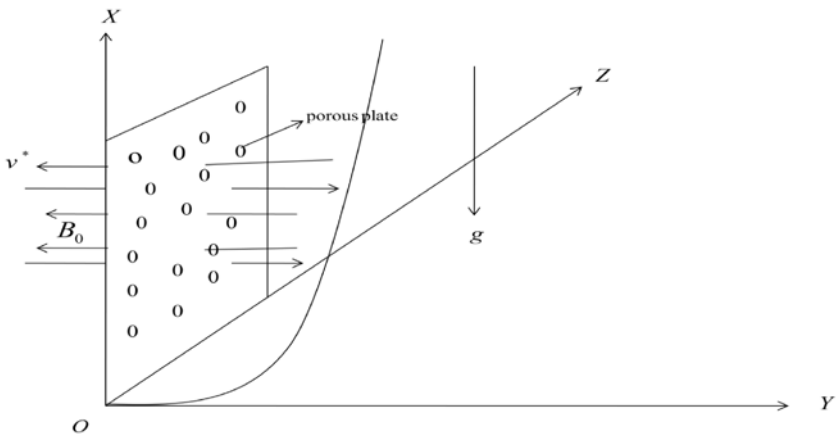

Flow configuration of the problem.

Our investigation is restricted to the following assumptions :

(*i*) All the fluid properties are considered constants except the influence of thevariation in density in the buoyancy force term.

(*ii*) Viscous dissipation and Ohmic dissipatrion of energy are negligible.

(*iii*) Magnetic Reynolds number is assumed to be small enough to neglect the induced magnetic field.

(*iv*) Induced electric field is neglected.

(*v*) Slip flow regime is considered.

The governing equations of motion are :

Equation of continuity :

$$\frac{\partial v^*}{\partial y^*} = 0 \qquad \ldots \quad (7)$$

Momentum equation :

$$\frac{\partial u^*}{\partial t^*} + v^* \frac{\partial u^*}{\partial y^*} = \frac{dU_\infty^*}{dt^*} - \frac{\sigma B_0^2}{\rho}\left(u^* - U_\infty^*\right) + \upsilon \frac{\partial^2 u^*}{\partial y^{*2}} + g\beta\left(T^* - T_\infty^*\right)$$

$$+ g\beta^*\left(C^* - C_\infty^*\right) - \frac{\upsilon}{k^*}\left(u^* - U_\infty^*\right) \qquad \cdots \quad (8)$$

Energy equation :

$$\rho C_p\left(\frac{\partial T^*}{\partial t^*} + v^* \frac{\partial T^*}{\partial y^*}\right) = \kappa \frac{\partial^2 T^*}{\partial y^{*2}} - \frac{\partial q_r^*}{\partial y^*} + Q^*\left(T^* - T_\infty^*\right) \qquad \ldots \quad (9)$$

Species continuity equation :

$$\frac{\partial C^*}{\partial t^*} + v^* \frac{\partial C^*}{\partial y^*} = D_M \frac{\partial^2 C^*}{\partial y^{*2}} + D_T \frac{\partial^2 T^*}{\partial y^{*2}} - K^*\left(C^* - C_\infty^*\right) \qquad \ldots \quad (10)$$

The slip flow boundary conditions are given by

$$\left.\begin{aligned} &u^* = u_w^* + h_1^* \frac{\partial u^*}{\partial y^*}; T^* = T_w^* + h_2^* \frac{\partial T^*}{\partial y^*}; C^* = C_w^* + h_3^* \frac{\partial C^*}{\partial y^*} \text{ at } y^* = 0 \\ &u^* \to U_\infty^* = U_0\left(1 + \varepsilon e^{\delta^* t^*}\right); T^* \to T_\infty^*; C^* \to C_\infty^* \text{ as } y^* \to \infty \end{aligned}\right\} \qquad \ldots \quad (11)$$

where ε and δ^* are scalar constants which are less than unity and $\varepsilon << 1$.

The plate is subjected to a variable suction and to satisfy the equation of continuity, v^* is chosen as follows:

$$v^* = -V_0\left(1+\varepsilon\alpha e^{\delta^* t^*}\right) \quad \ldots (12)$$

where α is a real positive constant, ε and $\varepsilon\alpha$ are small less than unity, V_0 is the scale of the suction velocity which has a non-zero positive constant.

The radiative heat flux term by using the Rosel and approximation is given by

$$q_r^* = \frac{4\sigma^*}{3k_1^*}\frac{\partial T^{*4}}{\partial y^*} \quad \ldots (13)$$

where σ^* and k_1^* are respectively the Stefan-Boltzmann constant and the mean absorption coefficient. We assume that the temperature difference within the flow are sufficiently small such that T^{*4} may be expressed as a linear function of the temperature. This is accomplished by expanding in a Taylor series about T_∞^* and neglecting higher order terms, thus

$$T^{*4} \cong 4T_\infty^{*3} - 3T_\infty^{*4} \quad \ldots (14)$$

For the sake of normalisation of the mathematical model of the physical problem, thefollowing non-dimensional quantities are defined:

$$u = \frac{u^*}{U_0}, v = \frac{v^*}{V_0}, t = \frac{t^* V_0^2}{\upsilon}, y = \frac{V_0 y^*}{\upsilon}, \delta = \frac{\delta^* \upsilon}{V_0^2}, u_w = \frac{u_w^*}{U_0},$$

$$U = \frac{U_\infty^*}{U_0},\ \theta = \frac{T^* - T_\infty^*}{T_w^* - T_\infty^*}, \phi = \frac{C^* - C_\infty^*}{C_w^* - C_\infty^*},\ k = \frac{k^* V_0^2}{\upsilon^2}, Pr = \frac{\mu C_p}{\kappa},$$

$$M = \frac{\sigma B_0^2 \upsilon}{\rho V_0^2} Gr = \frac{\upsilon g\beta\left(T_w^* - T_\infty^*\right)}{U_0 V_0^2}, Gm = \frac{\upsilon g\beta^*\left(C_w^* - C_\infty^*\right)}{U_0 V_0^2},$$

$$Sc = \frac{\upsilon}{D_M}, K = \frac{\upsilon K^*}{V_0^2}, Sr = \frac{D_M K_T\left(T_w^* - T_\infty^*\right)}{\upsilon T_M\left(C_w^* - C_\infty^*\right)}, Q = \frac{Q^*\upsilon^2}{\kappa V_0^2}, R = \frac{4\sigma^* T_\infty^{*3}}{k_1^*\kappa}.$$

The non-dimensional form of the equations (8)-(10) are :

$$\frac{\partial u}{\partial t}-\left(1+\varepsilon\alpha e^{\delta t}\right)\frac{\partial u}{\partial y}=\frac{dU}{dt}+\frac{\partial^2 u}{\partial y^2}+Gr\theta+Gm\phi-M\left(u-U\right)-\frac{\left(u-U\right)}{k} \quad \ldots(15)$$

$$\frac{\partial \theta}{\partial t}-\left(1+\varepsilon\alpha e^{\delta t}\right)\frac{\partial \theta}{\partial y}=\left(1-\frac{4R}{3}\right)\frac{1}{Pr}\frac{\partial^2 \theta}{\partial y^2}+\frac{Q}{Pr}\theta \quad \ldots \quad (16)$$

$$\frac{\partial \phi}{\partial t}-\left(1+\varepsilon\alpha e^{\delta t}\right)\frac{\partial \phi}{\partial y}=\frac{1}{Sc}\frac{\partial^2 \phi}{\partial y^2}+Sr\frac{\partial^2 \theta}{\partial y^2}-K\phi \quad \ldots \quad (17)$$

The corresponding boundary conditions are :

$$\left.\begin{aligned} &u=u_w+h_1\frac{\partial u}{\partial y},\theta=1+h_2\frac{\partial \theta}{\partial y},\phi=1+h_3\frac{\partial \phi}{\partial y} \text{ at } y=0\\ &u\to U(t)=1+\varepsilon e^{\delta t},\theta\to 0,\phi\to 0 \text{ as } y\to\infty \end{aligned}\right\} \quad \ldots \quad (18)$$

4. Method of solution

In order to solve the non-linear partial differential equations (15)-(17) subject to the condition (18), the expressions for the velocity, temperature and concentration are assumed to be of the asymptotic form :

$$\left.\begin{aligned} u&=u_0(y)+\varepsilon e^{\delta t}u_1(y)+O(\varepsilon^2)\\ \theta&=\theta_0(y)+\varepsilon e^{\delta t}\theta_1(y)+O(\varepsilon^2)\\ \phi&=\phi_0(y)+\varepsilon e^{\delta t}\phi_1(y)+O(\varepsilon^2) \end{aligned}\right\} \quad \ldots \quad (19)$$

On substituting of (19) in equations (15)-(17), the following ordinary linear differential equations are obtained

$$u_0''+u_0'-\left(M+\frac{1}{k}\right)u_0=-Gr\theta_0-Gm\phi_0-\left(M+\frac{1}{k}\right) \quad \ldots \quad (20)$$

$$u_1''+u_1'-\left(M+\delta+\frac{1}{k}\right)u_1=-Gr\theta_1-Gm\phi_1-\alpha u_0'-\left(M+\delta+\frac{1}{k}\right) \quad \ldots \quad (21)$$

$$\theta_0''+a_1\theta_0'+a_2\theta_0=0 \quad \ldots \quad (22)$$

$$\theta_1''+a_1\theta_1'+a_3\theta_1=-\alpha a_1\theta_0' \quad \ldots \quad (23)$$

$$\phi_0'' + Sc\phi_0' - ScK\phi_0 = -ScSr\theta_0'' \quad \ldots \quad (24)$$

$$\phi_1'' + Sc\phi_1' - Sc(K+\delta)\phi_1 = -\alpha Sc\phi_0' - ScSr\theta_1'' \quad \ldots \quad (25)$$

Subject to the boundary conditions

$$u_0 = u_w + h_1\frac{\partial u_0}{\partial y}, u_1 = h_1\frac{\partial u_1}{\partial y}, \theta_0 = 1 + h_2\frac{\partial \theta_0}{\partial y}, \theta_1 = h_2\frac{\partial \theta_1}{\partial y},$$

$$\phi_0 = 1 + h_3\frac{\partial \phi_0}{\partial y}, \phi_1 = h_3\frac{\partial \phi_1}{\partial y} \text{ at } y = 0$$

$$u_0 \to 0, u_1 \to 1, \theta_0 \to 0, \theta_1 \to 0, \phi_0 \to 0, \phi_1 \to 0 \quad \text{as} \quad y \to \infty \quad \ldots \quad (26)$$

The equations (20)-(25) are solved in sequence subject to the condition (26) and the solutions are given by

$$\theta_0 = A_1 e^{-m_1 y} \quad \ldots \quad (27)$$

$$\theta_1 = A_2 e^{-m_1 y} - A_2 A_3 e^{-m_2 y} \quad \ldots \quad (28)$$

$$\phi_0 = -A_4 e^{-m_1 y} + A_5 e^{-m_3 y} \quad \ldots \quad (29)$$

$$\phi_1 = A_6 e^{-m_3 y} - (A_7 + A_8) e^{-m_1 y} + A_9 e^{-m_2 y} + A_{10} e^{-m_4 y} \quad \ldots \quad (30)$$

$$u_0 = 1 + A_{11} e^{-m_1 y} - A_{12} e^{-m_3 y} + A_{13} e^{-m_5 y} \quad \ldots \quad (31)$$

$$u_1 = 1 + A_{14} e^{-m_1 y} + A_{15} e^{-m_2 y} - A_{16} e^{-m_3 y} - A_{17} e^{-m_4 y} + A_{18} e^{-m_5 y} + A_{19} e^{-m_6 y} \quad \ldots \quad (32)$$

Substituting equations (27)-(32) in equation (19), we obtain the expressions for the velocity, temperature and concentration fields in the boundary layer as follows :

$$u(y,t) = 1 + A_{11} e^{-m_1 y} - A_{12} e^{-m_3 y} + A_{13} e^{-m_5 y} + \varepsilon e^{\delta t}\left(1 + A_{14} e^{-m_1 y} + A_{15} e^{-m_2 y} - A_{16} e^{-m_3 y} - A_{17} e^{-m_4 y} + A_{18} e^{-m_5 y} + A_{19} e^{-m_6 y}\right) \quad \ldots \quad (33)$$

$$\theta(y,t) = A_1 e^{-m_1 y} + \varepsilon e^{\delta t}\left(A_2 e^{-m_1 y} - A_2 A_3 e^{-m_2 y}\right) \quad \ldots \quad (34)$$

$$\phi(y,t) = -A_4 e^{-m_1 y} + A_5 e^{-m_3 y} + \varepsilon e^{\delta t}\left(A_6 e^{-m_3 y} - (A_7 + A_8) e^{-m_1 y} + A_9 e^{-m_2 y} + A_{10} e^{-m_4 y}\right) \quad (35)$$

where

$$a_1 = \frac{Pr}{1-\frac{4R}{3}}, a_2 = \frac{Q}{1-\frac{4R}{3}}, a_3 = \frac{Q-\delta Pr}{1-\frac{4R}{3}}, \xi = M + \frac{1}{k},$$

$$m_1 = \frac{a_1 + \sqrt{a_1^2 - 4a_2}}{2}, m_2 = \frac{a_1 + \sqrt{a_1^2 - 4a_3}}{2}, \; m_3 = \frac{Sc + \sqrt{Sc^2 + 4ScK}}{2},$$

$$, m_4 = \frac{Sc + \sqrt{Sc^2 + 4Sc\left(K+\delta\right)}}{2}, m_5 = \frac{1+\sqrt{1+4\xi}}{2}, m_6 = \frac{1+\sqrt{1+4\left(\xi+\delta\right)}}{2},$$

$$A_1 = \frac{1}{1+h_2 m_1}, A_2 = \frac{\alpha a_1 m_1 A_1}{m_1^2 - a_1 m_1 + a_3}, A_3 = \frac{1+h_2 m_1}{1+h_2 m_2}, A_4 = \frac{ScSrm_1^2 A_1}{m_1^2 - Scm_1 - ScK},$$

$$A_5 = \frac{1+A_4\left(1+h_3 m_1\right)}{1+h_3 m_3}, \; A_6 = \frac{\alpha Scm_3 A_5}{m_3^2 - Scm_3 - Sc\left(K+\delta\right)},$$

$$A_7 = \frac{\alpha Scm_1 A_4}{m_1^2 - Scm_1 - Sc\left(K+\delta\right)}, A_8 = \frac{SrScm_1^2 A_2}{m_1^2 - Scm_1 - Sc\left(K+\delta\right)},$$

$$A_9 = \frac{SrScm_2^2 A_2 A_3}{m_2^2 - Scm_2 - Sc\left(K+\delta\right)},$$

$$A_{10} = \frac{-\left(1+h_3 m_3\right)A_6 + \left(1+h_3 m_1\right)\left(A_7 + A_8\right) - \left(1+h_3 m_2\right)A_9}{1+h_3 m_4},$$

$$A_{11} = \frac{GmA_4 - GrA_1}{m_1^2 - m_1 - \xi}, A_{12} = \frac{GmA_5}{m_3^2 - m_3 - \xi},$$

$$A_{13} = \frac{u_w - \left(1+h_1 m_1\right)A_{11} + \left(1+h_1 m_3\right)A_{12} - 1}{1+h_1 m_5},$$

$$A_{14} = \frac{Gm\left(A_7 + A_8\right) - GrA_2 + \alpha m_1 A_{11}}{m_1^2 - m_1 - \left(\xi+\delta\right)}, A_{15} = \frac{GrA_2 A_3 - GmA_9}{m_2^2 - m_2 - \left(\xi+\delta\right)},$$

$$A_{16} = \frac{GmA_6 + \alpha m_3 A_{12}}{m_3^2 - m_3 - \left(\xi+\delta\right)}, A_{17} = \frac{GmA_{10}}{m_4^2 - m_4 - \left(\xi+\delta\right)}, A_{18} = \frac{\alpha m_5 A_{13}}{m_5^2 - m_5 - \left(\xi+\delta\right)},$$

$$A_{19} = \frac{-\left(1+h_1 m_1\right)A_{14} - \left(1+h_1 m_2\right)A_{15} + \left(1+h_1 m_3\right)A_{16} + \left(1+h_1 m_4\right)A_{17} - \left(1+h_1 m_5\right)A_{18} - 1}{1+h_1 m_6}$$

5. Skin-friction

The non-dimensional skin-friction at the plate is given by

$$\tau = \left[\frac{\partial u}{\partial y}\right]_{y=0} \quad \ldots \quad (36)$$

$$= \left(-m_1 A_{11} + m_3 A_{12} - m_5 A_{13}\right) + \varepsilon e^{\delta t}\left(-m_1 A_{14} - m_2 A_{15} + m_3 A_{16} + m_4 A_{17} - m_5 A_{18} - m_6 A_{19}\right)$$

6. Rate of heat transfer

The rate of heat transfer in terms of Nusselt number at the plate is given by

$$Nu = -\left[\frac{\partial \theta}{\partial y}\right]_{y=0} \quad \ldots \quad (37)$$

$$= m_1 A_1 - \varepsilon e^{\delta t}\left(-m_1 A_2 + m_2 A_2 A_3\right)$$

7. Rate of mass transfer

The rate of mass transfer in terms of Sherwood number at the plate is given by

$$Sh = -\left[\frac{\partial \phi}{\partial y}\right]_{y=0}$$

$$= -m_1 A_4 + m_3 A_5 + \varepsilon e^{\delta t}\left(m_3 A_6 - m_1\left(A_7 + A_8\right) + m_2 A_9 + m_4 A_{10}\right) \quad \ldots (38)$$

8. Results and discussion

In order to get the physical insight of the problem, we have carried out numerical calculations for non-dimensional velocity field, temperature field, concentration field, coefficient of skin-friction at the plate, the rate of heat transfer and the rate of mass transfer at the plate for different values of the physical parameters involved and these are demonstrated in graphs. The value of Prandtl number *Pr* is chosen to be 0.71 which corresponds to air and the value of Schmidt number *Sc* is taken to be 0.22 which corresponds to 2*H* whereas the values of other parameters *viz*. thermal Grash of number *Gr*, solutal Grash of number *Gm*, magnetic parameter *M*, chemical reaction parameter *K*, Soret number *Sr* and heat source/sink parameter *Q* have been chosen arbitrarily.

Figures 1 - 8 exhibit the variation of the velocity distribution u versus normal coordinate y under the influence of magnetic parameter M, velocity ratio parameter u_w, chemical reaction parameter K, heat source/sink parameter Q, Soret number Sr, Radiation parameter R, thermal Grash of number Gr and solutal Grash of number Gm. Figure 1 shows that the fluid flow is retarded due to imposition of the transverse magnetic field. This phenomenon agrees with the physical fact that a magnetic field exerts a resistive body force known as the Lorentz force which retards the fluid motion. Figure 2 depicts that the flow is accelerated under the effect of velocity ratio parameter. Its influence is highly significant near the plate where as it remains uniform as it moves far away from the plate. The effect of chemical reaction parameter K is high lighted in figure 3. An increase of the chemical reaction leads to a decrease in the velocity field. In figure 4, the influence of the heat source/sink parameter Q on velocity has been depicted. It is observed that an increase in the values of Q leads to a fall in the velocity. The effect of Soret number Sr on the velocity distribution is shown in the figure 5. From this figure we see that velocity increases with increasing values of Sr for which we conclude that the fluid velocity rises due to greater thermal diffusion. Figure 6 illustrates the effect of radiation on the velocity. It is seen from this figure that there is asteady increase in fluid velocity due to radiation. The increase in this parameter leads to a increase in the boundary layer thickness and to reduce the heat transfer rate in presence of thermal bouyancy force. Figures 7 and 8 depict that thermal buoyancy force and solutalbuoyancy force causes the flow to accelerate to a good extent near the plate.

Figures 9-11 show that the change of behaviour of the temperature distribution due to variation of Pr, R and h_2. The effect of Prandtl number Pr on the temperature distribution is shown in figure 9. The temperature steadily increases with the increase in Prandtl number. It shows that an increase in Prandtl number results in a rise in the temperature distribution within boundary layer and temperature across the boundary layer becomes uniform. From figure 10 we observe that fluid temperature gets increased due to the effect of thermal radiation. The temperature of the flow field is decreased under the effect of slip parameter h_2 which reflected in figure 11.

Figures 12-15 demonstrate the variation of concentration field under the influence of the parameters *Sc*, *Sr*, h_3 and *R*. Figure 12 shows that the concentration level of the fluid is decreased for increasing Schmidt number. This is consistent with the fact that an increase in *Sc* means a decrease of molecular diffusivity which results in a fall in the thickness of the concentration boundary layer. It is seen from figure 13 that concentration level rises inpresence of thermal diffusion. It is noticed from figure 14 that there is a comprehensive fall in the concentration level of the fluid due to radiation which indicates a reduction in the thickness of the boundary layer. The impact of slip parameter due to jump in concentration is shown in figure 15. The concentration of the flow field is decreased with increase in slip parameter due to jump in concentration.

The effect of magnetic parameter *M*, chemical reaction parameter *K*, Soret number *Sr* and radiation parameter *R* on skin-friction is observed in figures 16-19. Figures 16 and 17 show that the coefficient of skin-friction is reduced under the application of transverse magnetic field and chemical reaction parameter whereas a reverse phenomenon is observed in figures 18 and 19 due to the effect of Soret number and radiation parameter. That is to say that the frictional resistance of the fluid at the plate falls comprehensively due to application of transverse magnetic field and chemical reaction.

Figures 20-21 display the variations in the rate of heat transfer due to Prandtl number *Pr* and radiation parameter *R*. It is seen that Prandtl number and radiation parameter reduce the rateof heat transfer from plate to the fluid.

The effects of Soret number *Sr*, radiation parameter *R* and Prandtl number *Pr* on the rate of mass transfer is demonstrated in figures 22-24. The rate of mass transfer falls under theeffect of thermal diffusion which is visualised in figure 22 whereas the rate is found to berising with the increase of radiation parameter and Prandtl number as observed in figures 23 and 24 respectively.

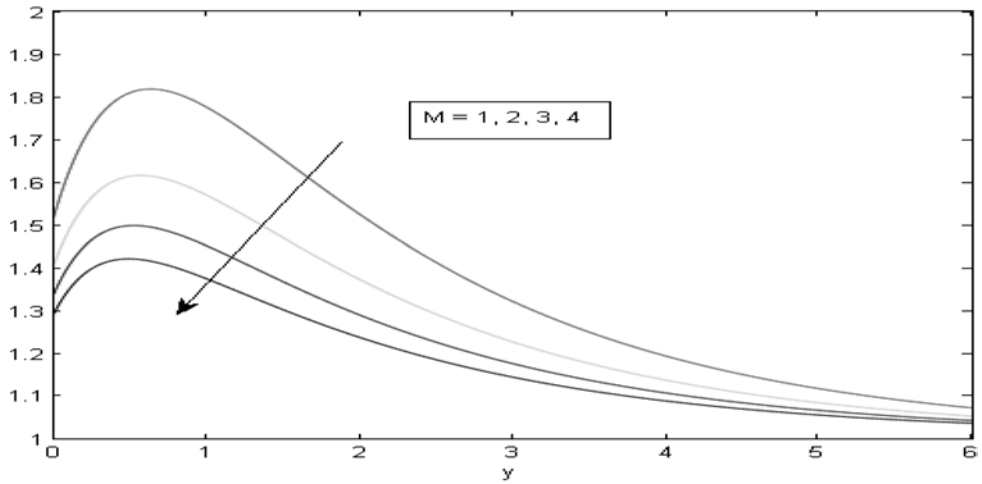

Figure 1

Velocity profile for variation in M when Q = 1; R =2; Sc =0.22; Sr =1; K =1; Gr =1; Gm =4; Pr =0.71; u_w =1; $\alpha = 1$; $\varepsilon = 0.01$; $\delta = 0.1$; t = 1; h_3 = 1; k = 1.

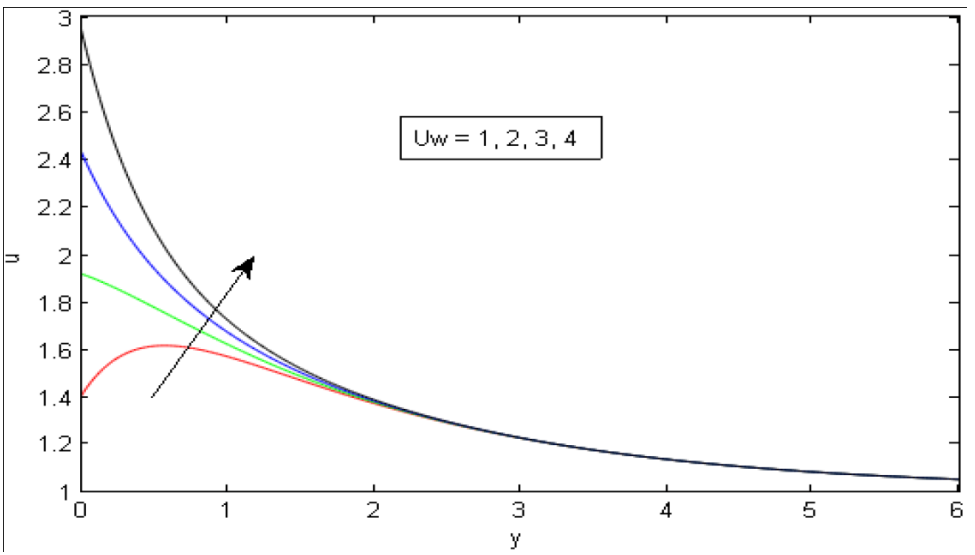

Figure 2

Velocity profile for variation in u_w when Q = 1; R = 2; Sc = 0.22; Sr = 1; K = 1; Gr = 1; Gm = 4; Pr = 0.71; M = 2; $\alpha = 1$; $\varepsilon = 0.01$; $\delta = 0.1$; t = 1; h_3 =1; k =1.

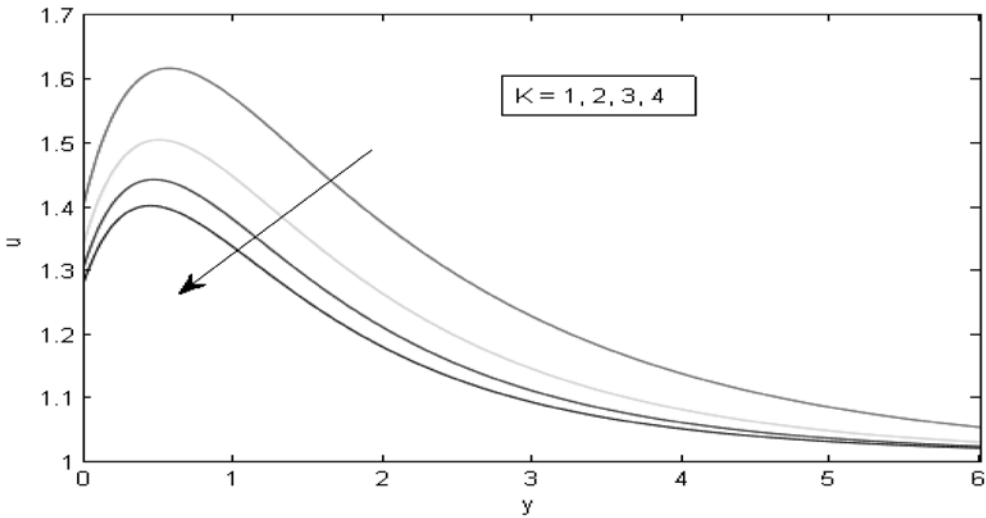

Figure 3

Velocity profile for variation in K when $Q = 1$; $R = 2$; $Sc = 0.22$; $Sr = 1$; $M = 2$; $Gr = 1$; $Gm = 4$; $Pr = 0.71$; $u_w = 1$; $\alpha = 1$; $\varepsilon = 0.01$; $\delta = 0.1$; $t = 1$; $h_3 = 1$; $k = 1$.

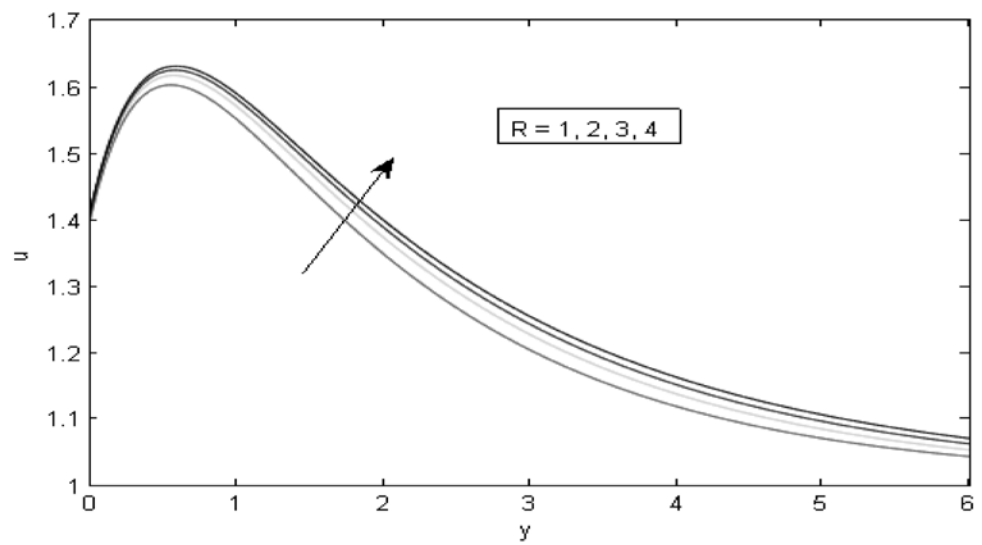

Figure 4

Velocity profile for variation in R when $Q = 1$; $M = 2$; $Sc = 0.22$; $Sr = 1$; $K = 1$; $Gr = 1$; $Gm = 4$; $Pr = 0.71$; $u_w = 1$; $\alpha = 1$; $\varepsilon = 0.01$; $\delta = 0.1$; $t = 1$; $h_3 = 1$; $k = 1$.

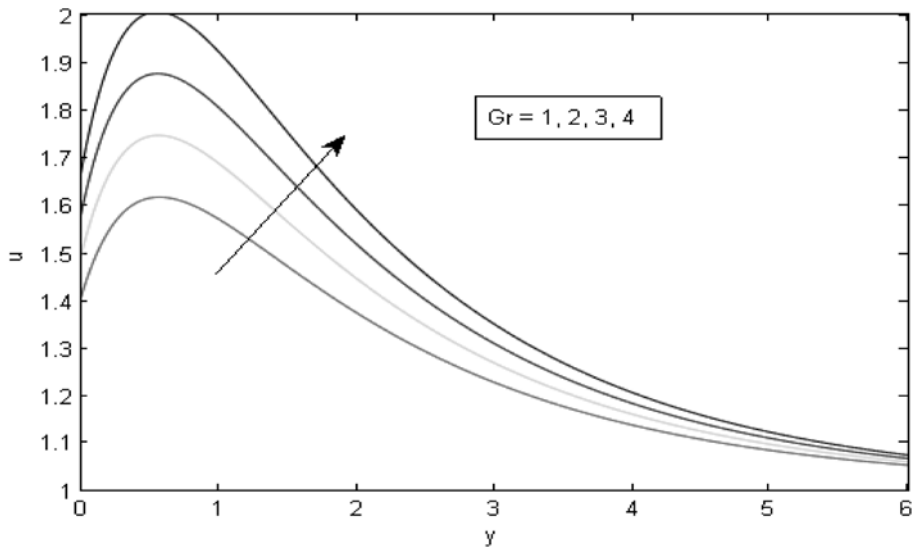

Figure 5

Velocity profile for variation in Gr when $Q = 1$; $R = 2$; $Sc = 0.22$; $Sr = 1$; $K = 1$; $M = 2$; $Gm = 4$; $Pr = 0.71$; $u_w = 1$; $\alpha = 1$; $\varepsilon = 0.01$; $\delta = 0.1$; $t = 1$; $h_3 = 1$; $k = 1$.

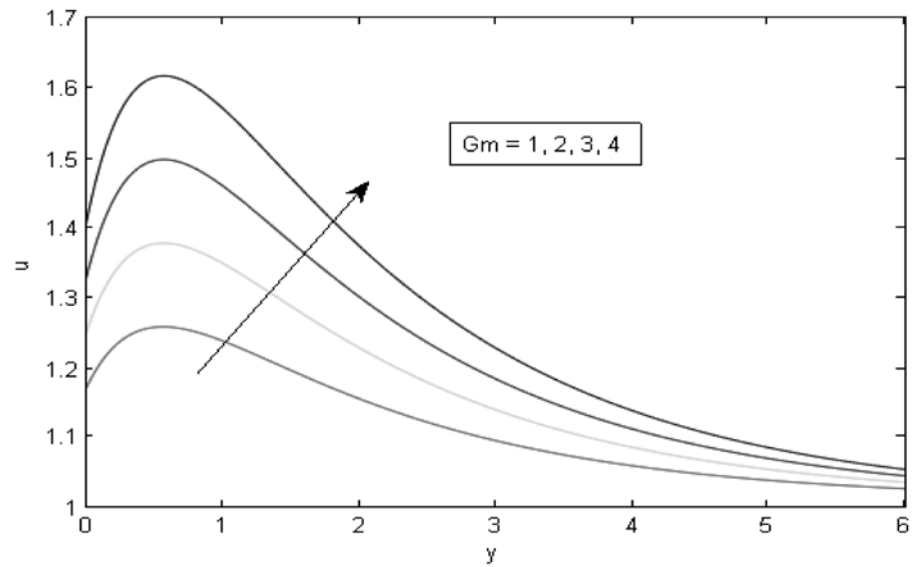

Figure 6

Velocity profile for variation in Gm when $Q = 1$; $R = 2$; $Sc = 0.22$; $Sr = 1$; $K = 1$; $Gr = 1$; $M = 2$; $Pr = 0.71$; $u_w = 1$; $\alpha = 1$; $\varepsilon = 0.01$; $\delta = 0.1$; $t = 1$; $h_3 = 1$; $k = 1$.

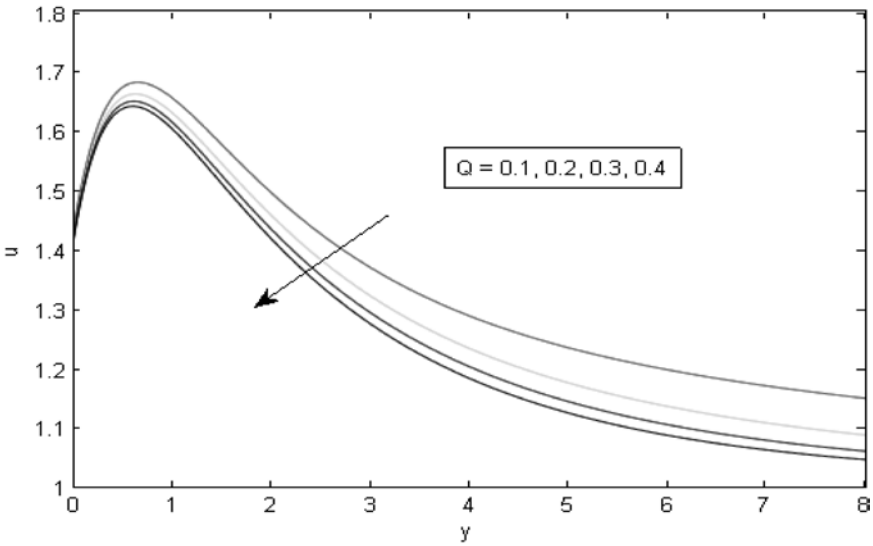

Figure 7

Velocity profile for variation in Q when $M = 2$; $R = 2$; $Sc = 0.22$; $Sr = 1$; $K = 1$; $Gr = 1$; $Gm = 4$; $Pr = 0.71$; $u_w = 1$; $\alpha = 1$; $\varepsilon = 0.01$; $\delta = 0.1$; $t = 1$; $h_3 = 1$; $k = 1$.

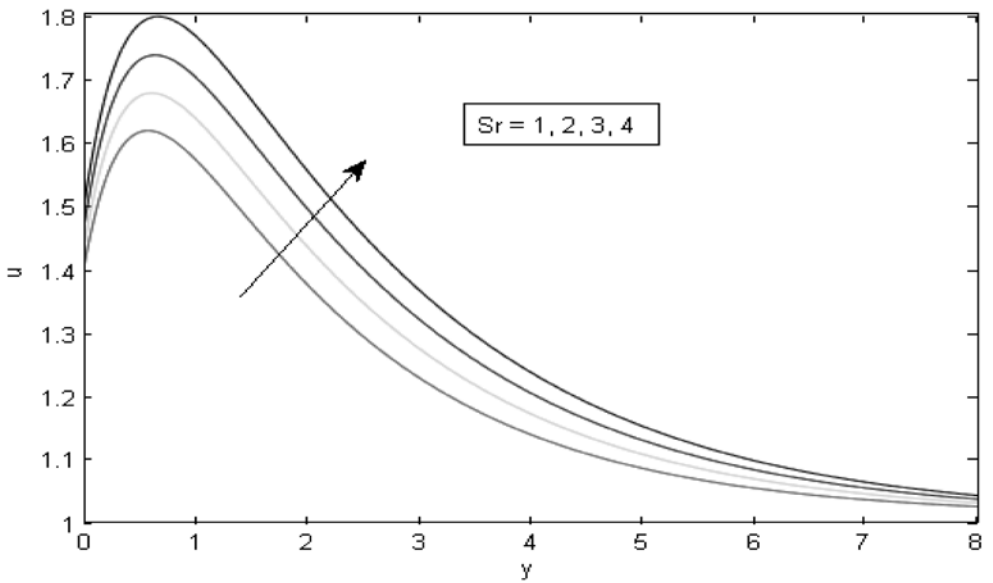

Figure 8

Velocity profile for variation in Sr when $Q = 1$; $R = 2$; $Sc = 0.22$; $M = 2$; $K = 1$; $Gr = 1$; $Gm = 4$; $Pr = 0.71$; $u_w = 1$; $\alpha = 1$; $\varepsilon = 0.01$; $\delta = 0.1$; $t = 1$; $h_3 = 1$; $k = 1$.

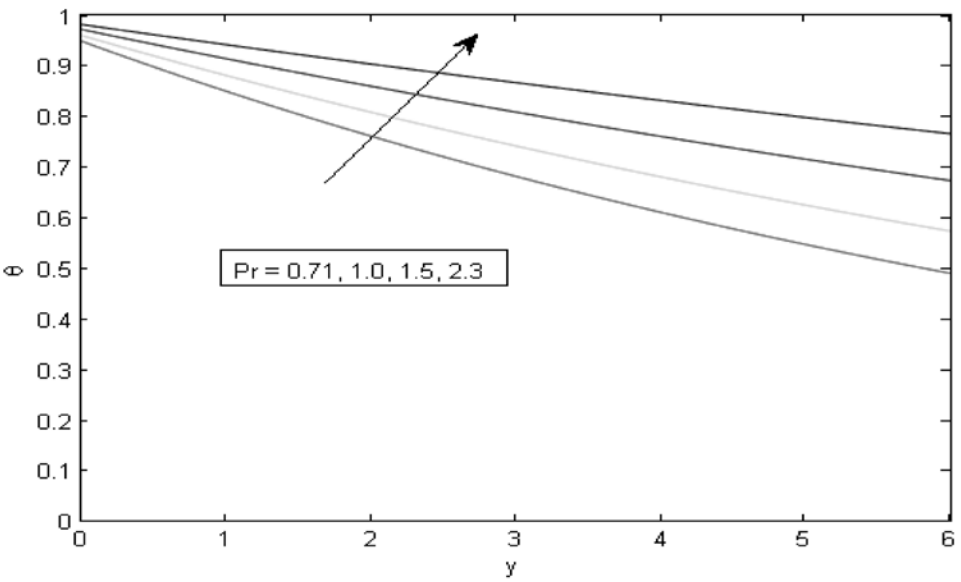

Figure 9
Temperature profile for variation in *Pr*.

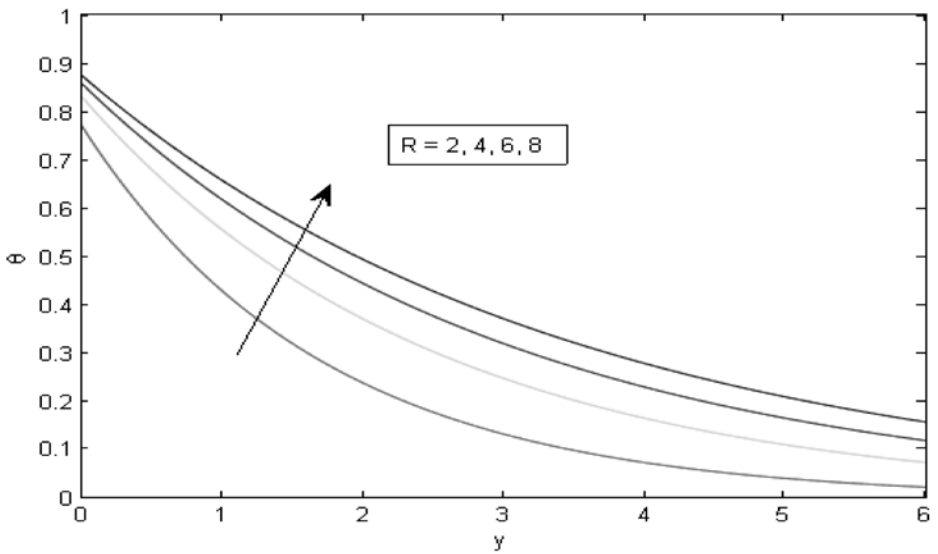

Figure 10
Temperature profile for variation in *R*.

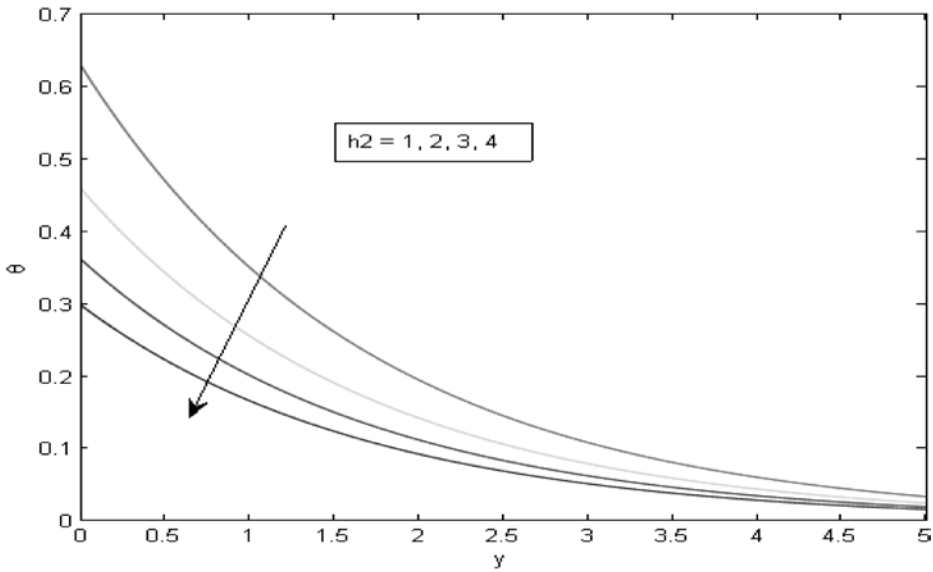

Figure 11
Temperature profile for variation in h_2.

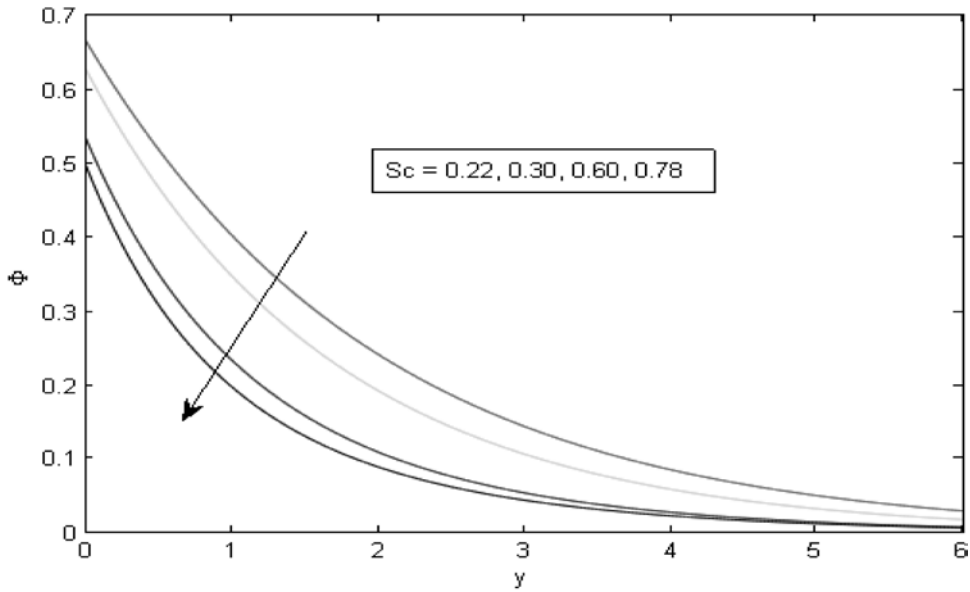

Figure 12
Concentration profile for variation in *Sc*.

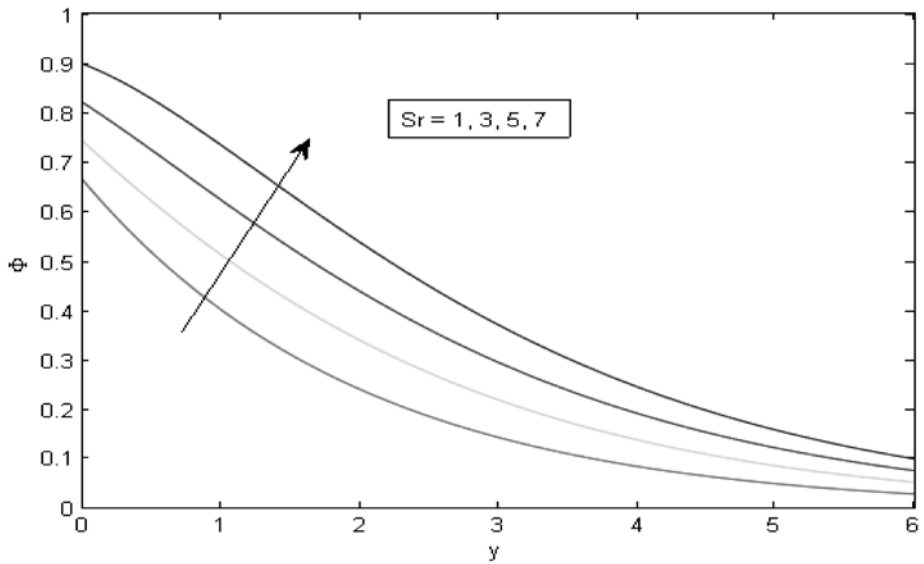

Figure 13
Concentration profile for variation in *Sr*.

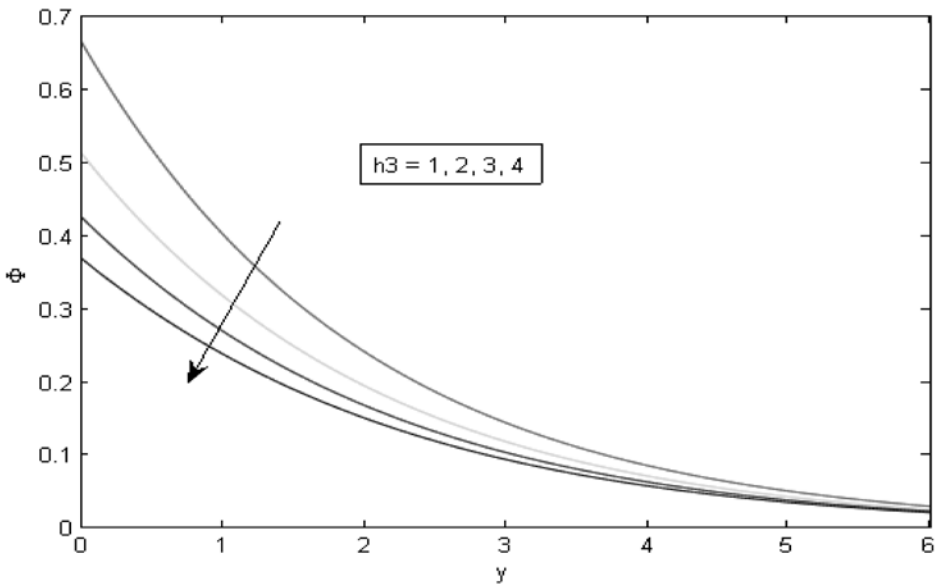

Figure 14
Concentration profile for variation in h_3.

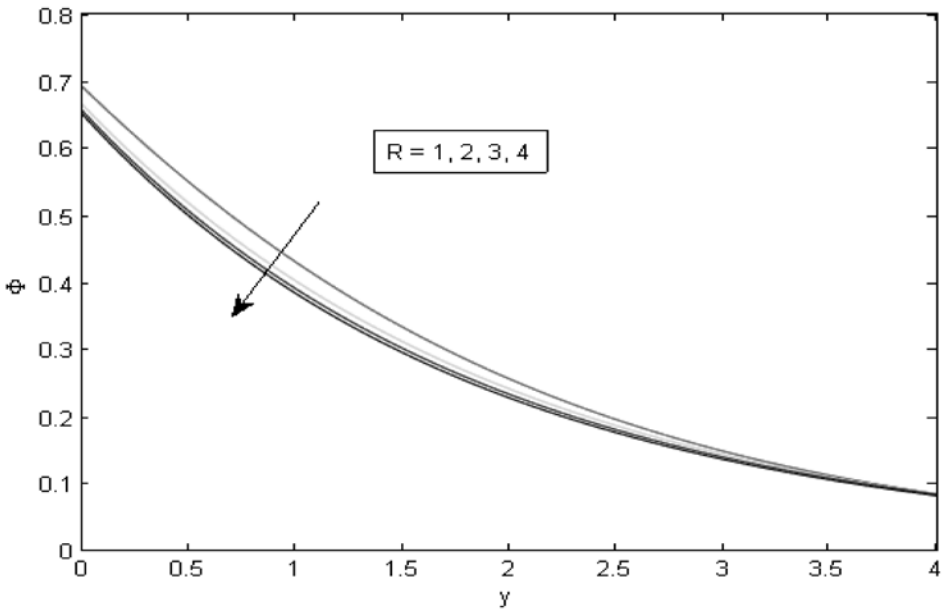

Figure 15
Concentration profile for variation in *R*.

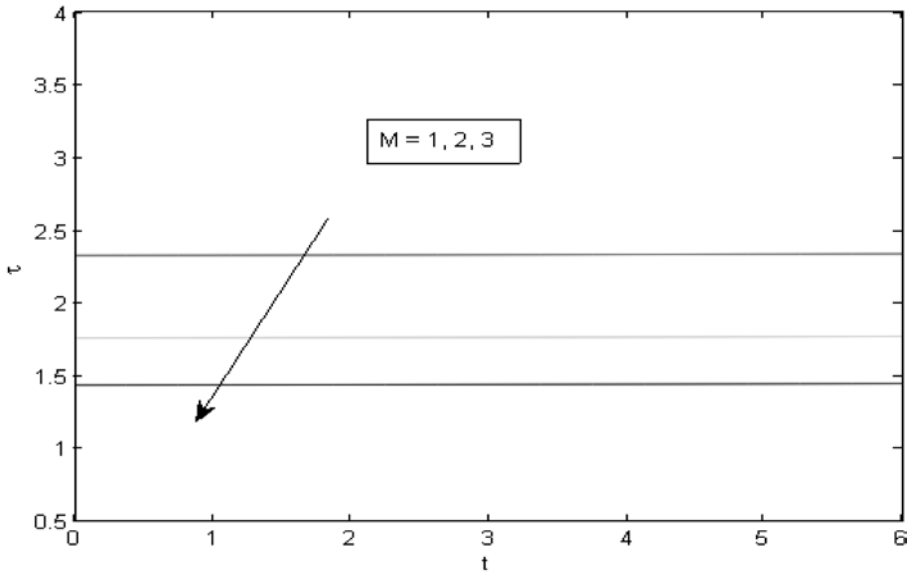

Figure 16
Skin-friction for variation in *M* when $Q = 1$; $R = 2$; $Sc = 0.22$; $Sr = 1$; $K = 1$; $Gr = 3$; $Gm = 4$; $Pr = 0.71$; $u_w = 1$; $\alpha = 1$; $\varepsilon = 0.01$; $\delta = 0.1$; $t = 1$; $h_3 = 1$; $k = 1$.

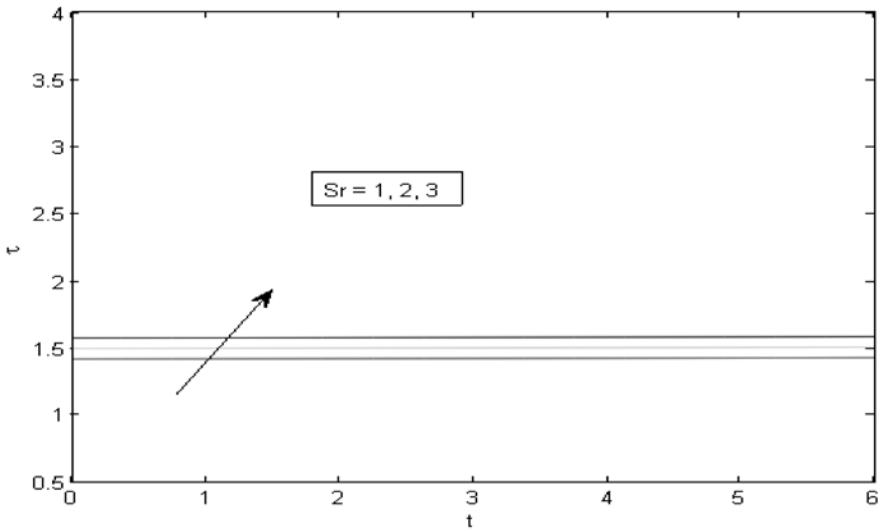

Figure 17

Skin-friction for variation in Sr when $Q = 1$; $R = 2$; $Sc = 0.22$; $M = 2$; $K = 1$; $Gr = 3$; $Gm = 4$; $Pr = 0.71$; $u_w = 1$; $\alpha = 1$; $\varepsilon = 0.01$; $\delta = 0.1$; $t = 1$; $h_3 = 1$; $k = 1$.

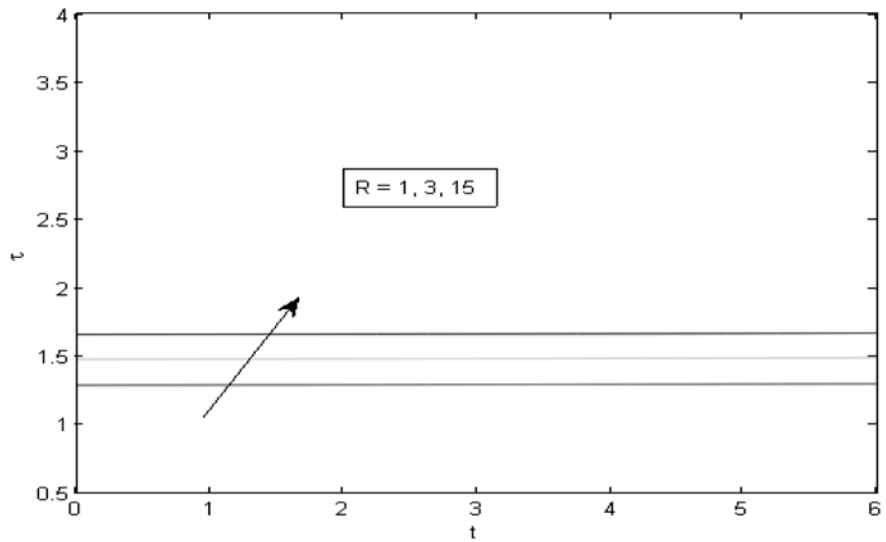

Figure 18

Skin-friction for variation in R when $Q = 1$; $M = 2$; $Sc = 0.22$; $Sr = 1$; $K = 1$; $Gr = 3$; $Gm = 4$; $Pr = 0.71$; $u_w = 1$; $\alpha = 1$; $\varepsilon = 0.01$; $\delta = 0.1$; $t = 1$; $h_3 = 1$; $k = 1$.

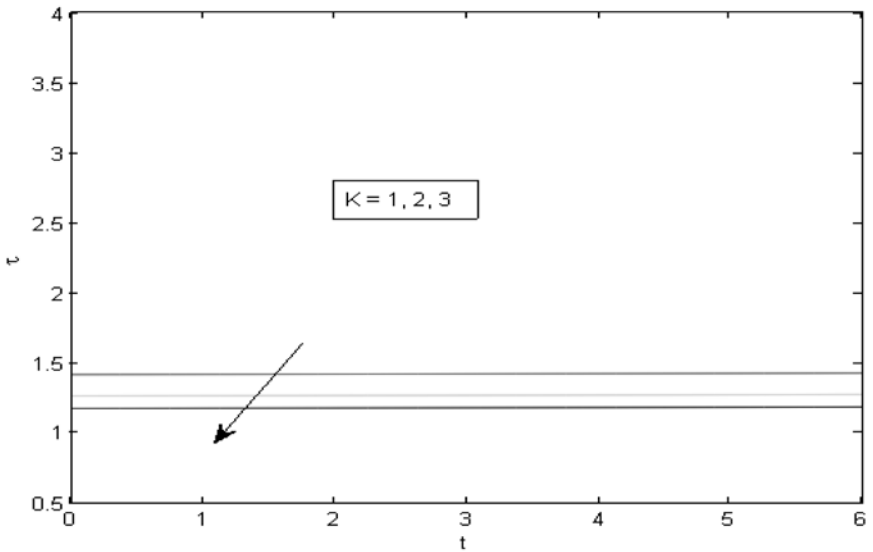

Figure 19
Skin-friction for variation in K when Q = 1; R = 2; Sc = 0.22; Sr = 1; M = 2; Gr = 3; Gm = 4; Pr = 0.71; u_w = 1; α = 1; ε = 0.01; δ = 0.1; t = 1; h_3 =1; k =1.

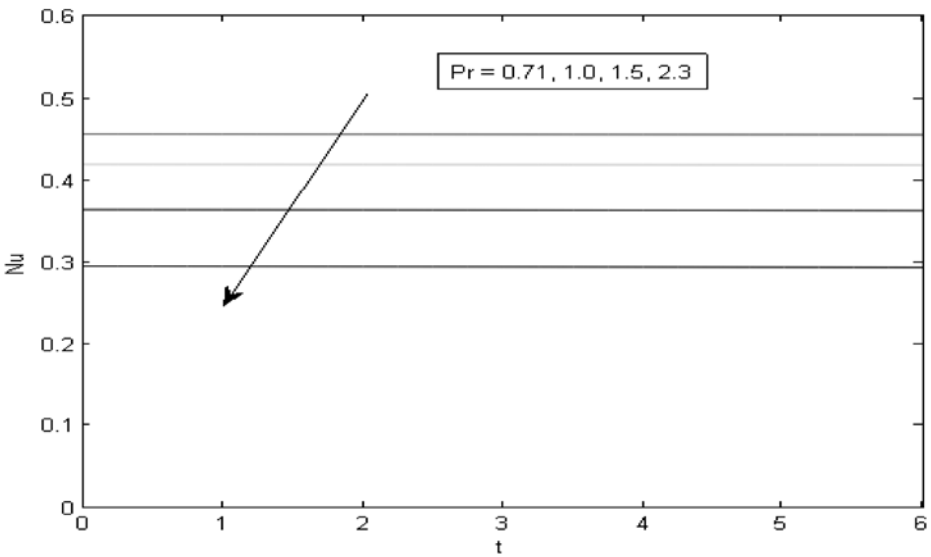

Figure 20
Nusselt number Nu for variation in Pr.

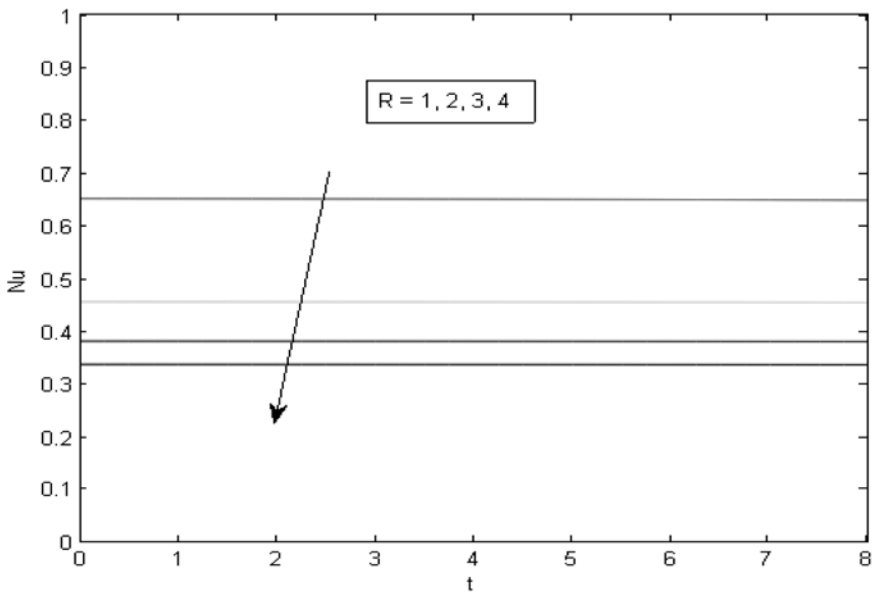

Figure 21
Nusselt number *Nu* for variation in *R*.

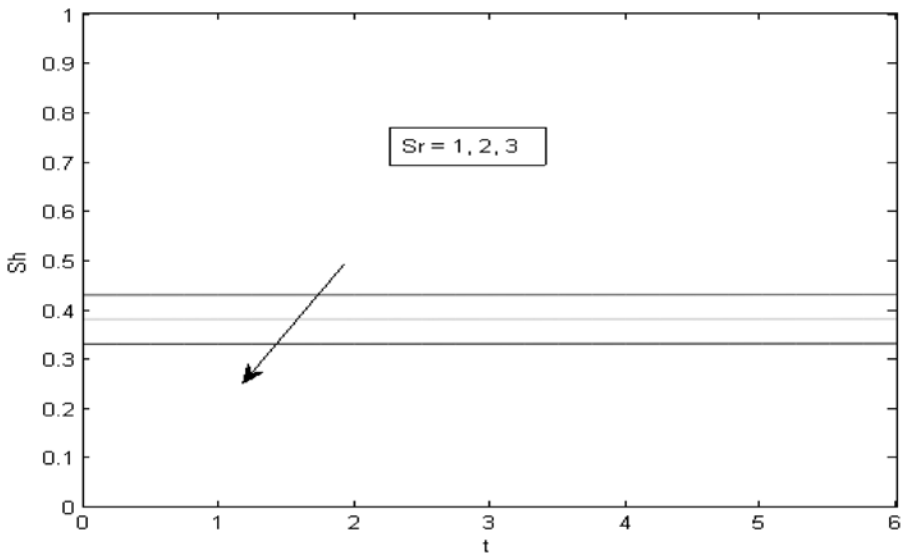

Figure 22
Sherwood number *Sh* for variation in *Sr*.

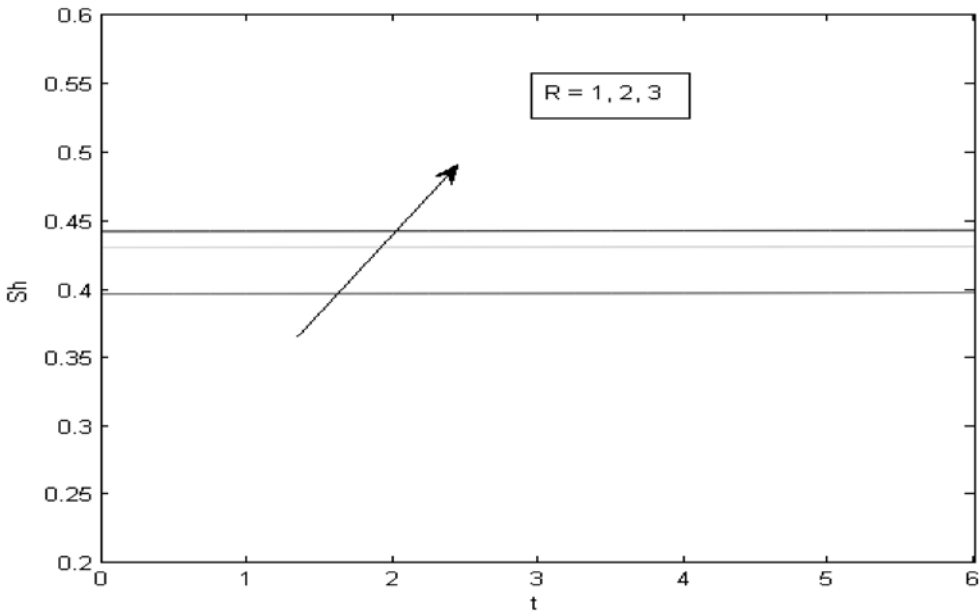

Figure 23
Sherwood number *Sh* for variation in *R*.

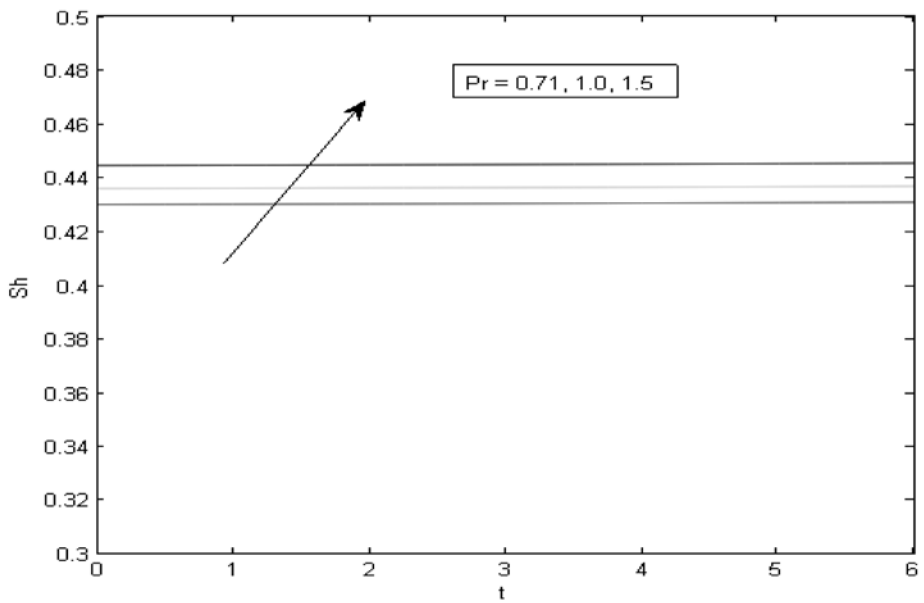

Figure 24
Sherwood number *Sh* for variation in *Pr*.

9. Conclusion

Our investigation of the problem leads to the following conclusions :

- The fluid velocity decreases as the effect of the magnetic field parameter becomes stronger.
- The fluid velocity is accelerated under the effects of thermal radiation, velocity ratio parameter and thermal diffusion.
- The temperature increases with the increase in Prandtl number and thermal radiation.
- The species concentration in the fluid decreases with the increase in Schmidt number, radiation and slip parameter.
- The viscous drag at the plate increases under the effects of thermal radiation and thermal diffusion.
- The rate of heat transfer at the plate is decreased due to radiation and Prandtl number.
- The rate of mass transfer from the plate to the fluid gets decreased under the effect of thermal diffusion.

References

1. Soundalgekar, V. and Takhar, H.S.− Radiative convective flow past a semi-infinite vertical plate, Modeling Measure and Control, Vol. **51**, pp. 31-40, (1992).
2. Hossain, A.M., Alim, M.A. and Rees, D.A.S.− Effect of Radiation on free convection from a porous vertical plate, Int. J. of Heat and Mass transfer, **42**, 181-191 (1999).
3. Raptis, A. − Radiation and flow through a porous medium, Journal of porous media,Vol. 4, No 3, 271-273 (2001).
4. Rajput, U.S.,Varshney, N.K. and Rajput, D.− Free convection flow of magneto polar fluid through porous medium in slip flow regime with mass transfer, Acta Ciencia Indica XXXIV M, **4**, 2045 (2008).
5. Johari, R., Saxena, A.M. and Jha, R.− Unsteady MHD flow through porous medium and heat transfer past a porous vertical moving plate with heat source, Acta Ciencia Indica XXXIV M, **4**, 1683 (2008).
6. Anjali Devi, S.P. and Raj, J.W.S. − Thermo diffusion effects on unsteady hydro-magnetic free convection flow with heat and mass transfer past a moving vertical plate with time dependent suction and heat source in a slip flow regime, Int. J. of Appl. Math. and Mech., **7**, 20-51 (2011).

7. Prakash, J., Sivaraj, R. and Kumar, B.R.− Influence of chemical reaction on unsteady MHD mixed convective flow over a moving vertical plate, Int. J. Fluid Mech., **3**, 1-14 (2011).
8. Raju, M.C., Varma, S.V.K. and Reddy, N.A.− Radiation and mass transfer effects on a free convection flow through a porous medium bounded by a vertical surface, Journal of future Engineering and Technology, Vol. 7, No. 2, pp.7-12, (2012).
9. Bhavana, M., Chenna Kesavaiah, D. and Sudhakaraiah, A.− The Soret effect on free convective unsteady MHD flow over a vertical plate with heat source, IJIRSET, **5**, 1617-1628 (2013).
10. Ahmed, N. and Das, K.K.− MHD Mass transfer flow past a vertical porous plate embedded in a porous medium in a slip flow regime with thermal radiation and chemical reaction, OJFD, **3**, 230-239 (2013).
11. Balamurugan, K.S., Ramaprasad, J. L. and Varma, S.V.K.− Unsteady MHD free convective flow past a moving vertical plate with time dependent suction and chemical reaction in a slip flow regime, Procedia Engineering, **127**, 516-523 (2015).
12. Ahmed, N. and Bhattacharyya, D. J.− MHD natural flow past an exponentially accelerated vertical plate, Allahabad Mathematical Society, **30**, 147-171 (2015).

INDIAN JOURNAL OF THEORETICAL PHYSICS, VOL. 64, NOS. 3 & 4, 2016

Wave particle duality from D-dimensional blackbody radiation

Joydip Mitra
Department of Physics, Scottish Church College
1 & 3 Urquhart Square, Kolkata-700006
E-mail: jmscphys@gmail.com

(Received for publication in August, 2016)

[**Abstract :** In 1900 Planck, while analyzing the blackbody radiation spectrum, proposed his hypothesis that exchange of energy between walls of cavity and radiation can only be exchanged in a discrete manner. Einstein later showed radiation itself is quantized and using statistical approach arrived at the fluctuation formula which shows wave and particle behavior of light is encoded in the blackbody radiation spectrum. Here we will first review the calculation made by Einstein and then generalize to *D*-dimensional black body radiation. It is shown that in *D*-dimensional world still wave-particle duality is manifested in Blackbody radiation spectrum. Some general consequences in a *D*-dimensional blackbody have also been discussed.]

Keywords : black body radiation, Fluctuation formula, wave-particle duality

1. Introduction

In his "annusmilabilis" (1905) Einstein published a revolutionary paper where he considered the electromagnetic radiation is itself quantized and by the introduction of those quanta, later named as "Photons" he successfully explained the Photoelectric effect. By calculating the entropy of cavity radiation, he argued that "monochromatic radiation of low intensity behaves in thermodynamic respect as if it consists of mutually independent energy quanta of magnitude $h\nu$"[1]. Hence light possesses a particle nature along with their wave nature. Later on, in 1909 paper[2], Einstein considered the relative mean-square energy fluctuation of the radiant energy in cavity radiation or Black body radiation, thereby showing that the wave–particle duality of light is encoded in the Black body spectrum. A historical overview can be found in[3,4] and references therein.

2. Einstein derivation of fluctuation formula

In the following we will first derive the relative mean square fluctuation of energy as in the canonical ensemble, given by

$$\frac{\left\langle \Delta \in^2 \right\rangle}{\left(\bar{\in}\right)^2} = \frac{1}{\left(\bar{\in}\right)^2} \frac{\partial \bar{\in}}{\partial \beta} \qquad \ldots \quad (1)$$

where $\beta = \frac{1}{\kappa T}$.

Also note that for a canonical ensemble, $\bar{\in} = \frac{\sum_{j} j e^{-\beta \in j}}{z}$ where Z is the canonical partition function. Therefore,

$$\frac{\partial \bar{\epsilon}}{\partial \beta} = \overline{\epsilon^2} - (\bar{\epsilon})^2 \qquad \ldots \quad (2)$$

or, $$\langle \Delta \epsilon^2 \rangle = kT^2 \frac{\partial \bar{\epsilon}}{\partial T} \ . \qquad \ldots \quad (3)$$

After writing down the fluctuation relation for the canonical ensemble, let us focus our attention to the equilibrium radiation in a hollow cavity of volume *V* at temperature *T*. Let *v* be a small volume in the hollow cavity (*V*). The mean spectral energy of radiation in the range between *v* and *v+dv*, according to Planck's law is given by

$$\bar{\epsilon} = \frac{8\pi\nu^2 d\nu}{c^3} v \ \frac{h\nu}{\frac{h\nu}{(e^{\overline{kT}}-1)}} \qquad \ldots \quad (4)$$

where $\frac{8\pi\nu^2 d\nu}{c^3}$ denotes the number of modes of *EM* radiation and the term $\frac{h\nu}{\left(\frac{h\nu}{ekT-1}\right)}$ denotes the average energy of the radiation.

Substituting (4) in (3), we obtain

$$kT^2 \frac{\partial \bar{\epsilon}}{\partial T} = \frac{8\pi h\nu^3 d\nu}{c^3} v \left[\frac{h\nu}{(e^{\frac{h\nu}{kT}} - 1)} + \frac{h\nu}{\left(e^{\frac{h\nu}{kT}} - 1 \right)^2} \right]$$

which after some simple algebra can be recast in the form

$$= h\nu\ \bar{\epsilon} + \frac{(\bar{\epsilon})^2}{\frac{8\pi\nu^2 d\nu}{c^3}v}\ .$$

Therefore, $\frac{\langle\Delta\epsilon^2\rangle}{(\bar{\epsilon})^2} = \frac{h\nu}{\bar{\epsilon}} + \frac{1}{\frac{8\pi\nu^2 d\nu}{c^3}v} = \frac{1}{\frac{\bar{\epsilon}}{h\nu}} + \frac{1}{\frac{8\pi\nu^2 d\nu}{c^3}v}$

Here $\frac{\bar{\epsilon}}{h\nu}$ represents the number of particles, now called photons each carrying an energy $h\nu = N_p$ and $\frac{8\pi\nu^2 d\nu}{c^3}v$ represents the number of wave modes in the frequency range ν and $\nu+d\nu = N_\nu$. Therefore, the relative mean square statistical fluctuation is given by $\frac{\langle\Delta\epsilon^2\rangle}{(\bar{\epsilon})^2} = \frac{1}{N_p} + \frac{1}{N_\nu}$. This breaking up of the fluctuations distinctly into particle and wave parts unambiguously manifests the wave-particle duality. We can explicitly show that $\frac{1}{N_p}$ results from Wien's Law , given by

$$\bar{\epsilon} = \frac{8\pi\nu^2 d\nu}{c^3} v\ h\nu e^{-\frac{h\nu}{kT}}$$

In this case,

$$\langle\Delta\epsilon^2\rangle = \frac{8\pi h\nu^3 d\nu}{c^3} v\ h\nu e^{-\frac{h\nu}{kT}} = \bar{\epsilon}\, h\nu.$$

Therefore,

$$\frac{\langle\Delta\epsilon^2\rangle}{(\bar{\epsilon})^2} = \frac{1}{\frac{\bar{\epsilon}}{h\nu}} = \frac{1}{N_p}$$

Similarly $\frac{1}{N_\nu}$ results from Rayleigh-Jeans law given by, $\bar{\epsilon} = \frac{8\pi\nu^2 d\nu}{c^3} v\ kT$

Therefore,

$$\langle\Delta\epsilon^2\rangle = kT^2 \frac{\partial\bar{\epsilon}}{\partial T} = \frac{8\pi\nu^2 d\nu}{c^3} v\ k^2T^2 = \frac{(\bar{\epsilon})^2}{\frac{8\pi\nu^2 d\nu}{c^3}v}$$

Or, $\frac{\langle\Delta\epsilon^2\rangle}{(\bar{\epsilon})^2} = \frac{1}{\frac{8\pi\nu^2 d\nu}{c^3}v} = \frac{1}{N_\nu}$

We also point out the fact that particle nature dominates in high frequency (Wien's law) and wave nature is dominant in low frequency (Rayleigh-Jeans law) of electromagnetic spectrum. Hence the wave particle duality is encoded in Black body radiation curve.

3. Blackbody radiation in D-dimensional universe

Here we consider electromagnetic radiation in a metallic cavity which has the shape of a *D*-dimensional cube (each side has length *L*) whose walls are maintained at a temperature *T*.

Now in a *D*-dimensional world, the electric field has *D*-components. Since electric fields are transverse in nature, so there will be (*D*-1) components for polarization. Hence, number of modes including all possible polarizations of the electric field is given by,

$$N(k)dk = (D-1)V\frac{dV_k}{(2\pi)^D}$$

where $V(=L^D)$ is the volume of *D*-dimensional cavity and dV_k is the volume in the k space. Now the *D*-dimensional volume element in k space is given by

$$dV_k = \frac{2\pi^{D/2}}{\Gamma\left(\frac{D}{2}\right)}k^{D-1}dk.$$

Since $k = \frac{2\pi\nu}{c}$, so the number of modes in the frequency interval ν to $\nu+d\nu$ is represented as[5,6]

$$N(\nu)d\nu = (D-1)V\frac{2}{\Gamma\left(\frac{D}{2}\right)}\left(\frac{\sqrt{\pi}}{c}\right)^D \nu^{D-1}d\nu.$$

To get a feeling about the number of modes for different dimensions, we see that

No. of modes	*D*=3	*D*=4	*D*=5
$N(\nu)d\nu$	$\frac{8\pi\nu^2 d\nu}{c^3}V$	$\frac{6\pi^2\nu^3 d\nu}{c^4}V$	$\frac{32\pi^2\nu^4 d\nu}{3c^5}V$

According to Planck, each mode has an average energy $\frac{h\nu}{\left(e^{\frac{h\nu}{kT}}-1\right)}$. So the spectral energy distribution in the interval ν to $\nu+d\nu$ is given by,

$$\rho(\nu)d\nu = (D-1)V\frac{2}{\Gamma\left(\frac{D}{2}\right)}\left(\frac{\sqrt{\pi}}{c}\right)^D \frac{h\nu^D}{\left(e^{\frac{h\nu}{kT}}-1\right)}d\nu$$

(Here we have used a more common notation $\rho(\nu)\, d\nu$ rather than $\bar{\epsilon}$ as used in the previous section.). It is easy to observe that total energy density over all frequencies can be obtained by integrating energy density over all frequencies *viz* $\int_0^\infty \rho(\nu)d\nu$ resulting in $C_D T^{D+1}$.

One of the important aspect of Planck Black body distribution is the Wien's displacement law. The law states that $\frac{\nu_{max}}{T} = \alpha =$ constant where ν_{max} is the frequency at which spectral energy density is maximum. The value of the constant depends upon the dimensionality.

Calculating $\frac{d\rho(\nu)}{d\nu} = 0$, we get a transcendental equation $(x = \frac{h\nu_m}{kT})$

$$e^{-x} = 1 - \frac{x}{D}.$$

The solution can be done numerically.Moreover, above Planck distribution as the spectral energy density in the interval λ and $\lambda+d\lambda$ can be represented as[7]

$$\rho(\lambda)d\lambda = (D-1)V\frac{2}{\Gamma\left(\frac{D}{2}\right)}\pi^{\frac{D}{2}}\frac{hc}{\lambda^{D+2}(e^{\frac{hc}{\lambda kT}}-1)}d\lambda$$

Employing $\frac{d\rho(\lambda)}{d\lambda} = 0$, we get a another transcendental equation $(y = \frac{hc}{\lambda_m kT})$

$$e^{-y} = 1 - \frac{y}{D+2}$$

which can also be solved numerically. We present below the solutions for *x* and *y* for different dimensions.

Quantity	*D*=3	*D*=4	*D*=5
x	2.821	3.920	4.965
y	4.965	5.984	6.993
$\lambda_m\nu_m$	0.568*c*	0.655*c*	0.799*c*

It then turns out the frequency at which $\rho(\nu)d\nu$ is maximum; the corresponding wavelength is not the wavelength λ_m at which $\rho(\lambda)d\lambda$ is maximum. This is due to the inherent asymmetric nature of the Blackbody radiation spectrum. Also note that

For $D\to\infty$ only $\nu_m\lambda_m \to c$.

To calculate the fluctuation in this general case, we use the same relation $\langle \Delta\epsilon^2 \rangle = kT^2 \frac{\partial \bar{\epsilon}}{\partial T}$. The Rayleigh-Jeans formula in *D*-dimensions take the form

$$\bar{\epsilon}_{RJ}(\nu)d\nu = (D-1)V \frac{2}{\Gamma\left(\frac{D}{2}\right)} \left(\frac{\sqrt{\pi}}{c}\right)^D \nu^{D-1}\, kT\, d\nu$$

whereas the Wien's formula takes the form

$$\bar{\epsilon}_{wien}(\nu)d\nu = (D-1)V \frac{2}{\Gamma\left(\frac{D}{2}\right)} \left(\frac{\sqrt{\pi}}{c}\right)^D h\nu^D e^{-\frac{h\nu}{kT}}\, d\nu\ .$$

The relative fluctuation in case of Rayleigh is then given by

$$\frac{\langle \Delta\epsilon^2 \rangle}{(\bar{\epsilon})^2} = \frac{1}{(D-1)V \frac{2}{\Gamma\left(\frac{D}{2}\right)} \left(\frac{\sqrt{\pi}}{c}\right)^D \nu^{D-1}}$$

Clearly this relation reflects the fact that Rayleigh-Jeans part of the Planck Blackbody spectrum shows the wave nature. In case of Wien, the relative fluctuation is given by $\frac{\langle \Delta\epsilon^2 \rangle}{(\bar{\epsilon})^2} = \frac{h\nu}{\bar{\epsilon}} = \frac{1}{N_p}$ which clearly shows the particle nature.

In case of Planck formula for general *D*-dimensions,

$$kT^2 \frac{\partial \bar{\epsilon}}{\partial T} = (D-1)V \frac{2}{\Gamma\left(\frac{D}{2}\right)} \left(\frac{\sqrt{\pi}}{c}\right)^D \nu^D \left[\frac{h\nu}{(e^{\frac{h\nu}{kT}} - 1)} + \frac{h\nu}{\left((e^{\frac{h\nu}{kT}} - 1\right)^2}\right]$$

which on further simplification, can be written as

$$\frac{\langle \Delta\epsilon^2 \rangle}{(\bar{\epsilon})^2} = \frac{1}{\frac{\bar{\epsilon}}{h\nu}} + \frac{1}{(D-1)V \frac{2}{\Gamma\left(\frac{D}{2}\right)} \left(\frac{\sqrt{\pi}}{c}\right)^D \nu^{D-1}} = \frac{1}{N_p} + \frac{1}{N_\nu}$$

This clearly shows that in *D*-dimensional Blackbody radiation, the relative fluctuation in case of Planck distribution breaks up into particle (Wien) and wave (Rayleigh) parts implying wave-particle duality in general *D*-dimensional world.

4. Conclusion

In 1909 Einstein, via statistical approach showed that Fluctuation of energy density in cavity radiation splits up into two parts, one representing the wave and the other representing the particle nature of *EM* radiation. Here we have generalized this case for a general *D*-dimensional blackbody showing that wave-particle duality still reigns supreme in general *D*-dimensional framework.

References

1. Einstein, A.− Annalen der Physik, **17**, 132-148 (1905).
2. Einstein, A.− Physikalische Zeitschrift, Vol.**10**, P. 185-193 (1909).
3. Varro, S.− Fluctuation and Noise Letters, Vol. **6**, No. 3, R11-R46 (2006).
4. Pais, A.− "Subtle is the Lord.The Science and the life of Albert Einstein", Oxford University Press, First Indian Edition, (2005).
5. Cardoso, T.R. et. al.− Rev.Bras.Ens.Fis., **27**, 559-563 (2005) and references therein.
6. Pardy, M.− Results in Physics, **3**, 70-73 (2013).
7. Lianxi, Ma, et. al.− Lat. Am. J. Phys. Educ., Vol. **3**, No. 3, Sept. (2009).

INDIAN JOURNAL OF THEORETICAL PHYSICS, VOL. 64, NOS. 3 & 4, 2016

Indication of azimuthal long-range correlation of pions in ultra-relativistic nuclear interactions

Md. Abdul Kayum Jafry[*]**,**
Department of Physics,
Shibpur Dinobundhoo Institution (College),
412/1 G.T. Road (South), Howrah-711102, India

Dipak Ghosh and Argha Deb
Nuclear and Particle Physics Research Centre,
Department of Physics,
Jadavpur University, Kolkata-700 032, India

(Received for publication in September, 2016)

[**Abstract :** This paper reports an investigation of the two-particle long-range azimuthal correlation of the pions produced in ^{16}O–*AgBr* interactions at 60 *AGeV* and ^{32}S–*AgBr* interactions at 200 *AGeV*. The experimental results are compared with those of Monte Carlo simulated events to look for dynamical correlation. The data show two-particle long-range correlation among the pions in azimuthal space at both the energies.]

Keywords : Heavy ion interactions, produced particles, two-particle azimuthal correlation.

PACS: 25.70 Pq, 25.75-q

1. Introduction

Studies of nuclear matter under extremes of energy and density have become a subject of increasing interest because of the possibility of observing some exotic phenomena. The study of correlations among the produced particles presents significant features of the nuclear interaction and is a potential source of information. These correlations can provide direct information about the later stage of the reaction when nuclear matter is highly excited and diffused[1]. Two-particle correlations give information about the space time structure and dynamics of the emitting source[2-4].

* Corresponding author : E-mail : akjafry@yahoo.com

Several studies using well-known two-particle and three-particle correlation functions have been reported in different types of interactions at various energies[5-16].

The particles produced in high energy interactions (like hadron-hadron, hadronnucleus) seem to prefer to be emitted in a correlated fashion. But it is not possible to say with certainty why they prefer to do so. The existing explanations are not conclusive. A detailed correlation study is essential to look for the exact reason of the correlated emission of the particles speculated by different theorists.

Generally short-range correlation of pions is studied though it is also important and interesting to study long-range correlation among pions. But long range correlation studies are very rare. For this reason, we are trying to study long-range correlation of pions in azimuthal angle space.

We have made an investigation on two-particle long-range correlations among pions in ^{16}O–$AgBr$ interactions at 60 *AGeV* and ^{32}S–$AgBr$ interactions at 200 *AGeV*. The experimental data on two particle long range correlation function for the produced particles is compared with those obtained by Monte-Carlo simulation (assuming an independent emission model) to search for true dynamical effect. Any significant excess of the experimental data over Monte Carlo values are termed as dynamical surplus. The dynamical surplus may signify the presence of dynamical correlation among the particles.

2. Experimental method

The data sets used in this present analysis were obtained from Illford *G*5 emulsion tracks exposed to ^{32}S beam of energy 200 *AGeV* and ^{16}O beam of energy 60 *AGeV* were obtained from *CERN SPS*. A Leitz Metaloplan microscope with a 10*x* objective and 10*x* ocular lens provided with a semi-automatic scanning stage was used to scan the plates. Each plate was scanned by two independent observers to increase the scanning efficiency. The final measurements were done using an oil-immersion 100*x* objective. The measuring system fitted with it has 1 μm resolution along the *x* and *y* axes and 0.5 μm resolutions along the *z*-axis.

Our detector can resolve particles differing by 0.1 unit in pseudorapidity scale and about 5^0 in azimuthal angle space. It is worthwhile to mention that the emulsion technique possesses a very high spatial resolution which makes it a very effective detector for studying correlation phenomena.

After scanning, the events were chosen according to the following criteria :

(*i*) The incident beam track should not exceed 3^0 from the main beam direction in the pellicle. It is done to ensure that we have taken the real projectile beam.

(*ii*) Events showing interactions within 20 μm from the top or bottom surface of the pellicle were rejected. It is done to reduce the loss of tracks as well as to reduce the error in angle measurement.

(*iii*) The selection of the primary interactions is made by following the incident beam track in the backward direction until it reaches the leading edge.

According to the emulsion terminology[17] the particles emitted after interactions are classified as :

(*a*) *Black particles* : Black particles consist of both single and multiple charged fragments. They are target fragments of various elements like carbon, lithium, beryllium etc with ionization greater or equal to 10 I_0, I_0 being the minimum ionization of a singly charged particle. Ranges of them are less than 3 *mm* and the velocity less than 0.3 *c* and the energy less than 30 *MeV*, where *c* is the velocity of light in vacuum.

(*b*) *Grey particles* : They are mainly fast target recoil protons with energy up to 400 *MeV*. They have ionization $1.4\ I_0 \leq I \leq 10 I_0$. Their ranges are greater than 3 *mm* and having velocities (*v*), $0.7\ c \geq v \geq 0.3\ c$.

(*c*) *Shower particles* : The relativistic shower tracks with ionization *I* less than or equal to 1.4 I_0 are mainly produced by pions and are not generally confined within the emulsion pellicle. These shower particles have energy in *GeV* range.

(*d*) The projectile fragments are different class of tracks with constant ionization, long range and small emission angle.

To ensure that the targets in the emulsion are silver or bromine nuclei, we have chosen only the events with at least eight heavy ionizing tracks of black and grey particles. For our present analysis, we have taken into consideration shower tracks (which are mostly pions) for azimuthal correlation.

According to the above selection procedure, we have chosen 250 events of ^{16}O–*AgBr* interactions at 60 *AGeV* and 140 events of ^{32}S–*AgBr* interactions at 200 *AGeV*. The shower tracks are identified from each event and their azimuthal angle (ϕ) were measured for each tracks by taking the coordinates of the interaction point (X_0, Y_0, Z_0), coordinates (X_1, Y_1, Z_1) at the end of the linear portion of each secondary track and coordinates (X_i, Y_i, Z_i) of a point on the incident beam. For our present analysis we have used the variable ϕ.

3. Method of analysis

3.1. Two-particle correlation :

For the phase space variable *z*, the two-particle normalized correlation function is defined[15] as

$$R(z_1, z_2) = \frac{\rho_2(z_1, z_2) - \rho_1(z_1)\rho_1(z_2)}{\rho_1(z_1)\rho_1(z_2)} = \frac{\rho_2(z_1, z_2)}{\rho_1(z_1)\rho_1(z_2)} - 1$$

where the quantities

$$\rho_1(z) = \frac{1}{\sigma}\frac{d\sigma}{dz};\ \rho_2(z_1, z_2) = \frac{1}{\sigma}\frac{d^2\sigma}{dz_1 dz_2}$$

represent one- and two-particle densities respectively.

In terms of number of particles, *R* can be represented as

$$R(z_1, z_2) = N_T \frac{N_2(z_1, z_2)}{N_1(z_1)N_1(z_2)} - 1$$

where N_T is the total number of inelastic events, N_1 (z_1) is the number of pions at the phase space interval z_1 to z_1+dz_1 and N_1 (z_2) is the number of

pions at the phase space interval z_2 to z_2+dz_2. N_2 (z_1, z_2) is the number of pairs of particles having one particle between the interval z_1 to z_1+dz_1 other particle between z_2 to z_2+dz_2 in an event.

For the purpose of study of azimuthal correlation among pions, ϕ is chosen as phase space variable (ϕ being the azimuthal angle of emission of the particles). In terms of ϕ,

$$R(\phi_1,\phi_2) = N_T \frac{N_2(\phi_1,\phi_2)}{N_1(\phi_1)N_1(\phi_2)} - 1 \qquad \ldots \quad (1)$$

The idea of using the correlation function of the above form comes from the work of Kirkwood[18] in statistical physics. $R = 0$ implies the absence of correlation, *i.e.* the case of completely independent particle emission.

3.2. Monte Carlo simulation:

Correlation between the particles produced in high energy heavy ion collisions can be studied by observing azimuthal correlation (ϕ) among them. Apart from the presence of any true dynamics, correlation may arise due to the following reasons:

(*a*) The broad multiplicity distribution of produced particles.

(*b*) The dependence of single particle spectrum $\frac{1}{\sigma}\frac{d\sigma}{dz}$ on the multiplicity.

(c) Trivial statistical fluctuations.

We have compared the experimental data with the data obtained by Monte Carlo simulation assuming independent emission model (*IEM*), to search for the non-trivial dynamical correlation among the produced particles in ^{16}O–*AgBr* interactions at 60 *AGeV* and ^{32}S–*AgBr* interactions at 200 *AGeV*. The simulation is made using the following assumptions :

(*a*) The produced particles (pions) are emitted independently.

(*b*) The multiplicity distribution of the Monte Carlo events is the same as the empirical multiplicity spectrum of the real ensemble.

(*c*) The single particle spectrum $\frac{1}{\sigma}\frac{d\sigma}{dz}$ of the simulated events reproduces the empirical multiplicity distribution $\frac{1}{\sigma}\frac{d\sigma}{dz}$ of the real ensemble.

It may be concluded that if one finds any excess in experimental values over the Monte Carlo simulated values, then there may be some kinematical reason within the reaction process which may leads towards long range dynamical correlation among produced particles. We will denote the experimental normalized correlation function by *R* and that of the Monte Carlo calculated events by R_M. The difference between experimental and Monte Carlo values can be interpreted as the dynamical surplus which arises due to some dynamics in the reaction process. The dynamical surplus can be written as

$$R_D = R - R_M \,. \qquad \ldots \quad (2)$$

4. Results and discussion

The normalized two-particle correlation function *R* is calculated for different values of azimuthal angle (ϕ) for both the data sets using Eq. (1) . We have calculated the correlation function *R* for the off-diagonal elements of the correlation matrix ($\phi_1 \neq \phi_2$). These off diagonal terms are the measures of the magnitude of the long-range correlation at different phase space intervals. We have also calculated the correlation function R_M for the simulated events for the same values of phase space intervals.

We have calculated the dynamical surplus values R_D from Eq. (2). It is observed that long-range dynamical correlations are very prominent in some azimuthal angle zones.

The details of which are shown in Table I.

Table I

The types of interactions with their specified energies, azimuthal angle ϕ_1, ϕ_2, the differences between ϕ_1 and ϕ_2 and few maximum values of the dynamical surplus R_D for each interactions.

Interactions	ϕ_1	ϕ_2	$\phi_1 \sim \phi_2$	R_D
$^{16}O - AgBr$	18	162	144	41.04
(60 *AGeV*)	54	162	108	43.11
	90	18	72	79.38
$^{32}S - AgBr$	18	198	180	39.58
(200 *AGeV*)	90	162	72	33.84

The table shows indication of significant dynamical long range azimuthal correlation both in ^{16}O–*AgBr* interactions at 60 *AGeV* and ^{32}S–*AgBr* interactions at 200 *AGeV*.

The data are new and important for better understanding of the dynamics of pionisation process at high and ultra high energies.

Acknowledgement

The authors are grateful to Prof. P.L. Jain, Buffalo State University, USA for providing us with the exposed and developed emulsion plates used for this analysis. Md. Abdul Kayum Jafry would like to acknowledge the financial help sanctioned by the University Grant Commission (Govt. of India) under his Minor Research Project.

References

1. Giacomelli, G. and Jacob, M. − Phys. Rep., 55 (1979).
2. Gyulassy, M., Kauffmann, S.K. and Wilson, L.W. − Phys. Rev., C **20**, 2267 (1979).
3. Boal, D.H., Gelbke, C.K. and Jennings, B.K. − Rev. Mod. Phys., **62** 553 (1990).
4. Heinz, U. and Jacak, B.V. − Ann. Rev. Nucl. Part. Sci., **49**, 529 (1999).

5. Plutta, J. et. al. − Eur. Phys. J., **A9**, 63 (2000).
6. Larionov, A.B. − Eur. Phys. J., **A7**, 507 (2000).
7. Anchishkin, D.V. − Eur. Phys. J., **A7**, 229 (2000).
8. El Naghy, A. et. al. − Nuovo Cimento, **A110**, 125 (1997).
9. Breakstone, A. et. al. − Mod. Phys. Lett., **A6**, 2785 (1991); Bopp, F.W. − Riv. Nuovo. Cim., **1**, 1 (1978).
10. Ghosh, D. et. al. − Phys. Rev., **D26**, 2983 (1982).
11. Ghosh, D. et. al. − Acta Phys. Slov., **47**, 425 (1997); Z. Phys., **A327**, 233 (1987); Indian J. Phys., A76, 277 (2002).
12. Derado, I. et. al. − Z. Phys., **C56**, 553 (1992).
13. Jain, P.L. and Singh, G.− Nucl. Phys., **A596**, 700 (1996); J. Phys., **G23**, 1655 (1997).
14. Levin, E. M. et. al. − Z. Phys., **C5**, 285 (1980).
15. Bell, W. et. al. − Z. Phys., **C22**, 109 (1984).
16. Berger, E.L. − Nucl. Phys., **B85**, 61 (1975); Chao, A.M. and Quigg, C.− Phys. Rev., D **9**, 2016 (1974); Quigg, C., Pirilla, P. and Thomas, G.H. − Phys. Rev. Lett., **34**, 2091 (1975).
17. Powell, C.F., Fowler, P.H. and Perkins, D.H. − The Study of Elementary Particles by Photographic Methods, Pergamon, Oxford, pp. 450-464 and references therein.
18. Kirkwood, I. − J. Chem. Phys., **7**, 919 (1935).

INDIAN JOURNAL OF THEORETICAL PHYSICS, VOL. 64, NOS. 3 & 4, 2016

MHD flow past a suddenly started infinite vertical plate with induced magnetic field

N. Ahmed
Department of Mathematics,
Gauhati University, Guwahati-781014,
Assam, India
E-mail: saheel_nazib@yahoo.com

(Received for publication in October, 2016)

[**Abstract :** A theoretical analysis of the problem of a free convective flow of an incompressible viscous electrically conducting Newtonian non-Gray fluid past a suddenly started infinite vertical plate with appreciable chemical reaction and radiation in presence of uniform transverse magnetic field taking into account the induced magnetic field, is presented. Assuming the fluid to be optically thin, the resulting system of the normalized governing equations is solved in closed form by adopting the Laplace transform technique. The effects of various physical parameters on the velocity, temperature and concentration fields, and skin friction, Nusselt number and Sherwood number at the plate, are demonstrated graphically and the results are discussed and physically interpreted.]

Keywords: Induced magnetic field**;** chemical reaction; thermal diffusion; thermal radiation; optically thin; magnetic diffusivity.

AMS 2000 subject classification: 76W05

Nomenclature

$\vec{B}$ – Magnetic induction vector or magnetic flux density ;

B_0 – Strength of the applied magnetic field, $\left[MT^{-1}Q^{-1}\right]$ *Tesla* ;

B_x' – Induced magnetic field ,$\left[MT^{-1}Q^{-1}\right]$, *Tesla* ;

B_x – Non-dimensional induced magnetic field ;

C_p – Specific heat at constant pressure, $\left[L^2T^{-2}\theta^{-1}\right], \frac{Joule}{kg\times K}$;

C' – Species concentration, $\left[(MOL)L^{-3}\right]\frac{Kmol}{m^3}$;

C'_{∞} – Species concentration far away from the plate, $\left[(MOL)L^{-3}\right], \frac{Kmol}{m^3}$;

C'_{w} – Species concentration at the plate for $t' > 0, \left[(MOL)L^{-3}\right], \frac{Kmol}{m^3}$;

D_M – Molar mass diffusivity, $\left[L^2T^{-1}\right], m^2s^{-1}$;

D_T – Thermal diffusivity, $\left[(MOL)L^{-1}\theta^{-1}T^{-1}\right], \frac{Kmol}{m\,K\,s}$;

$\vec{E}$ – Electric field ;

$e_{b\lambda}$ – Planck function, $\left(ML^{-1}T^{-3}\right)$;

$\overline{f}$ – Laplace transform of $f(t)$;

$\vec{g}$ – Gravitational acceleration vector;

Gr – Thermal Grashof number ;

Gm – Solutal Grashof number ;

g – Acceleration due to gravity, $\left[LT^{-2}\right], ms^{-2}$;

H_0 – Induced magnetic field at the plate for $t' > 0, \left[MT^{-1}Q^{-1}\right], Tesla$;

$\vec{J}$ – Current density vector ;

$\left|\vec{J}\right|$ – Magnitude of current density, $\left[QL^{-2}T^{-1}\right], Ampere/m^2$;

k – Thermal conductivity, $\left[MLT^{-3}\theta^{-1}\right] \frac{W}{mK}$;

K_{λ} – Absorption coefficient, $\left(L^{-1}\right) 1/m$;

$\overline{K}$ – Constant first order homogeneous reaction rate, T^{-1}, s^{-1} ;

K – Chemical reaction parameter ;

M – Magnetic parameter (square of the Hartmann number) ;

Pr – Prandtl number ;

Pm – Magnetic Prandtl number ;

p – Pressure, $\left[ML^{-1}T^{-2}\right]$, $Newton/m^2$ (Pascal) ;

$\vec{q}$ – Fluid velocity vector ;

Q – Radiation parameter ;

$\vec{q}$ – Radiative flux vector ;

q_r – Radiative flux, $\left[MT^{-3}\right], W/m^2$;

Sr – Soret number ;

Sc – Schmidt number ;

t' – Time, [T], second(s) ;

t_0 – Characteristic time, [T], second(s) ;

T_w' – Plate temperature for $t'>0, \left[\theta\right], K$;

T_∞' – Temperature far away from the plate, $\left[\theta\right], K$;

t – Non-dimensional time ;

T' – Fluid temperature, $\left[\theta\right], K$;

U_0 – Plate velocity, $\left[LT^{-1}\right], m/s$;

u' – X -component of $\vec{q}, \left[LT^{-1}\right], m/s$;

u – Non-dimensional fluid velocity ;

(x', y', z') – Cartesian coordinates, [L], meter(m) ;

y – Non-dimensional y-coordinate ;

ρ – Fluid density, $\left[ML^{-3}\right], Kg/m^3$;

ρ_∞ – Density far away from the plate, $\left[ML^{-3}\right], Kg/m^3$;

μ – Dynamic of viscosity, $\left[ML^{-1}T^{-1}\right], Kg/ms$;

μ_e – Magnetic permeability, $\left[MLQ^{-2}\right]$, *henry/ metre* ;

υ – Kinematic viscosity, $\left[L^2T^{-1}\right], m^2s^{-1}$;

$\bar{\varphi}$ – Viscous dissipation of energy per unit volume, $\left[ML^{-1}T^{-3}\right], J/m^3s$;

σ – Electrical conductivity, $\left[M^{-1}L^{-3}TQ^2\right], (ohm \times meter)^{-1}$;

η – Magnetic diffusivity, $\left[L^2T^{-1}\right], m^2s^{-1}$;

λ – Ratio of the plate induced magnetic field to the applied magnetic field;

β – Volumetric coefficient of thermal expansion, $\left[\theta\right]^{-1}, \frac{1}{K}$;

$\bar{\beta}$ – Volumetric coefficient for solutal expansion, $[MOL]^{-1}$, $\frac{1}{Kmol}$;

θ – Non-dimensional temperature ;

ϕ – Non-dimensional concentration ;

Subscript

w − Refers to the values of physical quantities at the plate ;

∞ − Refers to the values of the physical quantities away from the plate.

1. Introduction

MHD is the science of motion of electrically conducting fluids in presence of magnetic field. It concerns with the interaction of magnetic field and the fluid velocity of electrically conducting fluid. *MHD* generators, *MHD* pumps and *MHD* flow meters are some of the numerous examples of *MHD* principles. Dynamo and motor is a classical example of *MHD* principle. Convection problems of electrically conducting fluid in presence of magnetic field have got much importance because of its wide applications in Geophysics, Astrophysics, Plasma Physics, Missile technology etc. *MHD* principles also find its applications in Medicine and Biology. The present form of *MHD* is due to the pioneer contributions of several notable authors like Alfven[1], Cowling[2], Shercliff[3], Ferraro and Plumption[4] and Crammer and Pai[5].

The natural flow arises in fluid when the temperature as well as species concentration change causes density variation leading to buoyancy forces acting on the fluid. Free convection is a process of heat or mass transfer in natural flow. The heating of rooms and buildings by use of radiator is an example of heat transfer by free convection. On the other hand, the principles of mass transfer are relevant to the working of systems such as a home humidifier and the dispersion of smoke released from a chimney into the environment. The evaporation of alcohol from a container is an example of mass transfer by free convection. Radiation is also a process of heat transfer through electromagnetic waves. Rediative convective flows are encountered in countless industrial and environment process like heating

and cooling chambers, evaporation from large open water reservoirs, astrophysical flows and solar power technology. Due to importance of the above physical aspects, several authors have carried out model studies on the problems of free convective hydrodynamic and magnetohydrodynamic flows of incompressible viscous electrically conducting fluids under different flow geometries and physical conditions taking into account of thermal radiation. Some of them are Mansour[6], Ganesan and Loganathan[7], Mbeledogu, et. al.[8], Makinde[9], Samad and Rahman[10], Orhan and Ahmet[11], Prasad, et. al.[12], Takhar, et. al.[13] and Ahmed and Dutta[14]. Ezzat, et. al.[15] have analyzed the combined effects of heat and mass transfer on unsteady *MHD* flow of perfect conducting micro polar fluid with thermal relaxation.

Thermal diffusion effect which is also known as Soret effect concerns with the method of separating heavier gas molecules from lighter ones by maintaining temperature gradient over a given volume of a gas containing particles of different masses. This method is also used for separating the isotopes of an element. The Soret effect is concerned with the mass flux caused by the temperature gradient. Comprehensive literature on various aspects of thermal diffusion and diffusion – thermo effects on different mass transfer related problems can be found in Eckert and Drake[16], Postenlnicu[17] and Ahmed[18].

In many times, it is observed that the foreign mass reacts with the fluid and in such a situation chemical reaction plays an important role in chemical industry. The study of the effect of chemical reaction on heat and mass transfer in a flow is of great practical importance to the Engineers and Scientists because of its almost universal occurrence in many branches of science and technology. In the processes of drying, distribution of temperature and moisture over agricultural fields and graves of fruit trees, damage of crops due to freezing evaporation at the surface of water body, energy transfer in a wet cooling tower, and flow in a desert cooler, heat and mass transfer occur simultaneously. Possible applications of these types of flows can be found in many industries. Many investigators have studied the effect of chemical reaction on different convective heat and mass transfer flows, of whom Apelblat[19], Andersson, et. al.[20], Muthucumaraswamy,

et. al.[21] and Kundasamy, et. al.[22] are worth mentioning. In view of the practical importance of the above fields, very recently the problem of the transient *MHD* free convective flow of an incompressible viscous electrically conducting chemically reacting and thermal radiating optically thin non-Gray fluid past an impulsively started infinite vertical plate has been studied by Ahmed[23]. This work is an extension of the work investigated by Ahmed[17] to take into account the effect of first order homogeneous reaction on the chemically reacting flow. In most of the works done on hydro magnetic flows, it is not paid much attention to the effects on the flows caused due to existence of induced magnetic field. In general the induced magnetic field is neglected on the assumption that for most of the gases that exist in nature, the electrical conductivity is low for which the magnetic Reynolds number is very small. But when a high speed missile re-enters the earth's atmosphere, a very large amount of heat is generated due to the friction of the gas molecules and this viscous heating may sometimes be so considerable as to ionize the gas in particular air, near the forward stagnation point. Since the ionized gas in this stagnation region is electrically conducting a magnetic field maybe applied to it so as to induce e.m.f in the air, which in turn affects the motion. In other words the low conducting gases may also be considered to be good conductor under different physical circumstances. Further, we recall that the magnetic Reynolds number is the ratio of the induced magnetic field to the imposed magnetic field (Ref. Shercliff[31].That is to say that, if even the magnetic Reynolds number is very small, but the intensity of the imposed magnetic field is very high, the total ignorance of the induced magnetic field is not justified. Due to importance of the induced hydro magnetic effects on electrically conducting fluid flows, a good number of researchers have carried outtheir model studies on *MHD* flow problems under different physical and geometrical conditions. Some of them are Singh and Singh[24], Choudhury and Sharma[25] and Hossain and Khatun[26].

As the present author is aware, till now no attempt has been made to investigate the problem of a natural convective flow of an electrically conducting viscous incompressible Newtonian non-Gray fluid past a suddenly started infinite vertical plate with appreciable chemical reaction and radiation in presence of uniform transverse magnetic field taking into

account the induced magnetic field. In the present work, such an attempt has been made. Here our main objective is to study how the induced magnetic field, velocity, temperature and concentration fields, and the transport characteristics are influenced by the physical parameters involved in the problem. The basic difference between the present problem and that of the problem studied by Ahmed[23] is that here the induced magnetic field is considered, but the mathematical formulations of the two problems are not the same as the Maxwell's equations are concerned.

2. Mathematical formulation of the problem

The equations governing the motion of an incompressible, viscous, electrically conducting, chemically reacting and radiating fluid in presence of a magnetic field having constant mass diffusivity and thermal diffusivity are

Continuity equation :

$$\vec{\nabla}.\vec{q} = 0 \qquad \ldots \quad (1)$$

Magnetic field continuity equation :

$$\vec{\nabla}.\vec{B} = 0 \qquad \ldots \quad (2)$$

Ampere's law :

$$\vec{\nabla} \times \vec{B} = \mu_e \vec{J} \qquad \ldots \quad (3)$$

MHD momentum equation with buoyancy force :

$$\rho\left[\frac{\partial \vec{q}}{\partial t'} + \left(\vec{q}.\vec{\nabla}\right)\vec{q}\right] = -\vec{\nabla}p + \vec{J} \times \vec{B} + \rho\vec{g} + \mu\nabla^2\vec{q} \text{ (Ref. [27])} \qquad \ldots \quad (4)$$

Energy equation :

$$\rho C_p\left[\frac{\partial T'}{\partial t'} + \left(\vec{q}.\vec{\nabla}\right)T'\right] = k\nabla^2 T' + \bar{\varphi} + \frac{\vec{J}^2}{\sigma} - \vec{\nabla}.\vec{q}_r \qquad \ldots \quad (5)$$

Species continuity equation :

$$\frac{\partial C'}{\partial t'} + \left(\vec{q}.\vec{\nabla}\right)C' = D_M\nabla^2 C' + D_T\nabla^2 T' + \bar{K}\left(C'_\infty - C'\right) \qquad \ldots \quad (6)$$

Magnetic diffusion equation for small magnetic Reynolds number :

$$\frac{\partial \vec{B}}{\partial t'} = \eta \nabla^2 \vec{B} \qquad \ldots \quad (7)$$

All the physical quantities are defined in the nomenclature.

We now consider an unsteady radiative and chemically reactive *MHD* free convective flow of an incompressible viscous and electrically conducting optically thin non-Gray fluid past a suddenly moving infinite vertical plate in its own plane in presence of a transverse magnetic field of uniform strength B_0 taking into account the thermal diffusion effect.

In order to make the mathematical model of the present problem idealized, our investigation is restricted to the following assumptions :

(*i*) All the fluid properties are considered constant except the influence of the variation in density in the buoyancy force.

(*ii*) The viscous and Ohmic dissipations of energy are negligible.

(*iii*) The magnetic Reynolds number is small.

(*iv*) The flow is parallel to the plate.

(*v*) The plate is electrically non-conducting.

(*vi*) The radiation heat flux in the direction of the plate velocity is considered negligible in comparison to that in the norma direction.

(*vii*) No external electric field is applied for which the polarization voltage is negligible leading to $\vec{E} = \vec{O}$.

(*viii*) The chemical reaction is of first order and homogeneous.

(*ix*) The velocity field is independent of the distance parallel to the surface (as given in Schlichting[29]).

(*x*) The concentration field is independent of the distance parallel to the surface (as the mass transfer process in analogous to heat transfer).

Initially the plate and the surrounding fluid were at rest at the same temperature T'_∞ with concentration level C'_∞ at all points in the fluid. At time $t' > 0$, the plate is suddenly moved in its own plane with speed U_0. The plate temperature and concentration are instantly raised to $T'_w \left(T'_w > T'_\infty\right)$ and $C'_w \left(C'_w > C'_\infty\right)$ which are thereafter maintained constant.

We introduce a rectangular Cartesian coordinate system (x', y', z') with X'-axis along the plate in the upward vertical direction, Y'-axis normal to the plate and directed into the fluid region and Z'-axis along the width of the plate. Let $\vec{q} = (u', 0, 0)$ denote the fluid velocity and $B' = (B_x', B_0, 0)$ be the magnetic flux density at the point (x', y', z', t') in the fluid.

The radiative flux $\vec{q}_r$ is given by $\vec{q}_r = (0, q_r, 0)$

The equation (1) reduces to $\frac{\partial u'}{\partial x'} = 0$ which yields

$$\vec{u} = u'(y', t') \quad \ldots \quad (8)$$

The equation (2) gives,

$$\frac{\partial B_x'}{\partial x'} = 0 \text{ which leads to } B_x' = B_x'(y', t') \quad \ldots \quad (9)$$

Following the assumption (*vii*) and by the use of the equation (3), the momentum equation (4) transforms to

$$\rho \frac{\partial u'}{\partial t'} = \mu \frac{\partial^2 u'}{\partial y'^2} - \rho g - \frac{\partial p}{\partial x'} + \frac{B_0}{\mu_e} \frac{\partial B_x'}{\partial y'} \quad \ldots \quad (10)$$

and

$$0 = \frac{\partial p}{\partial y'} + \frac{B_x'}{\mu_e} \frac{\partial B_x'}{\partial y'} \quad \ldots \quad (11)$$

The equation (11) can be expressed as

$$0 = \frac{\partial p}{\partial y'} + \frac{1}{2\mu_e} \frac{\partial \left(B_x'\right)^2}{\partial y'} \quad \ldots \quad (12)$$

We recall that B_x' is small which suggests that $(B_x')^2$ can be neglected and as a consequence, the equation (12) takes the following form :

$$0 = \frac{\partial p}{\partial y'} \quad \ldots \quad (13)$$

The equation (13) shows that *p* is independent of y' indicating the fact that the pressure near the plate is the same as that far away from the plate along a normal to theplate. This phenomenon comprehensively establishes the fact that as we move far away from the plate, the equation (10) becomes

$$\frac{\partial p}{\partial x'} = -\rho_\infty g \quad \ldots \quad (14)$$

Elimination of $\frac{\partial p}{\partial x'}$ from (10) and (14) yields

$$\rho \frac{\partial u'}{\partial t'} = \mu \frac{\partial^2 u'}{\partial y'^2} + (\rho_\infty - \rho) g + \frac{B_0}{\mu_e} \frac{\partial B_x'}{\partial y'} \quad \ldots \quad (15)$$

The equation of state on the basis of classical Boussinesq approximation is

$$\rho = \rho_\infty \left[1 - \beta (T' - T_\infty') - \bar{\beta} (C' - C_\infty')\right]. \quad \ldots \quad (16)$$

On unification of the equations (15) and (16) accomplished by the fact $\rho_\infty \simeq \rho$, we derive the following linear partial differential equation

$$\frac{\partial u'}{\partial t'} = \upsilon \frac{\partial^2 u'}{\partial y'^2} + g\beta (T' - T_\infty') + g\bar{\beta} (C' - C_\infty') + \frac{\sigma B_0 \eta}{\rho} \frac{\partial B_x'}{\partial y'} \quad \ldots \quad (17)$$

The assumptions (*ii*) and (*ix*) lead the energy equation (5) to reduce to the form

$$\rho C_p \frac{\partial T'}{\partial t'} = k \frac{\partial^2 T'}{\partial y'^2} - \frac{\partial q_r}{\partial y'} \quad \ldots \quad (18)$$

The reduced form of the species continuity equation (6) based on axiom (*x*) is as given below

$$\frac{\partial C'}{\partial t'} = D_M \frac{\partial^2 C'}{\partial y'^2} + D_T \frac{\partial^2 T'}{\partial y'^2} + \bar{K} (C_\infty' - C') \quad \ldots \quad (19)$$

The magnetic diffusion equation (7) takes the form

$$\frac{\partial B_x'}{\partial t'} = \eta \frac{\partial^2 B_x'}{\partial y'^2} \quad \ldots \quad (20)$$

The appropriate initial and boundary conditions to be satisfied by the equations (17), (18), (19) and (20) are

$$u' = 0, \quad T' = T_\infty', \quad C' = C_\infty', B_x' = 0 \; \forall y \geq 0, \; t' \leq 0 \quad \ldots \quad (21)$$

$$\left.\begin{array}{lll} u' = U_0, & T' = T_w', \; C' = C_w', \; B_x' = H_0 & \text{at} \quad y' = 0 \\ u' = 0, & T' = T_\infty', \; C' = C_\infty', \; B_x' = 0 & \text{as} \quad y' \to \infty \end{array}\right\} \forall t' > 0 \quad \ldots \quad (22)$$

It is emphasized by Cogley, et. al.[28] that the rate of rediative flux in optically thin limit for a non-Gray gas near equilibrium is given by

$$\frac{\partial q_r}{\partial y'} = 4I\left(T' - T'_\infty\right) \quad \ldots \quad (23)$$

where

$$I = \int_0^\infty \left(K_\lambda\right)_\omega \left(\frac{\partial e_{b\lambda}}{\partial T'}\right)_\omega d\lambda \quad \ldots \quad (24)$$

On use of (23), (18) reduces to

$$\rho C_p \frac{\partial T'}{\partial t'} = k \frac{\partial^2 T'}{\partial y'^2} - 4I\left(T' - T'_\infty\right) \quad \ldots \quad (25)$$

Proceeding with the analysis, we introduce the following non-dimensional variables and similarity parameters to normalize the flow model.

$$u = \frac{u'}{U_0}, \quad y = \frac{y' U_0}{\upsilon}, \quad t = \frac{t' U_0^2}{\upsilon}, \quad Gr = \frac{\upsilon g \beta \left(T'_w - T'_\infty\right)}{U_0^3}, \quad Gm = \frac{\upsilon g \bar{\beta}\left(C'_w - C'_\infty\right)}{U_0^3},$$

$$\theta = \frac{T' - T'_\infty}{T'_w - T'_\infty}, \quad \phi = \frac{C' - C'_\infty}{C'_w - C'_\infty}, \quad Pr = \frac{\mu C_p}{k}, \quad Q = \frac{4I\upsilon^2}{kU_0^2}, \quad M = \frac{\sigma B_0^2 \upsilon}{\rho U_0^2},$$

$$Sc = \frac{\upsilon}{D_M}, \quad Sr = \frac{D_T\left(T'_w - T'_\infty\right)}{\upsilon\left(C'_w - C'_\infty\right)}, \quad K = \frac{\bar{K}\upsilon}{U_0^2}, \quad B_x = \frac{B_x'}{H_0},$$

$$\lambda = \frac{H_0}{B_0}, \quad Pm = \frac{\upsilon}{\eta} \quad \ldots \quad (26)$$

All the above quantities are defined in the nomenclature.

In the present investigation, there is no characteristic length and hence the magnetic Reynolds number or viscous Reynolds number does not appear explicitly. However, the induced hydromagnetic effect is characterized by the existence of the magnetic Prandtl number *Pm* as defined in the transformation (26).

By virtue of transformations cum definitions (26), the equations (17), (25), (19) and (20) in normalized form become

$$\frac{\partial u}{\partial t} = Gr\,\theta + Gm\,\phi + \frac{M\lambda}{Pm}\frac{\partial B_x}{\partial y} + \frac{\partial^2 u}{\partial y^2}, \qquad \ldots \quad (27)$$

$$Pr\frac{\partial \theta}{\partial t} = \frac{\partial^2 \theta}{\partial y^2} - Q\theta, \qquad \ldots \quad (28)$$

$$\frac{\partial \phi}{\partial t} = \frac{1}{Sc}\frac{\partial^2 \phi}{\partial y^2} + Sr\frac{\partial^2 \theta}{\partial y^2} - K\phi, \qquad \ldots \quad (29)$$

$$\frac{\partial B_x}{\partial t} = \frac{1}{Pm}\frac{\partial^2 B_x}{\partial y^2}. \qquad \ldots \quad (30)$$

The relevant initial and boundary conditions in non-dimensional form are as follows :

$$u = 0,\ \ \theta = 0,\ \ \phi = 0, B_x = 0 \ \ \forall y \geq 0,\ t \leq 0 \qquad \ldots \quad (31)$$

$$\left.\begin{array}{lll} u = 1, & \theta = 1, & \phi = 1,\ B_x = 1 \quad \text{at } y = 0 \\ u = 0, & \theta = 0, & \phi = 0, B_x = 0 \quad \text{as } y \to \infty \end{array}\right\}, t > 0 \qquad \ldots \quad (32)$$

3. Method of solution

On taking Laplace Transforms of the equations (30), (28), (29) and (27) and the conditions (31) and (32), the mixed initial and the boundary value problem reduces to a boundary value problem governed by the following equations :

$$\frac{d^2 \overline{B}_x}{dy^2} = Pm\,s\,\overline{B}_x, \qquad \ldots \quad (33)$$

$$\frac{d^2 \overline{\theta}}{dy^2} - (Q + Pr\,s)\overline{\theta} = 0, \qquad \ldots \quad (34)$$

$$\frac{d^2 \overline{\phi}}{dy^2} - (s + K)Sc\,\overline{\phi} = -Sc\,Sr\frac{d^2 \overline{\theta}}{dy^2}, \qquad \ldots \quad (35)$$

$$\frac{d^2 \overline{u}}{dy^2} - s\,\overline{u} = -Gr\,\overline{\theta} - Gm\,\overline{\phi} - \frac{M\lambda}{Pm}\frac{d\overline{B}_x}{dy}. \qquad \ldots \quad (36)$$

Subject to

$$\bar{u} = \frac{1}{s},\ \ \bar{\theta} = \frac{1}{s},\ \ \bar{\phi} = \frac{1}{s},\ \ \bar{B}_x = \frac{1}{s} \ \text{ at } y = 0, \qquad \ldots \quad (37)$$

$$\bar{u} = 0,\ \ \bar{\theta} = 0,\ \ \bar{\phi} = 0,\ \ \bar{B}_x = 0 \ \text{ as } y \to \infty. \qquad \ldots \quad (38)$$

The solutions of the equations (33), (34), (35) and (36) under the conditions (37) and (38) are

$$\bar{B}_x = \frac{1}{s} e^{-\sqrt{Pm\, s}\, y}, \qquad \ldots \quad (39)$$

$$\bar{\theta} = \frac{1}{s} e^{-\sqrt{Pr\, s + Q}\, y}, \qquad \ldots \quad (40)$$

$$\bar{\phi} = \left\{ \frac{1}{s}\left(1 + \lambda_1 A_1\right) + \frac{B_1 \lambda_1}{s + a_2} \right\} e^{-\sqrt{(s+K)Sc}\, y} - \lambda_1 \left(\frac{A_1}{s} + \frac{B_1}{s + a_2} \right) e^{-\sqrt{Pr(s+a_1)}\, y} \quad \ldots (41)$$

$$\bar{u} = \begin{cases}
S_1 e^{-\sqrt{s}y} - Gr\, S_2 e^{-\sqrt{\Pr(s+a_1)}y} - Gm\left[S_3 e^{-\sqrt{(s+K)Sc}y} - S_4 e^{-\sqrt{(s+a_1)\Pr}y} \right] + S_5 e^{-\sqrt{Pm\, s}y}; Pr \neq 1, Pm \neq 1, Sc \neq 1 \\
S_9 e^{-\sqrt{s}y} - \dfrac{Gr e^{-\sqrt{(s+Q)}y}}{Q s} - Gm\left[S_3 e^{-\sqrt{(s+K)Sc}y} - S_6 e^{-\sqrt{(s+Q)}y} \right] + S_5 e^{-\sqrt{Pm\, s}y}; Pr = 1, Pm \neq 1, Sc \neq 1 \\
S_{10} e^{-\sqrt{s}y} - Gr\, S_2 e^{-\sqrt{\Pr(s+a_1)}y} - Gm\left[S_3 e^{-\sqrt{(s+K)Sc}y} - S_4 e^{-\sqrt{(s+a_1)\Pr}y} \right] - y S_7 e^{-\sqrt{s}y}; Pr \neq 1, Pm = 1, Sc \neq 1 \\
S_{11} e^{-\sqrt{s}y} - Gr\, S_2 e^{-\sqrt{\Pr(s+a_1)}y} - Gm\left[S_8 e^{-\sqrt{(s+K)}y} - S_4 e^{-\sqrt{(s+a_1)\Pr}y} \right] + S_5 e^{-\sqrt{Pm\, s}y}; Pr \neq 1, Pm \neq 1, Sc = 1 \\
S_{12} e^{-\sqrt{s}y} - \dfrac{Gr e^{-\sqrt{(s+Q)}y}}{Q s} - Gm\left[S_3 e^{-\sqrt{(s+K)Sc}y} - S_6 e^{-\sqrt{(s+Q)}y} \right] - y S_7 e^{-\sqrt{s}y}; Pr = 1, Pm = 1, Sc \neq 1 \\
S_{13} e^{-\sqrt{s}y} - Gr\, S_2 e^{-\sqrt{\Pr(s+a_1)}y} - Gm\left[S_8 e^{-\sqrt{(s+K)}y} - S_4 e^{-\sqrt{(s+a_1)\Pr}y} \right] - y S_7 e^{-\sqrt{s}y}; Pr \neq 1, Pm = 1, Sc = 1 \\
S_{14} e^{-\sqrt{s}y} - \dfrac{Gr e^{-\sqrt{(s+Q)}y}}{Q s} - Gm\left[S_8 e^{-\sqrt{(s+K)}y} - S_6 e^{-\sqrt{(s+Q)}y} \right] + S_5 e^{-\sqrt{Pm\, s}y}; Pr = 1, Pm \neq 1, Sc = 1 \\
S_{15} e^{-\sqrt{s}y} - \dfrac{Gr e^{-\sqrt{(s+Q)}y}}{Q s} - Gm\left[S_8 e^{-\sqrt{(s+K)}y} - S_6 e^{-\sqrt{(s+Q)}y} \right] - y S_7 e^{-\sqrt{s}y}; Pr = 1, Pm = 1, Sc = 1
\end{cases} \quad \ldots (42)$$

where

$$a_1 = \frac{Q}{Pr}, a_2 = \frac{Pr\, a_1 - K\, Sc}{Pr - \mathrm{Sc}}, a_3 = \frac{Pr\, a_1}{Pr - 1}, a_4 = \frac{K\, Sc}{Sc - 1},$$

$$A_1 = \frac{a_1}{a_2}, B_1 = \frac{a_2 - a_1}{a_2}, \ \ \lambda_1 = \frac{Sc\, Sr\, Pr}{Pr - Sc},$$

$$S_1 = \frac{1}{s} + Gr\,S_2 + Gm\left(S_3 - S_4\right) - S_5,\ S_2 = \frac{1}{Pr-1}\left(\frac{A_2}{s} + \frac{B_2}{s+a_3}\right),$$

$$S_3 = \frac{1}{Sc-1}\left(\frac{A_3}{s} + \frac{A_4}{s+a_2} + \frac{A_5}{s+a_4}\right), S_4 = \frac{\lambda_1}{Pr-1}\left(\frac{B_3}{s} + \frac{B_4}{s+a_2} + \frac{B_5}{s+a_3}\right),$$

$$S_5 = \frac{M\lambda}{s\sqrt{s\,Pm}\left(Pm-1\right)}, A_2 = -B_2 = \frac{1}{a_3}, A_3 = \frac{1+\lambda_1 A_1}{a_4},$$

$$A_4 = \frac{B_1\lambda_1}{a_4 - a_2}, A_5 = -A_4 - A_3,\ B_3 = \frac{A_1}{a_3}, B_4 = \frac{B_1}{a_3 - a_2}, B_5 = -B_4 - B_3,$$

$$S_6 = \frac{\lambda_1}{Q}\left(\frac{A_1}{s} + \frac{B_1}{s+a_2}\right), S_7 = \frac{M\lambda}{2s},\quad S_8 = \frac{1}{K}\left(\frac{1+\lambda_1 A_1}{s} + \frac{B_1\lambda_1}{s+a_2}\right),$$

$$S_9 = \frac{1}{s} + \frac{Gr}{sQ} + Gm\left(S_3 - S_6\right) - S_5,\ S_{10} = \frac{1}{s} + GrS_2 + Gm\left(S_3 - S_4\right),$$

$$S_{11} = \frac{1}{s} + GrS_2 + Gm\left(S_8 - S_4\right) - S_5,\ S_{12} = \frac{1}{s} + \frac{Gr}{Qs} + Gm\left(S_3 - S_6\right),$$

$$S_{13} = \frac{1}{s} + GrS_2 + Gm\left(S_8 - S_4\right),\ S_{14} = \frac{1}{s} + \frac{Gr}{Qs} + Gm\left(S_8 - S_6\right) - S_5,$$

$$S_{15} = \frac{1}{s} + \frac{Gr}{Qs} + Gm\left(S_8 - S_6\right).$$

Taking inverse Laplace Transforms of (39), (40), (41) and (42), the representative induced magnetic field, and temperature, concentration and the velocity fields are obtained as follows :

$$B_x = \operatorname{erfc}\left(\frac{y\sqrt{Pm}}{2\sqrt{t}}\right), \qquad \ldots \quad (43)$$

$$\theta = f\left(y\sqrt{Pr}, a_1, t\right), \qquad \ldots \quad (44)$$

$$\phi = \left(1+\lambda_1 A_1\right)L_1 + B_1\lambda_1 L_2 - A_1\lambda_1 L_3 - B_1\lambda_1 L_4, \qquad \ldots \quad (45)$$

$$u=\begin{cases} M_1-\dfrac{Gr}{Pr-1}M_2-Gm\,M_3+\dfrac{M\lambda}{(Pm-1)\sqrt{Pm}}M_4;\ Pr\neq 1, Pm\neq 1, Sc\neq 1 \\ E_1-Gr\,E_2-Gm\,E_3+\dfrac{M\lambda}{(Pm-1)\sqrt{Pm}}M_4;\ Pr=1, Pm\neq 1, Sc\neq 1 \\ N_1-\dfrac{Gr}{Pr-1}M_2-Gm\,M_3-\dfrac{M\lambda}{2}N_4;\ Pr\neq 1, Pm=1, Sc\neq 1 \\ K_1-\dfrac{Gr}{Pr-1}M_2-Gm\,K_3+\dfrac{M\lambda}{(Pm-1)\sqrt{Pm}}M_4;\ Pr\neq 1, Pm\neq 1, Sc=1 \\ F_1-Gr\,E_2-Gm\,E_3-\dfrac{M\lambda}{2}N_4;\ Pr=1, Pm=1, Sc\neq 1 \\ G_1-\dfrac{Gr}{Pr-1}M_2-Gm\,K_3-\dfrac{M\lambda}{2}N_4;\ Pr\neq 1, Pm=1, Sc=1 \\ H_1-Gr\,E_2-Gm\,H_3+\dfrac{M\lambda}{(Pm-1)\sqrt{Pm}}M_4;\ Pr=1, Pm\neq 1, Sc=1 \\ J_1-Gr\,E_2-Gm\,H_3-\dfrac{M\lambda}{2}N_4;\ Pr=1, Pm=1, Sc=1 \end{cases} \quad \ldots (46)$$

where

$$L_1=f\left(y\sqrt{Sc},K,t\right),\quad L_2=e^{-a_2t}f\left(y\sqrt{Sc},K-a_2,t\right),$$

$$L_3=f\left(y\sqrt{Pr},a_1,t\right),\quad L_4=e^{-a_2t}f\left(y\sqrt{Pr},a_1-a_2,t\right),$$

$$M_1=\xi+\frac{Gr}{Pr-1}\xi_1+Gm\left(\frac{1}{Sc-1}\xi_2-\frac{\lambda_1}{Pr-1}\xi_3\right)+\xi_4,$$

$$M_2=A_2\,f\left(y\sqrt{Pr},a_1,t\right)+B_2\,e^{-a_3t}f\left(y\sqrt{Pr},a_1-a_3,t\right),$$

$$M_3=M_{3,1}-M_{3,2}.$$

$$M_{3,1}=\frac{1}{Sc-1}\Big[A_3f\left(y\sqrt{Sc},K,t\right)+A_4e^{-a_2t}f\left(y\sqrt{Sc},K-a_2,t\right)$$

$$+A_5e^{-a_4t}f\left(y\sqrt{Sc},K-a_4,t\right)\Big],$$

$$M_{3,2} = \frac{\lambda_1}{Pr-1}\Big[B_3 f\left(y\sqrt{Pr}, a_1, t\right) + B_4 e^{-a_2 t} f\left(y\sqrt{Pr}, a_1 - a_2, t\right) + B_5 e^{-a_3 t} f\left(y\sqrt{Pr}, a_1 - a_3, t\right)\Big],$$

$$M_4 = 2\sqrt{\frac{t}{\pi}} e^{-\frac{Pm\, y^2}{4t}} - y\sqrt{Pm}\, erfc\left(\frac{y\sqrt{Pm}}{2\sqrt{t}}\right),$$

$$\xi = erfc\left(\frac{y}{2\sqrt{t}}\right),\ \xi_1 = A_2\xi + B_2 e^{-a_3 t} f\left(y, -a_3, t\right),$$

$$\xi_2 = A_3\xi + A_4 e^{-a_2 t} f\left(y, -a_2, t\right) + A_5 e^{-a_4 t} f\left(y, -a_4, t\right),$$

$$\xi_3 = B_3\xi + B_4 e^{-a_2 t} f\left(y, -a_2, t\right) + B_5 e^{-a_3 t} f\left(y, -a_3, t\right),$$

$$\xi_4 = -\frac{M\lambda}{Pm\sqrt{Pm-1}}\left[2\sqrt{\frac{t}{\pi}} e^{-\frac{y^2}{4t}} - y\xi\right],$$

$$f\left(\xi, \eta, t\right) = \frac{1}{2}\left[e^{\xi\sqrt{\eta}}\, erfc\left(\frac{\xi}{2\sqrt{t}} + \sqrt{\eta t}\right) + e^{-\xi\sqrt{\eta}}\, erfc\left(\frac{\xi}{2\sqrt{t}} - \sqrt{\eta t}\right)\right],$$

$$E_1 = \xi + \frac{Gr}{Q}\xi + Gm\, E_{1,3} + \xi_4,$$

$$E_{1,3} = \frac{1}{Sc-1}\left[\xi_2 - \frac{\lambda_1}{Q}\left(A_1\xi + B_1 e^{-a_2 t} f\left(y, -a_2, t\right)\right)\right],$$

$$E_2 = \frac{1}{Q} f\left(y, Q, t\right),$$

$$E_3 = M_{3,1} - \frac{\lambda}{Q}\left[A_1 f\left(y, Q, t\right) + B_1 e^{-a_2 t} f\left(y, Q - a_2, t\right)\right],$$

$$N_1 = \xi + \frac{Gr}{Pr-1}\xi_1 + Gm\left(\frac{1}{Sc-1}\xi_2 - \frac{\lambda}{Pr-1}\xi_3\right),$$

$$N_4 = y\xi,$$

$$K_1 = \xi + \frac{Gr}{Pr-1}\xi_1 + Gm\left(\frac{1+\lambda_1 A_1}{K}\xi + \frac{B_1\lambda_1}{K}e^{-a_2 t} f\left(y,-a_2,t\right) - \frac{\lambda_1}{Pr-1}\xi_3\right) + \xi_4 ,$$

$$K_3 = \frac{1+\lambda_1 A_1}{K} f\left(y,K,t\right) + \frac{B_1\lambda_1}{K}e^{-a_2 t} f\left(y,K-a_2,t\right) - M_{3,2} ,$$

$$F_1 = \xi + \frac{Gr}{Q}\xi + Gm\, E_{1,3} ,$$

$$G_1 = \xi + \frac{Gr}{Pr-1}\xi_1 + Gm\left(\frac{1+\lambda_1 A_1}{K}\xi + \frac{B_1\lambda_1}{K}e^{-a_2 t} f\left(y,-a_2,t\right) - \frac{\lambda}{Pr-1}\xi_3\right),$$

$$H_1 = \xi + \frac{Gr}{Q}\xi + Gm\, H_{1,3} + \xi_4 ,$$

$$H_{1,3} = \frac{1+\lambda_1 A_1}{K}\xi + \frac{B_1\lambda_1}{K}e^{-a_2 t} f\left(y,-a_2,t\right) - \frac{\lambda_1}{Q}\left(A_1\xi + B_1 e^{-a_2 t} f\left(y,-a_2,t\right)\right),$$

$$H_3 = \frac{1+\lambda_1 A_1}{K} f\left(y,K,t\right) + \frac{B_1\lambda_1}{K}e^{-a_2 t} f\left(y,K-a_2,t\right) - \frac{\lambda_1}{Q}\Big[A_1 f\left(y,Q,t\right) + B_1 e^{-a_2 t} f\left(y,Q-a_2,t\right)\Big],$$

$$J_1 = \xi + \frac{Gr}{Q}\xi + Gm\, H_{1,3} .$$

4. Coefficient of skin-friction

The viscous drag at the plate per unit area in the direction of the plate velocity is quantified by the Newton's law of viscosity in the form :

$$\tau' = \frac{\mu\partial u'}{\partial y'}\Bigg]_{y'=0} = \rho U_0^2 \frac{\partial u}{\partial y}\Bigg]_{y=0} . \qquad \ldots \quad (47)$$

The coefficient of the skin-friction at the plate is as follows :

$$\tau = \frac{\tau'}{\rho U_0^2} = \frac{\partial u}{\partial y}\Bigg]_{y=0} ,$$

$$= \begin{cases} \psi_1 - \dfrac{Gr}{Pr-1}\psi_2 - Gm\psi_3 + \dfrac{M\lambda}{Pm-1}\sqrt{\dfrac{Pm}{\pi t}}; Pr \neq 1,\ Sc \neq 1, Pm \neq 1 \\ \psi_4 - \dfrac{Gr}{Q}\varphi(Q,t) - Gm\psi_5 + \dfrac{M\lambda}{Pm-1}\sqrt{\dfrac{Pm}{\pi t}}; Pr = 1,\ Sc \neq 1, Pm \neq 1 \\ \psi_6 - \dfrac{Gr}{Pr-1}\psi_2 - Gm\psi_3 - \dfrac{M\lambda}{2}; Pr \neq 1,\ Sc \neq 1, Pm = 1 \\ \psi_7 - \dfrac{Gr}{Pr-1}\psi_2 - Gm\psi_8 + \dfrac{M\lambda}{Pm-1}\sqrt{\dfrac{Pm}{\pi t}}; Pr \neq 1,\ Sc = 1, Pm \neq 1 \\ \psi_9 - \dfrac{Gr}{Q}\varphi(Q,t) - Gm\psi_5 - \dfrac{M\lambda}{2}; Pr = 1,\ Sc \neq 1, Pm = 1 \\ \psi_{10} - \dfrac{Gr}{Pr-1}\psi_2 - Gm\psi_8 - \dfrac{M\lambda}{2}; Pr \neq 1,\ Sc = 1, Pm = 1 \\ \psi_{13} - \dfrac{Gr}{Q}\varphi(Q,t) - Gm\psi_{12} + \dfrac{M\lambda}{Pm-1}\sqrt{\dfrac{Pm}{\pi t}}; Pr = 1,\ Sc = 1, Pm \neq 1 \\ \psi_{14} - \dfrac{Gr}{Q}\varphi(Q,t) - Gm\psi_{12} - \dfrac{M\lambda}{2}; Pr = 1,\ Sc = 1, Pm = 1 \end{cases} \quad \ldots \quad (48)$$

where

$$\psi_1 = \psi_{1,1} + Gm\left[\frac{1}{Sc-1}\psi_{1,2} - \frac{\lambda_1}{Pr-1}\psi_{1,3}\right] + \frac{M\lambda}{(Pm-1)\sqrt{Pm}},$$

$$\psi_2 = \sqrt{Pr}\left[A_2\,\varphi(a_1,t) + B_2 e^{-a_3 t}\varphi(a_1 - a_3, t)\right],$$

$$\psi_3 = \frac{1}{Sc-1}\psi_{3,1} - \frac{\lambda_1}{Pr-1}\psi_{3,2},$$

$$\psi_4 = -\frac{1}{\sqrt{\pi t}} - \frac{Gr}{Q\sqrt{\pi t}} + Gm\left[\frac{1}{Sc-1}\psi_{4,1} - \frac{\lambda_1}{Q}\psi_{4,2}\right] + \frac{M\lambda}{(Pm-1)\sqrt{Pm}},$$

$$\psi_5 = \frac{\sqrt{Sc}}{Sc-1}\psi_{5,1} - \frac{\lambda_1}{Q}\psi_{5,2},$$

$$\psi_6 = \psi_{1,1} + Gm\left[\frac{1}{Sc-1}\psi_{1,2} - \frac{\lambda_1}{\mathrm{Pr}-1}\psi_{1,3}\right],$$

$$\psi_7 = \psi_{1,1} + Gm\left[\psi_{7,1} - \frac{\lambda_1}{Pr-1}\psi_{7,2}\right] + \frac{M\lambda}{(Pm-1)\sqrt{Pm}},$$

$$\psi_8 = \frac{1+\lambda_1 A_1}{K}\varphi(K,t) + \frac{B_1\lambda_1}{K}e^{-a_2 t}\varphi(K-a_2,t) - \frac{\lambda_1}{\mathrm{Pr}-1}\psi_{3,2},$$

$$\psi_9 = -\frac{1}{\sqrt{\pi t}} - \frac{Gr}{Q\sqrt{\pi t}} + Gm\left[\frac{1}{Sc-1}\psi_{4,1} - \frac{\lambda_1}{Q}\psi_{4,2}\right],$$

$$\psi_{10} = -\frac{1}{\sqrt{\pi t}} - \frac{Gr}{Pr-1}\left[\frac{-A_2}{\sqrt{\pi t}} + B_2 e^{-a_3 t}\varphi(-a_3,t)\right] + Gm\left[\psi_{7,1} - \frac{\lambda_1}{Pr-1}\psi_{7,2} + B_5 e^{-a_3 t}\varphi(-a_3,t)\right],$$

$$\psi_{11} = -\frac{1+\lambda_1 A_1}{K}\frac{1}{\sqrt{\pi t}} + \frac{B_1\lambda_1}{K}e^{-a_2 t}\varphi(-a_2,t) - \frac{\lambda_1}{Q}\left[-\frac{A_1}{\sqrt{\pi t}} + B_1 e^{-a_2 t}\varphi(-a_2,t)\right],$$

$$\psi_{12} = -\frac{1+\lambda_1 A_1}{K}\varphi(K,t) + \frac{B_1\lambda_1}{K}e^{-a_2 t}\varphi(K-a_2,t) - \frac{\lambda_1}{Q}\left[A_1\varphi(Q,t) + B_1 e^{-a_2 t}\varphi(Q-a_2,t)\right],$$

$$\psi_{13} = -\frac{1}{\sqrt{\pi t}} - \frac{Gr}{Q\sqrt{\pi t}} + Gm\,\psi_{11} + \frac{M\lambda}{(Pm-1)\sqrt{Pm}},$$

$$\psi_{14} = -\frac{1}{\sqrt{\pi t}} - \frac{Gr}{Q\sqrt{\pi t}} + Gm\,\psi_{12} - \frac{M\lambda}{2},$$

$$\psi_{1,1} = -\frac{1}{\sqrt{\pi t}} - \frac{Gr}{Pr-1}\left(-\frac{A_2}{\sqrt{\pi t}} + B_2 e^{-a_3 t}\varphi(-a_3,t)\right),$$

$$\psi_{1,2} = -\frac{A_3}{\sqrt{\pi t}} + A_4 e^{-a_2 t}\varphi(-a_2,t) + A_5 e^{-a_4 t}\varphi(-a_4,t),$$

$$\psi_{1,3} = -\frac{B_3}{\sqrt{\pi t}} + B_4 e^{-a_2 t}\varphi(-a_2,t) + B_5 e^{-a_3 t}\varphi(-a_3,t),$$

$$\psi_{3,1} = \sqrt{Sc}\left[A_3\varphi(K,t) + A_4 e^{-a_2 t}\varphi(K-a_2,t) + A_5 e^{-a_4 t}\varphi(K-a_4,t)\right],$$

$$\psi_{3,2} = \sqrt{Pr}\left[B_3\varphi(a_1,t) + B_4 e^{-a_2 t}\varphi(a_1-a_2,t) + B_5 e^{-a_3 t}\varphi(a_1-a_3,t)\right],$$

$$\varphi(\eta,t) = -\frac{1}{\sqrt{\pi t}}e^{-\eta t} - \sqrt{\eta}\,erf\left(\sqrt{\eta t}\right),$$

$$\psi_{4,1} = -\frac{A_3}{\sqrt{\pi t}} + A_4 e^{-a_2 t}\varphi(-a_2,t) + A_5 e^{-a_4 t}\varphi(-a_4,t) = \psi_{1,2},$$

$$\psi_{4,2} = -\frac{A_1}{\sqrt{\pi t}} + B_1 e^{-a_2 t}\varphi(-a_2,t),$$

$$\psi_{5,1} = A_3\varphi(K,t) + A_4 e^{-a_2 t}\varphi(K-a_2,t) + A_5 e^{-a_4 t}\varphi(K-a_4,t),$$

$$\psi_{5,2} = A_1\varphi(Q,t) + B_1 e^{-a_2 t}\varphi(Q-a_2,t),$$

$$\psi_{7,1} = -\frac{1+\lambda_1 A_1}{K}\frac{1}{\sqrt{\pi t}} + \frac{B_1\lambda_1}{K}e^{-a_2 t}\varphi(-a_2,t),$$

$$\psi_{7,2} = -\frac{B_3}{\sqrt{\pi t}} + B_4 e^{-a_2 t}\varphi(-a_2,t) + B_5 e^{-a_3 t}\varphi(-a_3,t).$$

5. Coefficient of rate of heat transfer

The heat flux q^* from the plate to the fluid is quantified by the Fourier law of conduction in the form

$$q^* = -k\frac{\partial T'}{\partial y'}\Big]_{y'=0} = -k\frac{U_0}{\upsilon}(T'_w - T'_\infty)\frac{\partial\theta}{\partial y}\Big]_{y=0}. \qquad \ldots \quad (49)$$

The coefficient of the rate of heat transfer from the plate to the fluid in term of the Nusselt number is given by

$$Nu = \frac{\upsilon q^*}{kU_0(T'_w - T'_\infty)} = -\frac{\partial\theta}{\partial y}\Big]_{y=0} = \sqrt{Pr}\,\varphi(a_1,t). \qquad \ldots \quad (50)$$

6. Coefficient of mass transfer

The mass flux *Mw* at the plate is determined by the Fick's law of mass diffusion

$$M_w = -D_M\frac{\partial C'}{\partial y'}\Big]_{y'=0} = -\frac{D_M U_0}{\upsilon}(C'_w - C'_\infty)\frac{\partial\phi}{\partial y}\Big]_{y=0}. \qquad \ldots \quad (51)$$

The coefficient of mass transfer at the plate in terms of Sherwood number is given by

$$Sh = \frac{\upsilon M_w}{D_M U_0(C'_w - C'_\infty)} = -\frac{\partial\phi}{\partial y}\Big]_{y=0}$$

$$= -\begin{bmatrix}(1+\lambda_1 A_1)\sqrt{Sc}\;\varphi(K,t) + B_1\lambda_1\sqrt{Sc}\,e^{-a_2 t}\,\phi(K-a_2,t)\\ -\lambda_1 A_1\sqrt{Pr}\,e^{-a_2 t}\,\phi(a_1-a_2,t)\end{bmatrix}. \qquad \ldots \quad (52)$$

7. Results and discussion

In order to get clear insight of the physical problem, numerical computations from the analytical solutions for representative induced magnetic field, velocity field, temperature field, concentration field, and the coefficient of skin-friction, the coefficientof the rate of heat transfer in term of Nusselt number and the rate of mass transfer in term of Sherwood number at the plate have been carried out by assigning some arbitrarily chosen specific admissible values to the similarity parameters like magnetic parameter M (square of the Hartmann number), chemical reaction parameter K, radiation parameter Q, magnetic Prandtl number Pm, time t and the normal coordinate y. Throughout our investigation, the values of the Prandtl number Pr, Soret number Sr, thermal Grashof number Gr, solutal Grashof number Gm, Schmidt number Sc and the ratio of the plate induced magnetic field to the applied magnetic field λ have been fixed at 0.71, 1, 30, 20, 0.6 and 0.5 respectively as the numerical computations are concerned. We recall that Pr = 0.71 corresponds to air and Sc = 0.60 represents water vapor diffused inair at temperature 25^0C and 1 atmospheric pressure. In other words, the dilute mixture with air has been chosen as the solvent and water vapor as the solute. Further it may be stated that normal dry air is not a good conductor, but under certain physical conditions, air may be considered as a reasonably good conductor. Even, in the presence of impurities (*i.e.* chemical species, moisture), the electrical conductivity of the air-impurity mixture gets enhanced. On the basis of this fact, we have chosen some moderate values for Pm, although Pm is very small for normal dry air. The numerical results computed from the analytical solutions of the problem have been illustrated in figure 1 to figure 15.

The variations in the induced magnetic field B_x versus the normal coordinate y under the influence of magnetic Prandtl number Pm are demonstrated in the figure 1. Figure 1 shows that the induced magnetic field B_x falls asymptotically as moved away from the plate. It is inferred from figure 1 that there is a comprehensive rise in induced magnetic field as Pm decreases indicating the fact that increasing magnetic diffusivity causes B_x to increase substantially. This result is consistent to the physical fact that the magnetic lines become freer to pass though a medium of high magnetic diffusivity for which induced magnetic field gets increased.

The velocity profiles under the influence of the chemical reaction parameter K, magnetic Prandtl number Pm, magnetic parameter M, and the

radiation parameter Q are exhibited in figures 2–5. Figures 3 and 4 show that the fluid motion is accelerated under the effect of increasing magnetic Prandtl number Pm as well as thermal radiation. We recall that an increase in Pm means a decrease in magnetic diffusivity when the viscosity of the fluid is kept fixed. It establishes the fact that a fall in magnetic diffusivity of the medium results in a gradual increase in the fluid velocity. It is inferred from figure 2 that an increase in the magnetic parameter M has an inhibiting effect on the fluid velocity to some extent. The fluid velocity u gets continuously reduced in slow rate with increasing M. In other words, the imposition of the transverse magnetic field causes the flow to retard slowly and steadily. This phenomenon has an excellent agreement with the physical fact that the Lorentz force that appears due to interaction of the transverse magnetic field and the fluid velocity acts as a resistive force to the fluid flow which serves to decelerate the flow. The variation in fluid velocity under the effect of first order homogeneous chemical thermal radiation is presented in figure 5. It is observed in this figure that like magnetic field, the effect of consumption of species leads also to a substantial decrease in the fluid velocity. As such the imposition of the magnetic field as well as the consumption of species through chemical reaction is an effective regulatory mechanism for the flow regime. All the figures 2–5 uniquely establish the fact that the fluid velocity first increases in a thin layer adjacent to the plate and thereafter it decreases asymptotically indicating the fact that the buoyancy force has a significant effect on the flow near the plate and its effect gets nullified far away from the plate. In our model the plate temperature is greater than the undisturbed temperature (temperature far away from the plate). Similar result holds good for concentration also. This temperature or concentration gradients result in a density variation in the fluid adjacent to the plate and this density variation causes the buoyancy force to exist. As a resultant effect, an upward vertical fluid velocity in addition to the plate velocity is induced. Due to this fact, the fluid velocity in a very thin layer adjacent to the plate exceeds the plate velocity which is clearly reflected in the figures 2–5 for velocity distributions.

Figure 6 corresponds to the temperature distribution against the normal coordinate y under the influence of Q. A trend of decay in the temperature distribution of the fluid isclearly marked in figure 6 due to radiation and increasing normal coordinate y, thereby reducing comprehensively the thickness of the thermal boundary layer.

The variation in the species concentration ϕ under the influence of thermal radiation and chemical reaction are exhibited in figures 7 and 8. These figures indicate that the species concentration ϕ is enhanced near the plate under the effect of radiation whilst it falls due to effect of chemical reaction. This observation is consistent to the physical fact that when some of the species in a solvent are consumed, and then there is a natural tendency of drop of concentration level of the diffusing medium. One interesting observation is marked in figure 7. There is an indication on the basis of this figure that,for high radiation, the concentration level of the fluid first increases in a very thin layer adjacent to the plate and thereafter it decreases asymptotically to its minimum value as $y \to \infty$, whilst for relatively small radiation it directly falls asymptotically as we move away from the plate.

Figures 9–12 show how the skin friction at the plate is affected due to increasing values of the physical similarity parameters *Pm, M, K* and *Q* at different times. All the figures clearly register the fact that the viscous drag at the plate gets enhanced as time progresses irrespective on the choice of the values of the above parameters. It is further inferred from these figures that an increase in each of the values of the parameters *Pm, M, K* and *Q* results in a steady growth in the frictional force at the plate.

Figures 13 presents, how the Nusselt number *Nu* at the plate $y = 0$ is affected by *Q*, *Pr* and time *t*. The figure establishes the result of enhancement of the rate of heat transfer of the plate under the thermal radiation effect. The influence of *Q* on *Nu* seems to bepronounced in initial stage and thereafter the rate of heat transfer is stabilized. Further it is seen from this figure that initially the rate of fall of the Nusselt number *Nu* is very high and as time progresses the rate of fall of *Nu* becomes almost zero and thereby the rate heat transfer gets stagnated.

The behavior of the Sherwood number which determines the rate of mass transfer from the plate to the fluid is analogous to the behavior of the Nusselt number as the time is concerned as visualized from the figures 14 and 15. The same figures clearly show that the rate of mass transfer is continuously reduced due to radiation as well as chemical reaction indicating the fact that the rate of mass transfer may be inhibited to a marginal extent by making some suitable arrangements so that chemical reaction may take place.

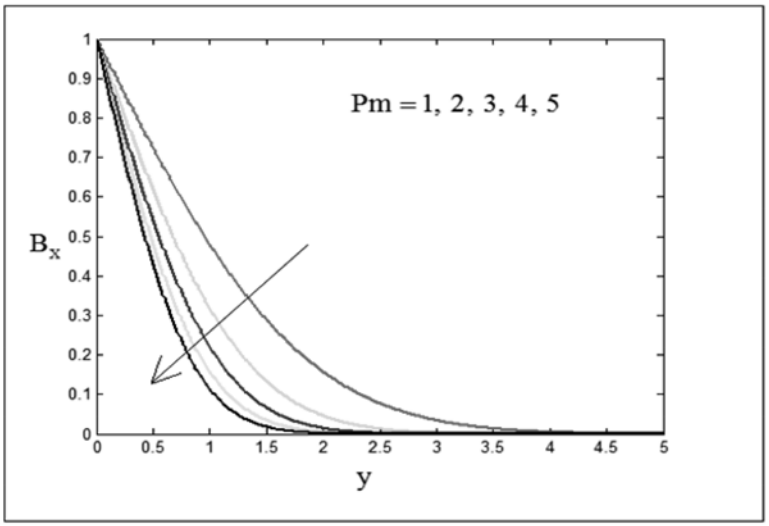

Figure 1
Induced magnetic field versus y for t = 1.

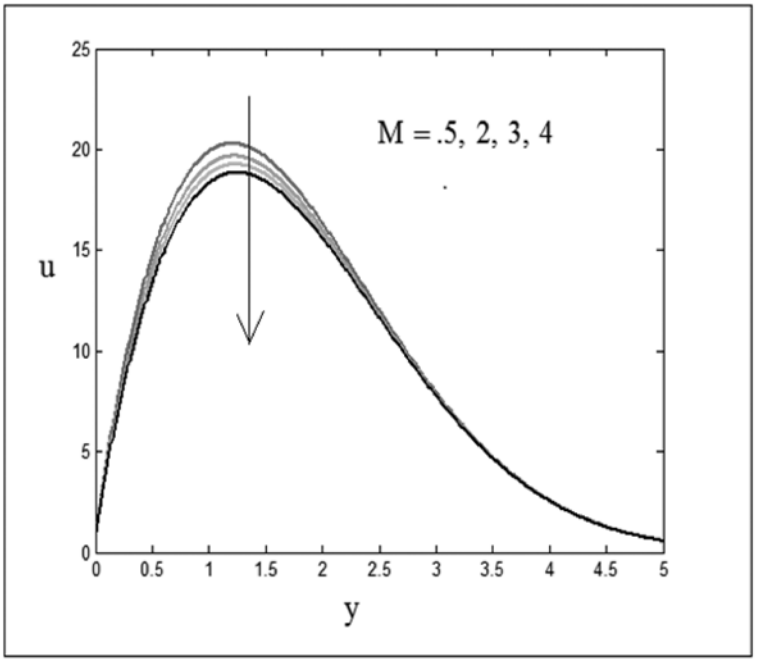

Figure 2
Velocity versus y for Gr = 30, Gm = 20, Pr = .71, Sc = .60, Sr = 1, Pm = 2, Q = .5, K = .5, t =1, λ=.5.

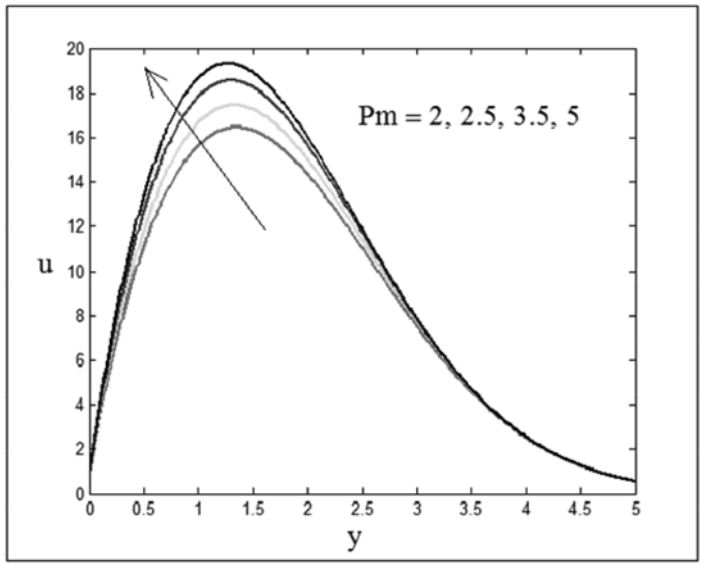

Figure 3
Velocity versus y for $Gr = 30$, $Gm = 20$, $Pr = .71$, $Sc = .60$, $Sr = 1$, $M = 10$, $Q = .5$, $K = .5$, $t=1$, $\lambda=.5$

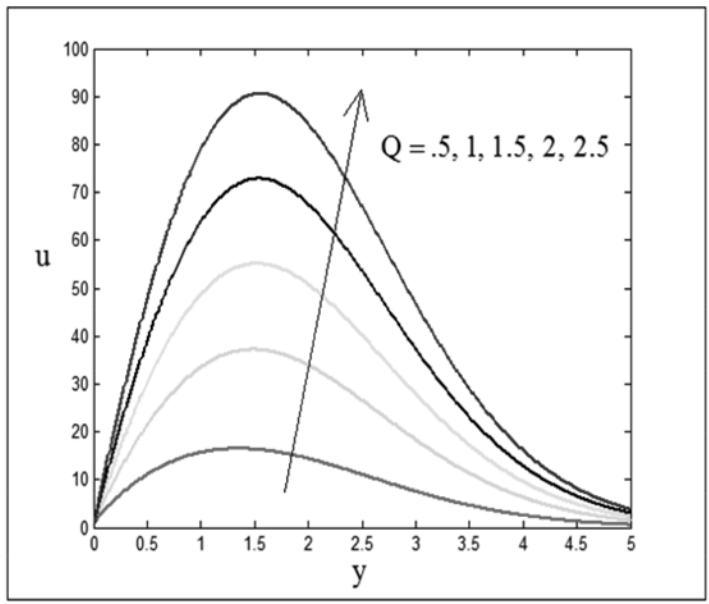

Figure 4
Velocity versus y for $Gr = 30$, $Gm = 20$, $Pr = ·71$, $Sc = ·60$, $Sr = 1$, $Pm = 2$, $M = 10$, $K = ·5$, $t=1$, $\lambda=·5$.

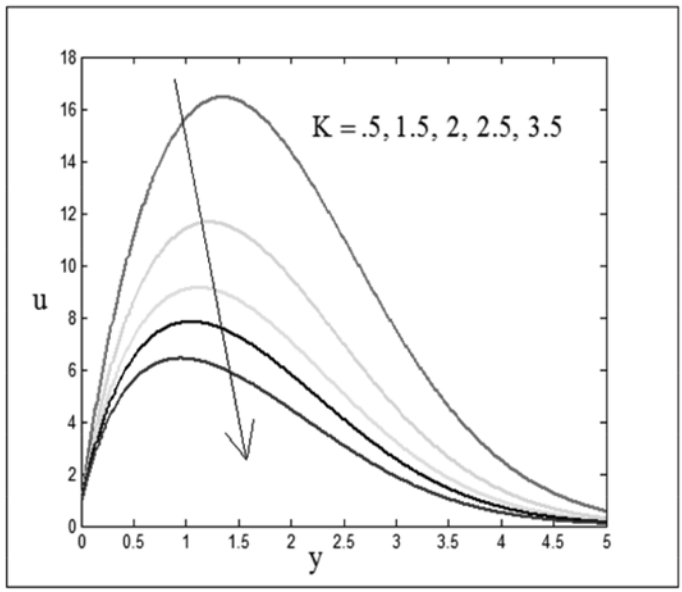

Figure 5
Velocity versus y for $Gr = 30$, $Gm = 20$, $Pr = 0.71$, $Sc = 0.60$, $Sr = 1$, $Pm = 2$, $M = 10$, $Q = 0.5$, $t=1$, $\lambda = 0.5$.

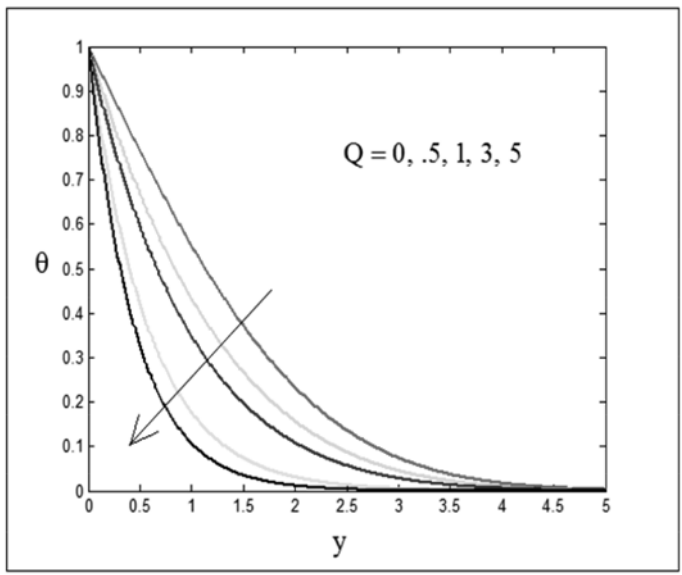

Figure 6
Temperature versus y for $Pr = 0.71$, $t = 1$.

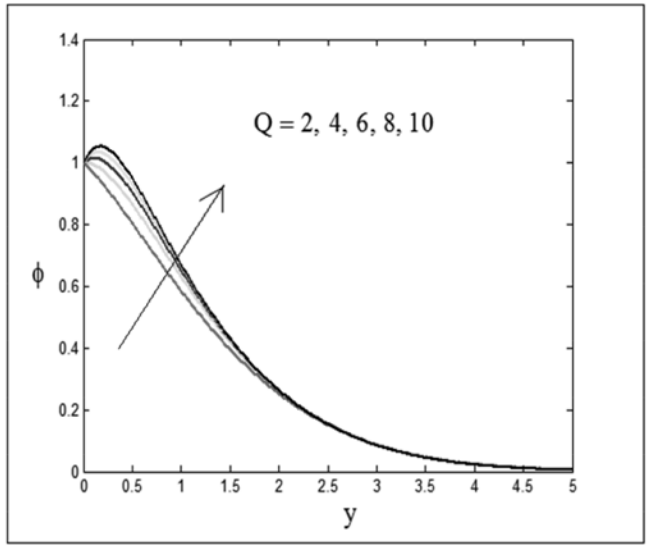

Figure 7
Concentration versus y for $Pr = 0.71$, $Sc = 0.60$, $Sr = 1$, $K = 1$, $t = 1$.

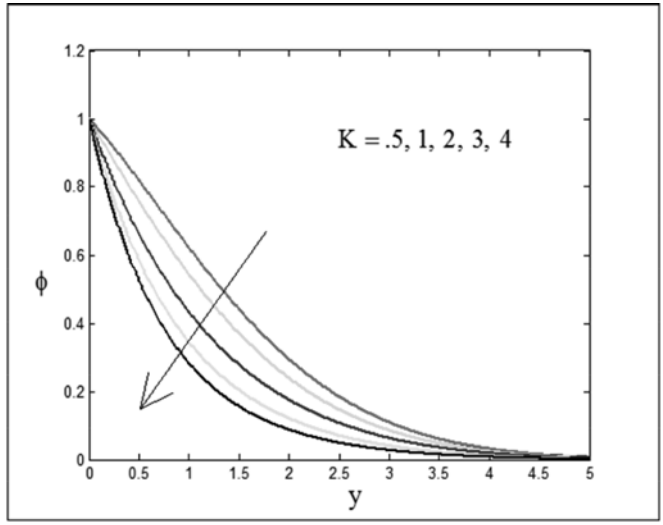

Figure 8
Concentration versus y for $Pr = 0.71$, $Sc = 0.60$, $Sr = 1$, $Q = 1$, $t = 1$.

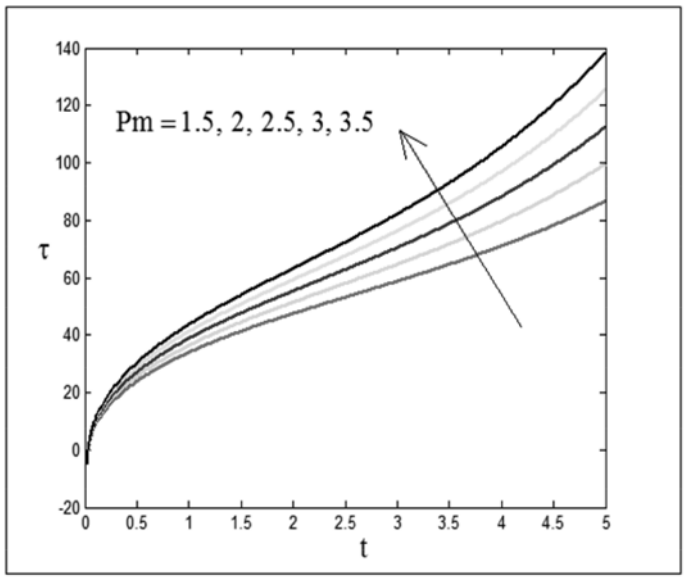

Figure 9
Skin-friction versus y for $Gr = 30$, $Gm = 20$, $Pr = 0.71$, $Sc = 0.60$, $Sr = 1$, $M = 10$, $Q = 0.5$, $K = 0.5$, $\lambda = 0.5$.

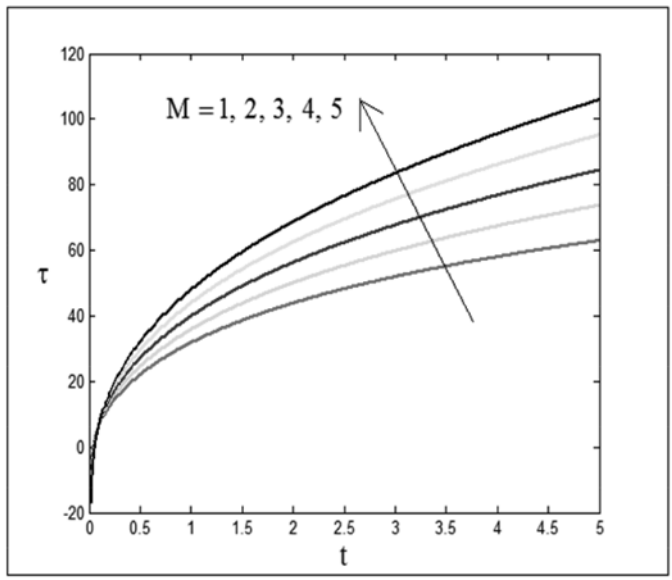

Figure 10
Skin-friction versus y for $Gr = 30$, $Gm = 20$, $Pr = 0.71$, $Sc = 0.60$, $Sr = 1$, $Pm = 2$, $Q = 0.5$, $K = 0.5$, $t = 1$, $\lambda = 0.5$.

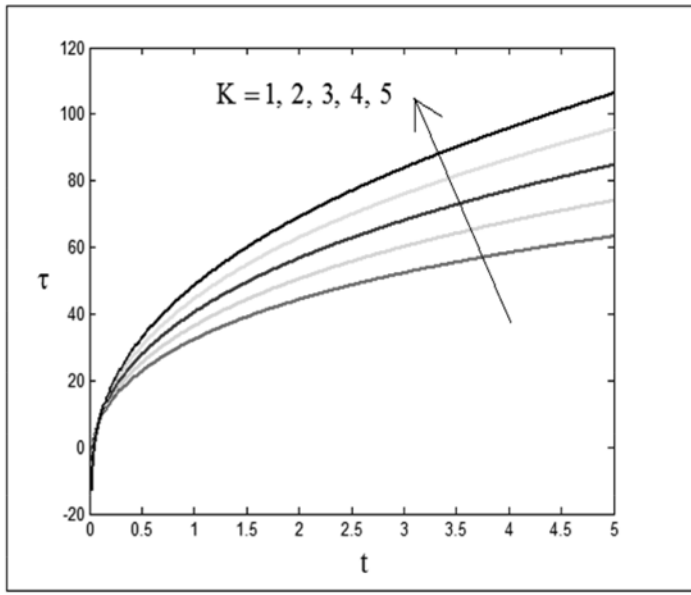

Figure 11
Skin-friction versus y for $Gr = 30$, $Gm = 20$, $Pr = 0.71$, $Sc = 0.60$, $Sr = 1$, $M = 10$, $Q = 0.5$, $Pm = 2$, $\lambda = 0.5$.

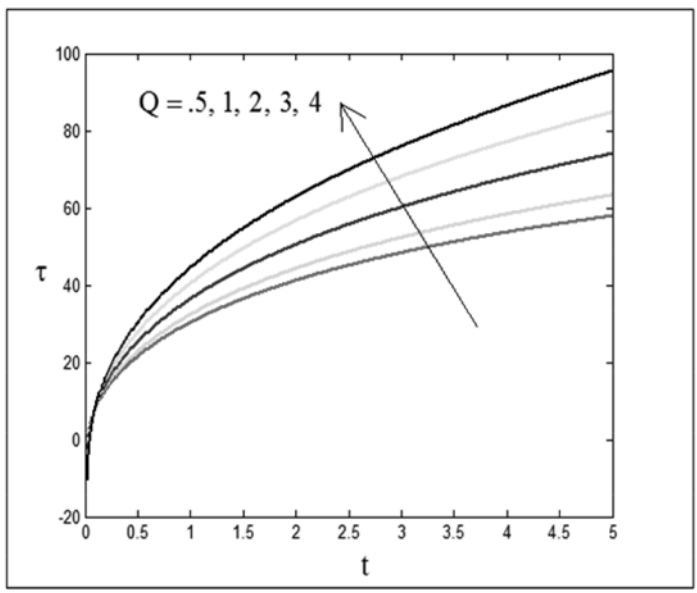

Figure 12
Skin-friction versus y for $Gr = 30$, $Gm = 20$, $Pr = 0.71$, $Sc = 0.60$, $Sr = 1$, $M = 10$, $Pm = 2$, $K = 0.5$, $\lambda = 0.5$.

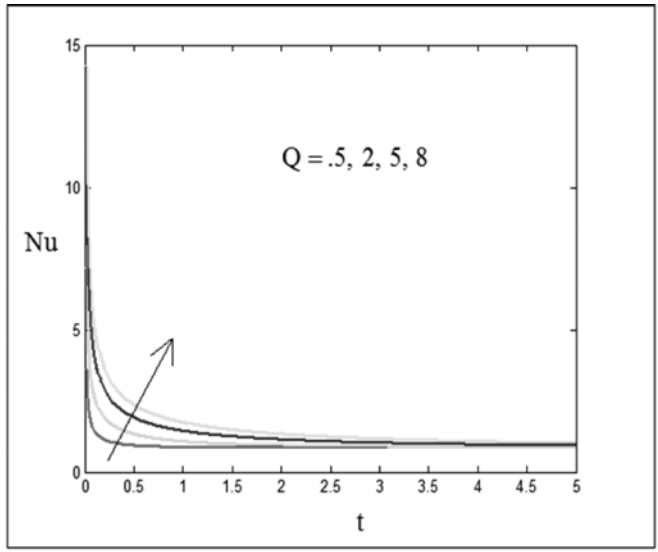

Figure 13
Nusselt number versus t for Pr = ·71.

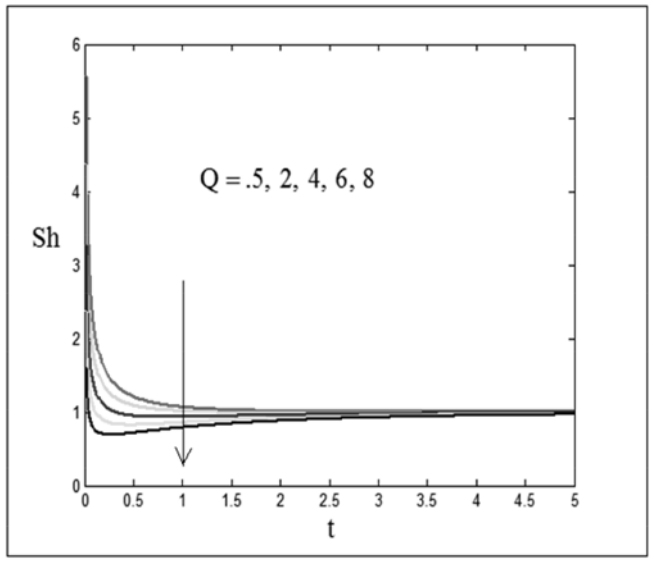

Figure 14
Sherwood number versus t for Pr = ·71, Sc = ·60, Sr=1, K=1.

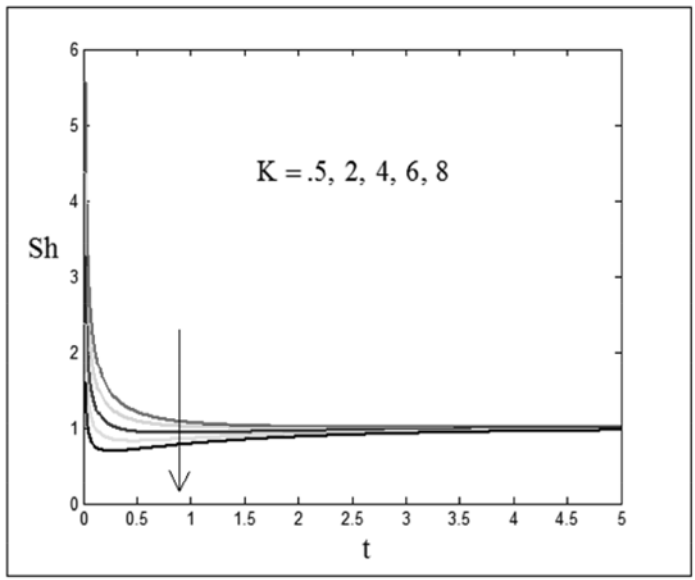

Figure 15
Sherwood number versus t for Pr = ·71, Sc = ·60, Sr = 1, Q = ·5.

8. Conclusions

(*i*) The fluid motion is accelerated under the effect of low magnetic diffusivity as well as thermal radiation.

(*ii*) The imposition of the transverse magnetic field or species consumption causes the flow to retard comprehensively.

(*iii*) The rate of mass transfer is continuously reduced due to radiation as well as chemical reaction effect.

(*iv*) The species concentration ϕ is enhanced near the plate under the effect of radiation whilst it falls due to effect of chemical reaction.

(*v*) The viscous drag at the plate gets enhanced as time progresses irrespective on the choice of the values of the physical parameters.

(*vi*) Initially the rate of fall of the Nusselt number Nu is very high and as time progresses the rate of fall of Nu becomes almost zero and thereby the rate heat transfer gets stagnated.

(*vii*) An increase in magnetic diffusivity causes B_x to increase substantially.

Acknowledgement

The author is highly thankful to CSIR-HRDG for funding this research work under Research Grant-in-aid No. 25(0209)/12/EMR-II.

References

1. Alfven, H. – Discovery of Alfven Waves, Nature, **150,** 405-406 (1942).
2. Cowling, T.G. – Magnetohydrodynamics, Willey Inter Science, NewYork (1957).
3. Shercliff, J.A. – A text book of Magnetohydrodynamics, Pergomon Press, London (1965).
4. Ferraro, V.C.A. and Plumpton, C. – An introduction to Magnetic Fluid Mechanics, Clarandon Press, Oxford (1966).
5. Crammer, K.R. and Pai, S. L. – Magneto Fluid Dynamics for Engineers and Applied Physicist, Mc Grow-Hill Book Co. New York (1973).
6. Mansour, M.A. – Radiation and free convection effects on the oscillatingflow past a vertical plate, Astrophysics and Space Science, **166(2),** 269-275. DOI : 10. 1007/BF 01094898 (1990).
7. Ganesan, P. and Loganathan, P. – Radiation and mass transfer effects onflow of an incompressible viscous fluid past a moving vertical cylinder, International journal of Heat and Mass Transfer, **45(21)**, 4281-4288.DOI : 10. 1016/S 0017-9310(02) 00140-0 (2002).
8. Mbeledogu, I.U., Amakiri, A.R.C. and Ogulu, A. – Unsteady MHD free convection flow of a compressible fluid past a moving vertical plate in the presence of radiative heat transfer, Int. J. Heat and Mass Transfer, **50** (9-10), 326-331.DOI : 10. 1016/j. ijheatmasstransfer .2006.10. 032 (2007).
9. Makinde, O.D.− Free Convection flow with thermal radiation and mass transfer past a moving vertical porous plate, International Communications in Heat and Mass Transfer, **32**(10), 1411-1419. DOI: 10. 1016/j.icheatmasstransfer2005. 07. 005 (2005).
10. Samad, M.A. and Rahman, M.M. – Thermal radiation interaction withunsteady MHD flow past a vertical porous plate immersed in a porous medium, Journal of Naval Architecture and Marine Engineering, **3(1),** 7-14 (2006).
11. Orhan, A. and Ahmet, K. – Radiation effect on MHD mixed convectionflow about a permeable vertical plate, Heat and Mass Transfer., DOI : 10.1007/S00281-008-0428-y (2008).
12. Prasad, N.R., Reddy, N.B. and Muthucumaraswamy, R. – Transient radiation hydro-magnetic free convection flow past an impulsively started vertical plate with uniform heat and mass flux, Theoret. Appl. Mech., **33(1)**, 31-63 (2006).

13. Takhar, H.S., Gorla, R.S.R. and Soundalgekar, V.M. – Radiation effects on MHD free convection flow of a radiating gas past a semi infinite vertical plate, Int. J. Numerical Methods Heat Fluid Flow, **6(**2), 77-83 (1996).
14. Ahmed, N. and Dutta, M. – Analytical Analysis of Magnetohydrodynamic transient flow past a suddenly started infinite vertical plate with thermal radiationand ramped wall temperature, Journal of Heat Transfer (ASME) , **136**(4), 041703-041711.DOI : 10. 1115/1. 4026052 (2014).
15. Ezzat, M., El-Bary, A.A. and Ezzat, S. – Combined heat and mass transferfor unsteady MHD flow of perfect conducting micro polar fluid with thermal relaxation, Energy Conversion and Management, **52**(2), 934-945 (2011).
16. Eckert, E.R.G. and Drake, R.M.− Analysis of Heat and Mass Transfer, McGraw-Hill, New York (1972).
17. Postenlnicu, A. – Influence of a magnetic field on heat and mass transferby natural convection from vertical surface in porous media considering Soret and Dufour effects, Int. J. Heat and Mass Transfer, **47,** 1467-1472 (2004).
18. Ahmed, N. – Soret and radiation effects on transient MHD free convectionfrom an impulsively started infinite vertical plate, Journal of Heat Transfer (ASME), **134**/062701-1-9. DOI: 10. 1115/1. 4005749 (2012).
19. Apelblat, A. − Mass transfer with chemical reaction of first order, Effect of axial diffusion, The Chemical Engineering Journal, **23(2)**, 193-203.DOI:org/10.1016/0300-9467(82)80011-7 (1982).
20. Andersson, H.I., Hansen, O.R. and Holmedal, B. – Diffusion of a chemically reactive species from a stretching sheet, Int. J. Heat and Mass Transfer, **37**/4, 659-664.DOI: 00179310/37/4 (1994).
21. Muthuwmaraswamy, R. and Ganesan, P. – Effect of the chemical reactionand injection an flow characteristics in an unsteady upward motion of an isothermal plate, Journal of Applied Mechanics and Technical Physics, **42(**4), 665-671.DOI: 10.1023/A: 1019259932039 (2001).
22. Kundasamy, R., Periasamy, K. and Prabhu, K.K.S. – Effects of chemical reaction, heat and mass transfer along a wedge with heat source and concentration in the presence of suction or injection, Int. J. Heat and Mass Transfer, **48**(7), 1388-1394.DOI::10.1016/j.ijheatmasstransfer.2004.10.008 (2005).
23. Ahmed, N. – Effect of chemical reaction on a transient MHD flow past a suddenly started infinite vertical plate with thermal diffusion and radiation, Journal of Calcutta Mathematical Society, **10(1)**, 9-36 (2014).

24. Singh, N.P. and Singh, A.K. – MHD effects on heat and mass transfer in flow of a viscous fluid with induced magnetic field, Indian Journal of Pure and Applied Physics, **38**, 182-189 (2000).
25. Choudhury, R.C. and Sharma, B. K . – Combined heat and mass transfer by laminar mixed convection flow from a vertical surface with induced magnetic field, J. Appl. Phys., **99**, 034901-034910 (2006).
26. Hossain, M.M.T. and Khatun, M. – Study of diffusion-thermo effect on laminar mixed convection flow and heat transfer from a vertical surface with induced magnetic field, Int. J. of Appl. Math. and Mech., **8**(5), 40-60 (2012).
27. Chorlton, F. – Textbook of Fluid Dynamics, CBS Publishers, New Delhi -110032 (India) (1985).
28. Cogley, A.C.L., Vincenti, W.G. and Gilles, E.S. – Differential approximation for radiative heat transfer in a Gray gas near equilibrium, American Institute of Aeronautics and Astronautics, **6**(3), 551-553 (1968).
29. Schlichting, H. – Boundary-layer theory, 6th ed., New York, McGraw-Hill (1968).

ISSN : 0019-5693

INDIAN JOURNAL
OF
THEORETICAL PHYSICS

[Founder President : Late Prof. K. C. Kar, D.Sc.]

VOLUME 64

2016

Published by the

CALCUTTA INSTITUTE OF THEORETICAL PHYSICS
(Formerly, INSTITUTE OF THEORETICAL PHYSICS)
"BIGNAN KUTIR"
4/1, MOHAN BAGAN LANE, KOLKATA-700 004

(UGC approved and refereed Journal)

INFORMATION TO AUTHORS

Manuscripts should represent results of original works on theoretical physics or experimental physics with theoretical background or on applied mathematics. Letters to the Editor and Review articles in emerging areas are also published. Submission of the manuscript will be deemed to imply that it has not been published previously and is not under consideration for publication elsewhere (either partly or wholly) and further that, if accepted, it will not be published elsewhere. It is the right of the Editorial Board to accept or to reject the paper after taking into consideration the opinions of the referees.

Manuscripts may be submitted in pdf/MS word format to **admin@citphy.org or susil_vcsarkar@yahoo.co.in** Online submission of the paper through our **website: www.citphy.org** is also accepted. The file should be prepared with 2.5 cm margin on all sides and a line spacing of 1.5.

The title of the paper should be short and self-explanatory. All the papers must have an abstract of not more than 200 words, the abstract page must not be a part of the main file. Abstract should be self-contained. It should be clear, concise and informative giving the scope of the research and significant results reported in the paper. Below the abstract four to six key words must be provided for indexing and infornjation retrieval.

The main file should be divided into sections (and sub-sections, if necessary) starting preferably with introduction and ending with conclusion. Displayed formula must be clearly typed (with symbols defmed) each on a separate /'ine and well-separated from the adjacent text. Equations should be numbered with on the right-hand side consecutively throughout the text. Figures and Tables with captions should be numbered in Arabic numerals in the order of occurrence in the text and these should be embedded at appropriate places in the text. Associated symbols must invariably follow SI practice.

References should be cited in the text by the Arabic numerals as superscript. All the references to the published papers should be numbered serially by Arabic numerals and given at the end of the paper. Each reference should include the author's name, title, abbreviated name of the journal, volume number, year of publication, page numbers, as in the simple citation given below :

For Periodicals : Sen, N.R. - On decay of energy spectrum of Isotopic Turbulence, 1. Appl. Phys. **28,** No. l0, l09-110 (1999).

1. Mikhilin, S. G. - Integral Equations, Pergamon Press, New York (1964).
2. Hinze, A. K. - Turbulence Study of Distributed Turbulent Boundary Layer Flow, Ph.D, Thesis, Rorke University (1970).

The corresponding author will receive page proof, typically as a pdf file. The proof should be checked carefully and returned to the editorial office within two or three days. Corrections to the proof should be restricted to printing errors and made according to standard practice. At this stage any modifications (if any) made in the text should be highlighted.

To support the cost of publication of the journal, the authors (or their Institutions) are requested to pay publication charge Rs.200/- per printed page for authors of Indian Institutes and US$ 20 for others. Publication charges to be sent directly to **CALCUTTA INSTITUTE OF THEORETICAL PHYSICS, 'BIGNAN KUTIR', 4/1, MOHAN BAGAN LANE, KOLKATA-700 004, INDIA.**

A pdf of the final publisher's version of the paper will be sent to the corresponding author shortly after print publication by our Co-publisher, **Wilcox Books & Periodicals Co. (wilcoxbooks@gmail.com)**

All communications are to be sent to the Secretary, Calcutta Institute of Theoretical Physics, 'Bignan Kutir', 4/1, Mohan Bagan Lane, Kolkata-700 004.

Indian Journal of Theoretical Physics is in the list of Journals approved by UGC.

For details please visit our website www.citphy.org

INDIAN JOURNAL OF THEORETICAL PHYSICS

International Board of Editorial Advisors

B. Das Gupta, (*USA*)
Nao-Aki Noda, (*Japan*)
D. S. Roy, (*India*)
A. Sen, (*India*)
A. Roy Chaudhury, (*India*)
S. Raha, (*India*)
A. H. Siddiqi, (*India*)
N. K. Gupta, (*India*)
K. Ghatak, (*India*)
O. P. Agarwal, (*USA*)
Ching-Kong Chao, (*Taiwan*)
M. R. Islami, (*Iran*)
Halina Egner, (*Poland*)
K. C. Deshmukh, (*India*)
A. Kundu, (*India*)
B. Chakraborty, (*India*)
A. N. Sekhar Iyengar, (*India*)

BOARD OF EDITORS

D. K. Basu
C. Dutta
S. K. Biswas
R. K. Bera
D. Syam
I. Bose
M. Kanoria
P. R. Ghosh
Rita Chaudhuri
S. K. Sarkar
D. C. Sanyal
P. K. Chaudhuri
D. Sarkar
A. Sanyal
J. Mukhopadhyay
A. K. Ghosh

***Editorial Secretary* : D. C. Sanyal**

CALCUTTA INSTITUTE OF THEORETICAL PHYSICS

(Formerly, Institute of Theoretical Physics)

[Established in 1953 by Late Prof. K. C. Kar, D.Sc.]

***Director* : D. K. Basu** ***Secretary* : S. K. Sarkar**
***Registrar* : C. Dutta** ***Asst. Secretary* : M. Kanoria**
***Members* : P. R. Ghosh, A. Roy, D. C. Sanyal, Sudip Kr. Sarkar, J. Mukhopadhyay, M. Chakraborti, P. S. Majumdar**

PUBLICATIONS
OF
CALCUTTA INSTITUTE OF THEORETICAL PHYSICS

"BIGNAN KUTIR"
4/1, Mohan Bagan Lane, Kolkata - 700 004, India
Phone: +91-33-25555726

INDIAN JOURNAL OF THEORETICAL PHYSICS (lSSN : 0019-5693)

Research Journal containing Original Papers, Review Articles and Letters to the Editor is published quarterly in March, June, September and December and circulated all over the world.

Subscription Rates

₹ 1500 per volume (for Bonafide Indian Party)
US $ 350 (for Foreign Party)

Back Volume Rates

₹ 1500 per volume (for Bonafide Indian Party)
US $ 350 per volume or Equivalent Pounds per volume

Books Written by Prof. K. C. Kar, D. Sc.

- **INTRODUCTION TO THEORETICAL PHYSICS**
  [Vol. I and Vol. II (Accoustics)]
  Useful to students of higher physics
  Price : ₹ 60 or US $ 10 per volume
- **WAVE STATISTICS : Its principles and Applications**
  [Vol. I and Vol. II]
  Useful to Post Graduate and Research students
  Price : ₹ 80 or US $ 12
- **STATISTICAL MECHANICS : Principles and applications**
  [Vol. I and Vol. II]
  Useful to Advanced students of Theoretical Physics
  Price : ₹ 120 orUS $ 15
- **A NEW APPROACH TO THE THEORY OF RELATIVITY**
  Useful to post Graduate and Advanced students
  Price : ₹ 50 or US $ 8

Order may be sent directly to Calcutta Institute of Theoretical Physics
"Bignan Kutir", 4/1, Mohan Bagan Lane, Kolkata -700 004, India

---

All rights (including Copyright) reserved by the Calcutta Institute of Theoretical Physics.
Unimage, 10, Roy Bagan Street, Kolkata-700 006 and published by Dr. S. K. Sarkar, Secretary, on behalf of Calcutta Institute of Theoretical Physics, 4/1, Mohan Bagan Lane, Kolkatta -700 004, India.

INDIAN JOURNAL OF THEORETICAL PHYSICS

VOLUME 64, 2016

C O N T E N T S

JANUARY – JUNE, 2016

JULY – DECEMBER, 2016

Detailed information about our other Journals

1. Name of the Journal : **Bengal Past & Present**
   ISSN :..... **0005-8807**
   Frequency:..... **Annually (Latest Vol. 136,2017)**
   Price: .....(a) In India: Institutions: **500-00**
   .....(b) Overseas : **$ 150-00**
   Postage:..... **Post Free**
   * Discount :.... To Subscription Agencies: **25%**
   ..... To Institutions :..... **Fixed Price**
2. Name of the Journal:..... **Journal of the Indian Anthropological Society**
   ISSN :..... **0019-4387**
   Frequency:..... **Three Issues in a year (March, July & November)**
   Price:..... (a) In India: Institutions: **1500-00 (Latest Vol. 51, 2016)**
   ..... (b) Overseas..... **$ 300-00**
   Postage:..... **Post Free**
   * Discount: To Subscription Agencies: **25%**
   ..... To Institutions :..... **Fixed Price**
3. Name of the Journal: ..... **Journal of Surface Science and Technology**
   ISSN :..... **0970-1893**
   Frequency:..... **Quarterly**
   Price:..... (a) In India: Institutions: **1800-00 (Latest Vol. 33, 2017)**
   ..... (b) Overseas..... **$ 300-00**
   Postage :.....**Post Free**
   * Discount: To Subscription Agencies: **25%**
   ..... To Institutions :..... **Fixed Price**
4. Name of the Journal: **The Journal of the Indian Academy of Philosophy**
   ISSN: .....
   Frequency:..... **Bi-Annual**
   Price:..... (a) In India: Institutions: **200-00 (Latest Vol. 52, 2013)**
   ..... (b) Overseas..... **$ 30-00**
   Postage :..... **Post Free**
   * Discount :... To Subscription Agencies: **25%**
   ..... To Institutions :..... Fixed Price
5. Name of the Journal: **The Quarterly Review of Historical Studies**
   ISSN:..... 0033-5800
   Frequency:..... **Quarterly**
   Price:..... (a) In India: Institutions: **1500-00 (Latest Vol. 57, 2017-18)**
   ..... (b) Overseas..... **$ 400-00**
   Postage:..... **Post Free**
   * Discount :... To Subscription Agencies: **25%**
   ..... To Institutions: **Fixed Price**
6. Name of the Journal: **Indo-Iranica**
   ISSN:.....03789-0856
   Frequency:..... **Quarterly**
   Price:..... (a) In India: Institutions: **1500-00 (Latest Vol. 69, 2016)**
   ..... (b) Overseas..... **$ 350-00**
   Postage:.....**Post Free**
   * Discount : To Subscription Agencies: **25%**
   ..... To Institutions :..... **Fixed Price**

For more Journals Visit our website : www.wilcoxjournals.com

*** For Foreign Subscriptions Only**

Order should be sent to :

Wilcox Books and Periodicals Co.
8/2/A, Neogi Para Road,
Kolkata - 700036 (India)
Email : wilcoxbooks@gmail.com
: wilcoxbooks@yahoo.co.in